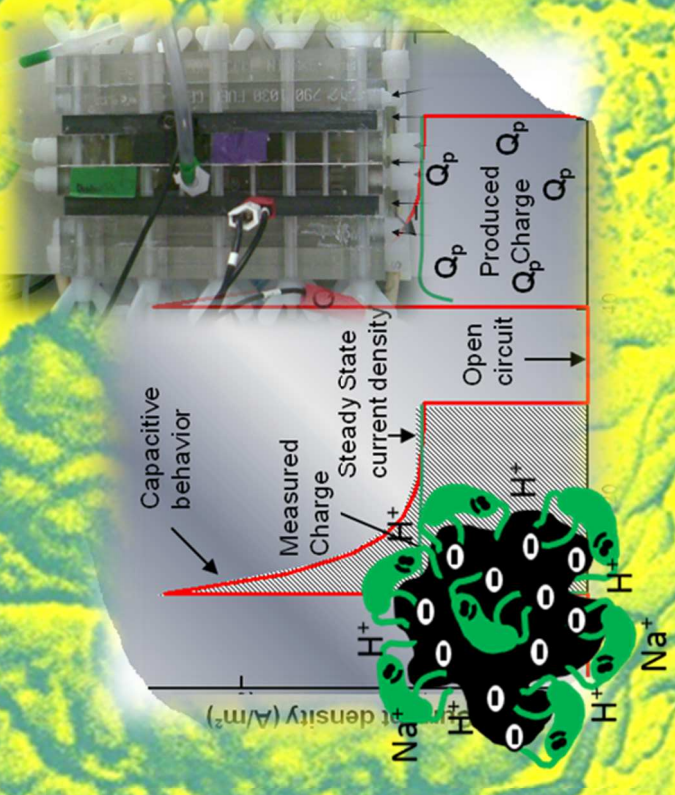


# Capacitive bioanodes for electricity storage in Microbial Fuel Cells



Alexandra Deeke

Capacitive bioanodes for electricity Storage in Microbial Fuel Cells

A. Deeke

# **Capacitive bioanodes for electricity storage in Microbial Fuel Cells**

**Alexandra Deeke**

## **Thesis committee**

### **Promotor**

Prof. Dr C.J.N. Buisman

Professor of Biological Recovery and Reuse Technology

Wageningen University

### **Co-promotors**

Dr H.V.M Hamelers

Scientific Program Director

Wetsus Centre of Excellence for sustainable Water Technology, Leeuwarden

Dr A. ter Heijne

Assistant professor, Sub-department of Environmental Technology

Wageningen University

### **Other members**

Prof. Dr A.J.M. Stams, Wageningen University

Dr A.W. Jeremiase, Magneto Special Anodes BV, Schiedam

Prof. Dr G.J. Witkamp, Delft University of Technology

Prof. Dr L.T. Angenent, Cornell University, Ithaca, USA

This research was conducted under the auspices of the Graduate School SENSE  
(Socio-Economic and Natural Sciences of the Environment)

# Capacitive bioanodes for electricity storage in Microbial Fuel Cells

Alexandra Deeke

## **Thesis**

submitted in fulfillment of the requirements for the degree of doctor

at Wageningen University

by the authority of the Rector Magnificus

Prof. Dr M.J. Kropff,

in the presence of the

Thesis Committee appointed by the Academic Board

to be defended in public

on Friday 10 October 2014

at 4 p.m. in the Plaza Hall of the Post Plaza Leeuwarden.

Alexandra Deeke

Capacitive bioanodes for electricity storage in Microbial Fuel Cells,  
168 pages.

PhD thesis, Wageningen University, Wageningen, NL (2014)

With references, with summaries in English, Dutch and German

ISBN 978-94-6257-110-5

# Chapter 1

## General Introduction

## 1.1 Introduction

The size of the world population is increasing. As of today, already 7 billion people live on earth and this number is expected to increase even more (WHO, 2012). Not only the number of humans living on earth is expected to grow but also their wealth and therefore the demand for energy will increase. Especially energy in the form of electricity is becoming more and more important for our modern society (see Figure 1.1). From 1973 till 2008 the share of electricity in our energy consumption increased from 9.4% to 17.2%, while the total energy use almost doubled.

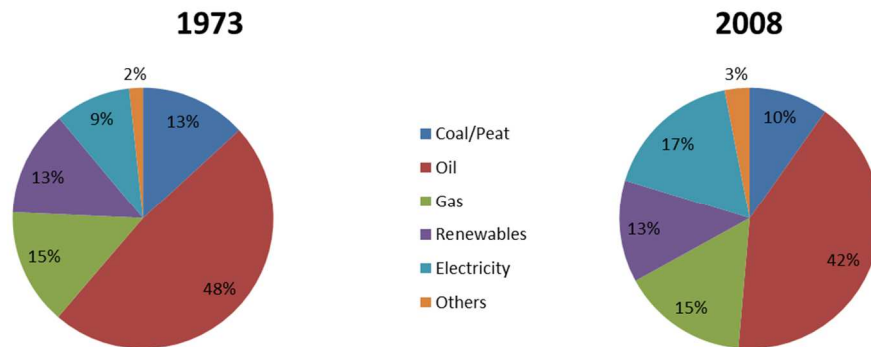


Figure 1.1: Fuel shares of our final consumption in percentages, comparison of 1973 and 2008 (based on IEA, 2011)  
In the 1970s, electricity was mainly used to operate the household appliances and for lighting in the evening hours <sup>1</sup> (Cooking was done on gas stoves.). But since the beginning of the 21th century more and more electricity is used for newly developed gadgets, like mobile phones, notebooks and televisions, but also for heating Figure 1.2.

This behaviour will increase our need for electricity even more <sup>2</sup>. At the same time the use of electrically fuelled cars, which is expected to rise significantly in the coming decades, will further increase the demand for electricity <sup>1,3</sup>.

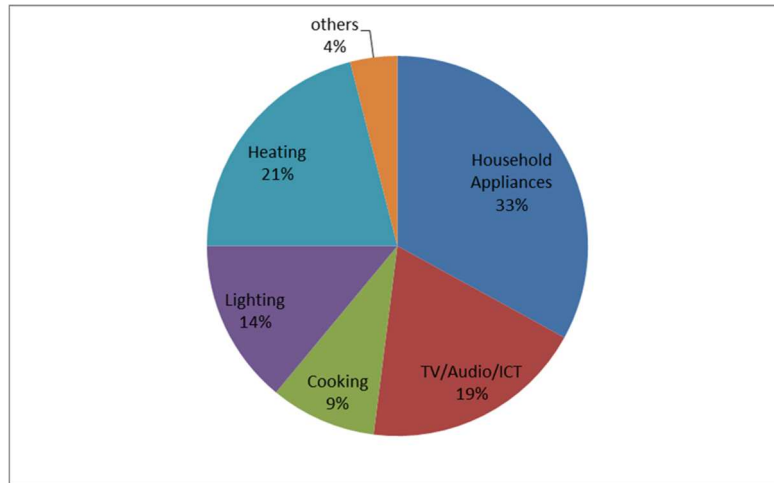


Figure 1.2: Average electricity use of Dutch Households (CBS, 2011)

The awareness of the pollution of the atmosphere as a result of burning fossil fuels and the depletion of the fossil fuels is not only driving the development of electrically fuelled cars, but it is also an important incentive for policy makers to change the way electricity is produced. Germany is the European country where policy makers had a huge influence on the further development and the use of electricity from renewable resources. Here policy makers took many decisions, which put Germany in the leading position regarding their use of renewable electricity. Figure 1.3 shows the development of renewable electricity production in Germany in the period from 1990 to 2012. In the 1990s, renewable electricity was mainly produced by hydropower and incineration of biomass. This was supported by a national directive, which enabled the electricity produced by hydropower to be introduced into the electricity grid. From the year 2000 on, a renewable energy directive (EEG) was introduced, which aimed at increasing the production of electricity from renewable resources up to 35% by 2020. This European energy directive was reinforced in 2004, 2009 and in January 2012, to restrict the carbon dioxide emissions even more and to support the use of renewable energy sources for electricity production. In Figure 1.3, an extra increase in the amount of

electricity produced from wind, biomass and solar sources after 2011 can be seen. This shift was induced by the reactor melt down of the nuclear power plant in Fukushima Japan (11.03.2011). This nuclear meltdown in Fukushima and its consequences increased the awareness of the risks of nuclear electricity production. Many people realized the safety hazards which rise during operation of the nuclear power plant, but also afterwards in the question how to deal with the radioactive waste. Therefore the German government was urged to switch off all nuclear power plants. From April 2011 till August 2011 all nuclear power plants of Germany had to pass a "Stress-test" to verify if they were safe enough to be connected to the grid again. Most power plants passed this test and are producing electricity again, but they do not produce as much electricity anymore as before; in 2010, 22% of Germany's electricity was produced by nuclear power plants, this was lowered to only 16% in 2012. At the same time the electricity production by renewable sources increased from 16% in 2010 to 22% in 2012<sup>4</sup>.

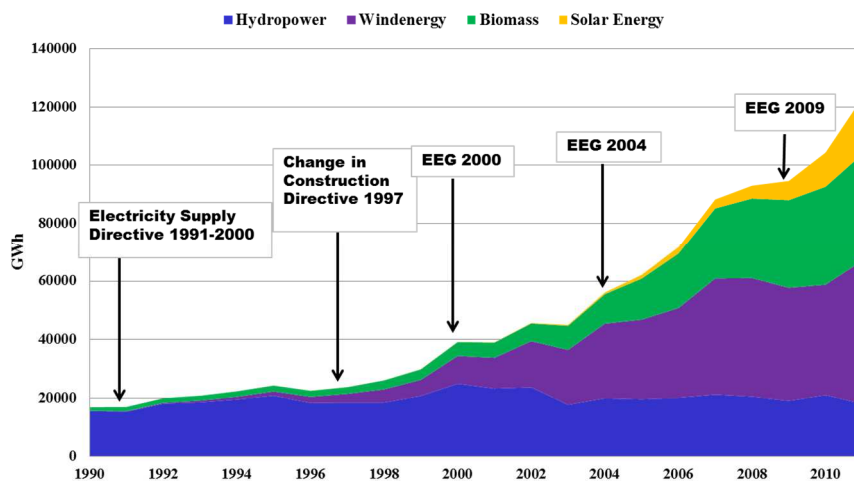


Figure 1.3: Renewable electricity production in Germany from 1990 towards 2012 (Ministry of the Environment)

Worldwide, electricity is mainly produced using either fossil fuels, which are depleting and emitting carbon dioxide and fine dust into the atmosphere, or

nuclear fuels, which are a safety hazard, as mentioned above (see Table 1.1, Figure 1.1). But the demand for electricity is increasing; therefore different sources are necessary. These challenges urge for a clean electricity production using renewable sources. But there are also challenges to tackle, when producing electricity with the renewable sources. When using hydropower for electricity production, there needs to be a considerable height difference, and therefore its application is limited to specific locations. When using wind and solar energy for electricity production the storage of the electricity is an important factor, since the electricity production is dependent on the day/night cycle or the wind speed, which usually does not match with the demand. So far, biomass is only used for electricity production via incineration, with low conversion rates from thermal to electrical energy. Advantages of biomass are its availability in many places in the world, and the fact that it can be stored.

Table 1.1: Fuel Types used for electricity production and their challenges

<b>Fuel type for electricity production</b>	<b>Challenge</b>
Fossil Fuels	Carbon dioxide, scarcity, political tensions, fine dust emissions
Nuclear Fuels	Waste, safety
Hydro Power	Location
Solar, Wind	Storage,
Biomass	Conversion

A new technology which uses biomass in the form of wastewater for electricity production is the Microbial Fuel Cell (MFC). In an MFC, the organic compounds

from wastewater (chemical energy) are converted directly by microorganisms into electrical energy. The direct conversion of the organic compounds into electricity results in higher efficiencies than the current biomass conversion technologies, which are using either incineration or the gasification of the organic compounds.

## 1.2 Microbial Fuel Cells

### 1.2.1 Introduction to Microbial Fuel Cells

An MFC (Figure 1.4) consists of two compartments: the anode and the cathode compartment. Those two compartments are separated by a membrane. In the anode compartment electrochemically active bacteria grow on the electrode and convert the biodegradable organic compounds in wastewater into carbon dioxide, protons and electrons.

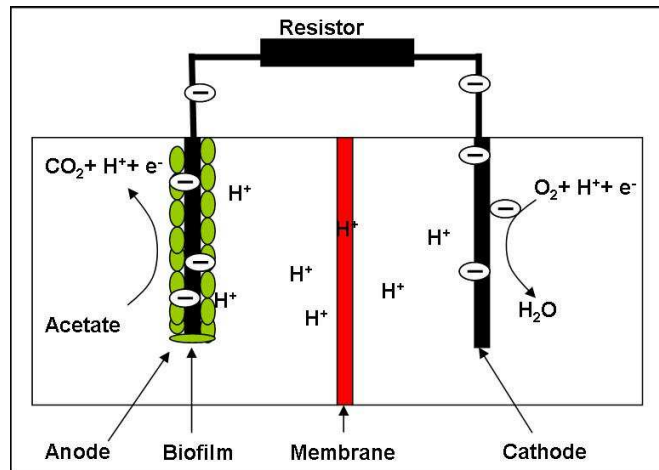


Figure 1.4: A typical two-chamber MFC

The protons and other positive ions are transferred through the membrane (cation exchange membrane) to the cathode compartment. The electrons pass through the external electric circuit from the anode to the cathode electrode. At the cathode the

protons and electrons react with the oxygen to form water. The electricity, which is produced by the MFC, is tapped off from the external circuit <sup>5</sup>. Many studies focussed on improving the power output of the MFCs by optimizing the anode <sup>6-10</sup>, cathode <sup>11-15</sup> and membrane materials <sup>16,17</sup>. The development of the power output over time achieved in studies performed on MFCs is in Figure 1.5. The power output achieved during these studies shows that, while significant improvements have been made in the first years, from 2007 the increase in power density levelled off. A maximum power output of 3.1W/m<sup>2</sup> is achieved so far, but further improvements are necessary to make the use of MFCs economical feasible.

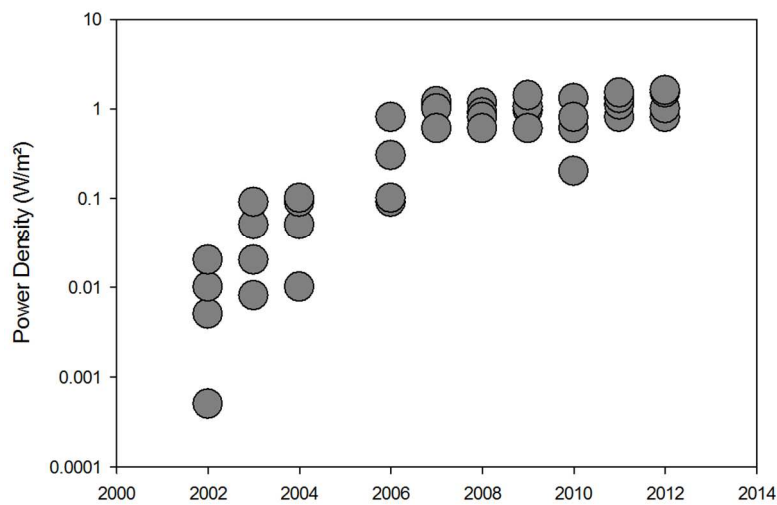


Figure 1.5: Development of the Power Output from MFCs throughout the years 2000 till 2013 (note that the y-axis has a logarithmic scale)

There are many challenges which have to be overcome for further increase in the power output of MFCs, like: the overpotential at the cathode, the overpotential at the anode, chemical use at the anode, ion transport through the membrane and material costs. Due to the unselective migration of positive ions through the membrane to the cathode compartment and the consumption of protons in the

cathode reaction, the pH increases in the catholyte. This increase in pH leads to an increase in overpotential and is thereby affecting the overall cell performance. At the same time the protons are accumulating in the anode compartment due to the limited transport through the membrane. To prevent the acidification of the anode compartment chemicals are used intensively. Phosphate buffers are used to keep the pH of the anolyte around 7 and to increase the conductivity of the medium for increased current density<sup>18</sup>. Furthermore the improvement of MFCs is limited by the cost of the materials, mainly for the electrodes and the membrane<sup>19</sup>. Another challenge which has to be overcome, that has not been addressed, until now, is related to storage; the MFC produces electricity constantly, since there is a continuous flow of wastewater. Storage of the wastewater would be a costly alternative as the average Dutch person produces 120L of wastewater per day (CBS, 2012). So, in case of a city with 100,000 inhabitants, this means a total wastewater production of 12,000 m<sup>3</sup> per day (or 500m<sup>3</sup> per hour). If this wastewater is treated in an MFC only when the electricity is demanded, a large storage tank is required of at least 6000m<sup>3</sup> (enables storage of ~12h of wastewater production) . The use of an electrochemical capacitor to store the electricity produced by the MFC and release it on demand, is a cost-effective alternative<sup>20</sup>.

### **1.2.2 Electrochemical Capacitors**

Electrochemical capacitors, also known as supercapacitors, represent an important group of capacitors. Research on electrochemical capacitors (supercapacitors) was intensified, when the need for storage of electricity increased<sup>21,22</sup>. Two main charge mechanisms are differentiated: the electrochemical double layer capacitance (EDLCs) or the Pseudocapacitance. In EDLCs the electrostatic charge is stored within the double layer on the electrode-electrolyte interphase<sup>23</sup>. Whereas in Pseudocapacitors the storage is achieved by redox reactions on the surface of the electrode which result in a reversible faradaic charge transfer. Both, the double-

layer capacitance and the pseudocapacitance contribute to the total capacitance of a supercapacitor. They also play an important role during the studies for this thesis. Usually, the electrochemical capacitor (EC) consists of two electrodes, which are separated by an electrolyte to enable the transport of ions. The principle of the charging process of an electrochemical capacitor is shown in Figure 1.6. The electrochemical capacitor consists of two electrodes that are covered with a layer of activated carbon. The electrodes of the electrochemical capacitor are connected to the external electric circuit. The ions of the electrolyte are attracted by the electrode with the opposite charge and are forming an electrical double layer close to the electrode. The amount of charge which can be stored in an electrochemical capacitor is determined by the material properties, such as the choice of the electrolyte (conductivity), the salt concentration and the properties of the activated carbon, such as the thickness and specific surface area. The electrochemical capacitor is discharged, when the direction of the electron-flow is reversed and the double-layer is disappearing.

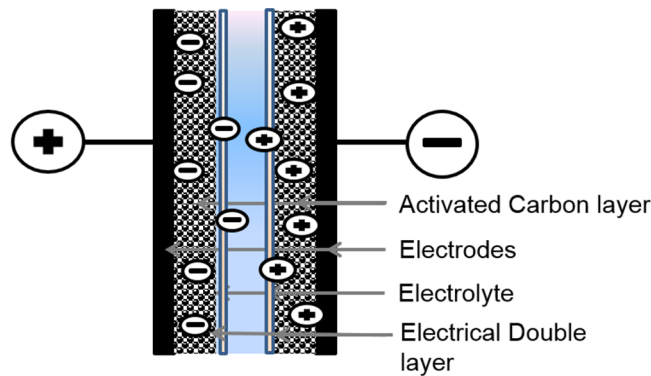


Figure 1.6: The charge-mechanism of an electrochemical capacitor

### 1.3 Combination of Microbial Fuel Cells and Electrochemical Capacitors

Combination of the MFC with an electrochemical capacitor enables the direct storage of the electricity, which is produced by the MFC. There are two possible ways to combine the operation of a Microbial Fuel Cell with that of an electrochemical capacitor. 1) The electric circuit of the MFC is connected to a capacitor and the electricity produced by the MFC is stored inside this capacitor. 2) The EC is integrated into the MFC, inserted into the anode compartment of an MFC to form a capacitive bioanode. This means that the microorganisms which usually grow on the anode electrode, will grow on the capacitive electrode. Thereby this capacitive electrode is both one electrode of the capacitor, and also the bioanode of the MFC. The principle of this capacitive bioanode is shown in Figure 1.7.

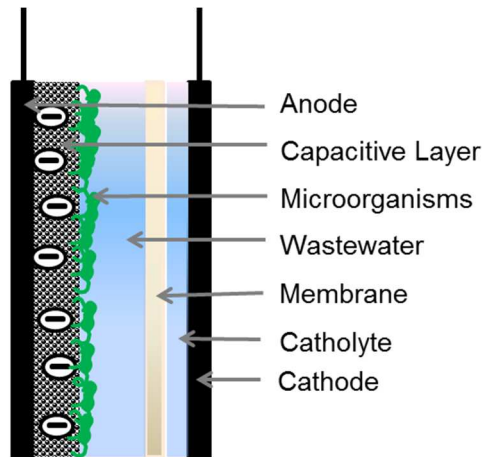


Figure 1.7: The principal of the bioelectrochemical charging in case of the capacitive bioanode

During the charging process, the capacitive bioanode is not connected to the cathode through the external electrical circuit. The microorganisms convert the organic compounds from the wastewater to protons, electrons and carbon dioxide,

and donate the electrons to the capacitive bioanode. The electrons are stored inside the capacitive electrode and the protons and other cations build up in the double layer. When the external electric circuit is closed, the capacitive bioanode discharges. At the same time, the microorganisms still convert the organic compounds of the wastewater, meaning that there are two sources of electric current: from the electrons which have been stored inside the capacitive electrode plus the electrons which are produced continuously. This capacitive current increases the amount of current we can harvest from the MFC. The use of this capacitive bioanode has several advantages compared to the use of an external capacitor, it is cheaper regarding material costs and a simple set-up regarding the external electric circuit. Less material costs for the integrated system compared to the external system are achieved, since the membrane, which separates the anode and the cathode compartment, also acts as a separator for the capacitor and the wastewater, which contains the food-supply for the microorganisms acts as the electrolyte for the capacitor. Due to the operation of the capacitive electrode in the charging and discharging mode other challenges in MFC optimization might be tackled as well. Since the protons and other positive ions are gathered in a layer in front of the capacitive material during the charging period, the pH-drop in the anode is less drastical and less buffer chemicals are needed. The ions are bound to the anode during the discharging period and are released upon discharging only. The flow of positive ions between the anode and the cathode compartment is balanced. Upon discharging, the electrons and the positive ions are released, this increases the conductivity of the anolyte and thereby improves the current flow since the internal resistance is lowered. The MFC can operate at lower COD concentrations due to the larger surface area (more biomass), which is increasing the coulombic efficiency.

### 1.3.1 Charging and Discharging

As shown in Figure 1.4, the electricity produced by the MFC is usually harvested continuously at the resistor. By inserting the capacitive electrode into the anode compartment, we enable also other ways of using the electricity. It is now possible to charge and discharge the electrode, meaning the electric circuit can be opened (electrical disconnection of anode and cathode) for the charging period and closed (electrical connection of anode and cathode) for the discharging period. When measuring the current density during this charge-discharge experiment the profile is different from the polarization curves obtained with noncapacitive bioanodes. An example of a profile measured with a capacitive bioanode is shown in Figure 1.8.

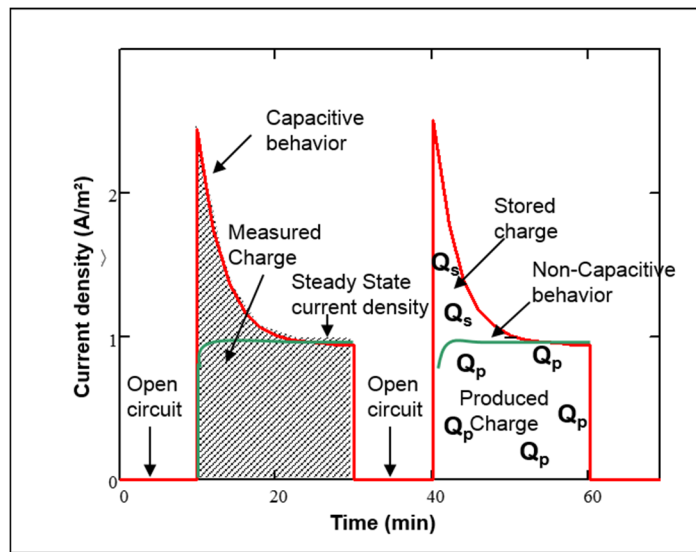


Figure 1.8: Current density measured during a charge-discharge experiment and its charge-distribution

During the charging period, the electrical circuit is opened and therefore we measure zero current (indicated in the figure by open circuit). Upon closing the electrical circuit and thereby discharging the capacitive bioanode, there is a sudden rise in current density, giving a peak. This peak in current density then levels off towards the steady state current density. The presence of this peak in current

density indicates the capacitive behavior of the electrode. The amount of charge produced by the capacitive bioanode is represented by the surface area under this current density graph. During the charging period, when the electric circuit is open, measured current density is zero and produced current density is stored as charge on the capacitive electrode

**Equation 1.1** 
$$i_m = 0; i_p = \frac{dQ_s}{dt}$$

, where  $Q_s$  is the stored charge (C/m<sup>2</sup>).

During the discharge period, measured current density is equal to produced current density plus stored charge (see Figure 1.8)

**Equation 1.2** 
$$i_m = i_p + \frac{dQ_s}{dt}$$

Theoretical it is possible to calculate an estimate for the produced charge (surface area under the green line) and the stored charge (surface area under the red line minus the surface area under the green line), but this is only an estimate. Therefore further calculations are made to determine the amount of measured charge (produced charge plus stored charge). Measured charge ( $Q_m$  in C/m<sup>2</sup>) is the integral of the current density curve from the charge-discharge experiment (shaded area in Figure 1.8)

**Equation 1.3** 
$$Q_m = \int_0^{t_o} i_m dt$$

Substituting the measured current density in Equation 1.3 leads to:

**Equation 1.4** 
$$Q_m = \int_{t_c}^{t_o} (i_p + \frac{dQ_s}{dt}) dt$$

**Equation 1.5** 
$$Q_m = i_p(t_o - t_c) + \Delta Q_s$$

, where  $t_o$  is the overall time of the charge-discharge cycle (s) and  $t_c$  is the charging time (s). The expected charge can be calculated as:

**Equation 1.6** 
$$Q_{cont,d} = i_s t_d$$

, where  $Q_{cont,d}$  is the expected charge (C),  $i_s$  is the steady state current (A) from the noncapacitive electrode taken from the polarization curves at an anode potential of -0.300 V, and  $t_d$  is the discharge time ( $t_d = t_o - t_c$ ).

To assess the effectiveness of each electrode the charge recovery ( $\eta_{rec}$ ) is introduced:

**Equation 1.7** 
$$\eta_{rec} = \frac{\sum Q_{m,k}}{n * Q_{cont,d,k}}$$

The charge recovery relates the measured charge from each experiment to the expected charge for each experiment.

The charge recovery and the relative charge recovery can reach three different states: (a)  $\eta_{rec} \leq 1$ , (b)  $\eta_{rec} = 1$ , and (c)  $\eta_{rec} \geq 1$ . When the recovery is lower than 1, measured charge is lower than the expected charge. When the recovery is equal to 1, measured charge is equal to the expected charge and when the recovery is larger than 1, measured charge is higher than the expected charge.

### 1.3.2 Capacitive Fluidized MFC

As shown earlier, the operational method with charging and discharging periods is advantageous<sup>24</sup>. Usually the whole MFC would have to operate continuously, since

the wastewater needs to be treated continuously. Therefore, the operation of the MFC in the charging and discharging mode offers a cheaper alternative, as the wastewater can be treated constantly, but the electricity will only be tapped off, when demanded.

The capacitive bioanode is a promising concept for a next generation MFC where the charging process is physically separated from the discharging process. Advantages of separating the charging and the discharging process are, that optimal circumstances can be created both for the charging process, which is occurring slowly, depending on the microorganisms, and the discharging process, which is occurring at a higher rate. By physical separating the charging from the discharging process the fluidized capacitive MFC is created. The principle of the fluidized capacitive MFC is shown in Figure 1.9.

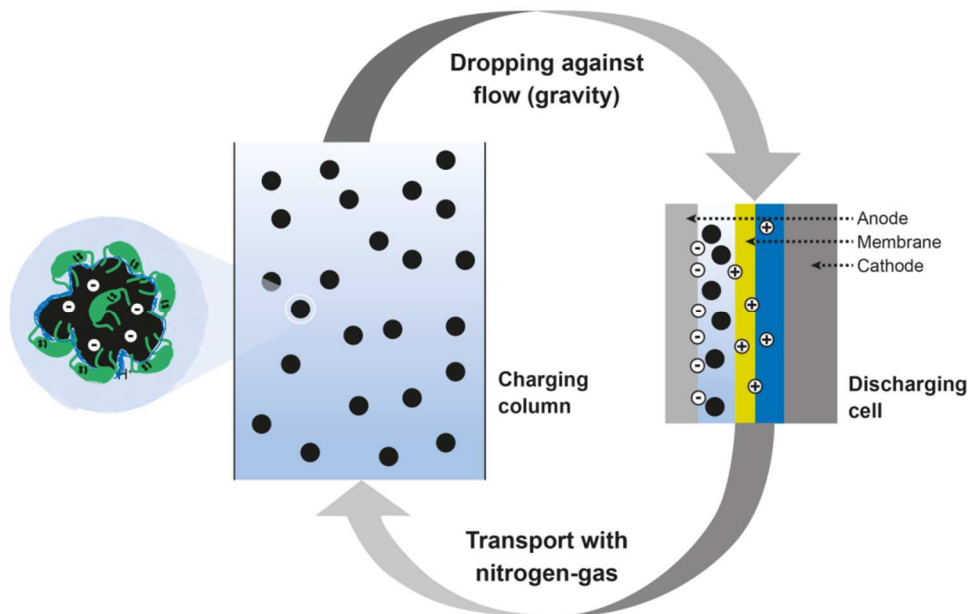


Figure 1.9: The principle of the fluidized capacitive anode

The fluidized capacitive anode consists of a charging column, a transport mechanisms and a discharging cell. In the charging column activated carbon

granules are fluidized in the wastewater using nitrogen gas. The microorganisms grow on these granules, converting the organic material from the wastewater into electrons, protons and carbon dioxide. The electrons are stored inside of the granules and the protons and other positive ions are gathered in the double layer around the granule. Like this the granules get charged by the microorganisms, for discharging the granules are transported into the discharging cell. In the discharging cell the granules make contact with the current collector thereby releasing their charge. Afterwards the granules will be transported back into the charging column.

This fluidized capacitive anode enables us to use a large anode compartment in which carbon granules are acting as the capacitive part of the electrode. By fluidizing the carbon granules, the distribution of medium towards the microorganisms is improved and it might decrease the risk of clogging as well.

#### **1.4 Thesis Outline**

The aim of this thesis is to enable on-demand electricity production with an integrated capacitive bioanode inside the Microbial Fuel Cell

**Chapter 2** analyses the performance of a capacitive bioanode in a two chamber flat plate MFC. A first integrated capacitive bioanode is compared with a noncapacitive bioanode, based on polarization curves and charge-discharge experiments. It is shown that the capacitive bioanode outperforms the noncapacitive bioanode during all experiments. The capacitive bioanode achieved a maximum current density of 1.02 A/m<sup>2</sup>. Furthermore it was able to store 22,831C/m<sup>2</sup> during the charge-discharge experiment with 5min of charging and 20 min of discharging. This represents a charge recovery of 1.53.

In **Chapter 3** we aimed at the improvement of the capacitive bioanode by changing the thickness of the capacitive layer. Since the storage capacity is dependent on the material parameters, we compared three different capacitive bioanodes regarding their performance in polarization curves and charge-discharge experiments. For

the proof-of-principle experiment we used a capacitive electrode with a thickness of 0.5mm. We compared the performance of a bioanode with this thickness to a capacitive bioanode with thicknesses of 0.2mm and 1.5mm. The capacitive bioanode with a thickness of 0.2mm was outperforming the other two electrodes during most of the experiments.

But even more parameters might influence the performance of the capacitive bioanodes, therefore we varied the PVDF-content of the capacitive bioanode in **Chapter 4**. Beforehand the capacitive bioanodes always contained 14% (weight-%) of PVDF. We used this study to further improve the recipe used for the production of the capacitive bioanodes. Six different PVDF-contents were tested and compared during material analyses (SEM, AFM and BET) and electrochemical experiments (polarization curves and charge-discharge experiments). The different PVDF-contents were: 2%, 4%, 10%, 14%, 21% and 46%. The capacitive bioanode with 21% of PVDF-content was operating stable throughout all the experiments and it was able to store more charge than the other electrodes.

In **Chapter 5** we introduce the proof-of-principle of the capacitive fluidized anode. In this reactor concept, the anode has a large volume, which is filled with fluidizing granules. These granules are charged by the microorganisms in the fluidizing part of the reactor and they are discharged when contacting the current collector of the small discharge cell. After discharging the granules are transported back into the fluidizing charging column. In the proof-of-principle stage, we show that this reactor concept is already able to operate 3 times as efficient compared to the noncapacitive bioanodes.

**Chapter 6** describes the factors limiting the power output of Microbial Fuel Cells as we experienced them during this thesis.



## Chapter 2

# Capacitive Bioanodes enable renewable energy storage in Microbial Fuel Cells

This chapter has been published as:

Deeke, A., Sleutels, T. H. J. A., Hamelers, H. V. M., & Buisman, C. J. N. (2012).  
Capacitive Bioanodes Enable Renewable Energy Storage in Microbial Fuel  
Cells. *Environmental Science & Technology*, 46(6), 3554–3560.  
doi:10.1021/es204126r

## Abstract

We developed an integrated system for storage of renewable electricity in a microbial fuel cell (MFC). The system contained a capacitive electrode that was inserted in the anodic compartment of a MFC to form a capacitive bioanode. This capacitive bioanode was compared with a noncapacitive bioanode based on performance and storage capacity.

The performance and storage capacity were investigated during polarization curves and charge-discharge experiments. During polarization curves the capacitive electrode reached a maximum current density of  $1.02 \pm 0.04$  A/m<sup>2</sup>, whereas the noncapacitive electrode reached a current density output of only  $0.79 \pm 0.03$  A/m<sup>2</sup>. During the charge-discharge experiment with 5 minutes of charging and 20 min of discharging the capacitive electrode was able to store a total of 22,831 C/m<sup>2</sup>, whereas the noncapacitive electrode was only able to store 12,195 C/m<sup>2</sup>. Regarding the charge recovery of each electrode, the capacitive electrode was able to recover 52.9% more charge during each charge-discharge experiment compared with the noncapacitive electrode.

The capacitive electrode outperformed the noncapacitive electrode throughout each charge-discharge experiment. With a capacitive electrode it is possible to use the MFC simultaneously for production and storage of renewable electricity.

## 2.1 Introduction

Energy production from renewable energy sources receives more and more attention, because of the depletion of fossil fuels and the social urgency to decrease greenhouse gas emissions. Sun, wind and biomass are huge renewable energy sources, available all over the world<sup>25,26</sup>. However, when using sun and wind as sources, it becomes difficult to match supply and demand of energy because of fluctuation of both demand and availability of renewable resources (e.g. day/night cycle, variable wind speeds). This is especially true for energy in the form of electricity, as an electrical grid has low intrinsic storage capabilities. Electricity storage capacity is a good option to match electricity production with the demand of the electricity market<sup>20</sup>. The advantage of biomass as a source for renewable energy is its worldwide availability and storage possibility. Storage however, is only practical for biomass with high organic concentrations (low water volumes) because of the required storage capacity. An example for biomass with low organic concentrations (high water volumes) is wastewater. Wastewater is produced continuously all over the world, and even though it contains low organic concentrations it is an attractive source for sustainable electricity production from a Microbial Fuel Cell (MFC).

The MFC is a recently developed technology for production of renewable energy, which can efficiently convert organic matter from wastewater into electricity<sup>27</sup>. The mechanism of an MFC is described in<sup>28</sup>. To harvest more energy from the MFC; the MFC would either have to be disconnected at certain times or the storage of the produced electricity would be required. Production of electricity in an MFC would be more attractive with a possibility to store electricity. Hence, we investigated the use of a capacitive bioanode in an MFC as storage option for renewable energy from wastewater. Electrochemical capacitors (ECs) are most widely used capacitors to store electricity. ECs consist of two electrodes that are separated by a spacer

material and an electrolyte. In an EC, electricity is stored as charge at the electrical double layer interphase between electrode and electrolyte<sup>29</sup>.

Dewan<sup>24</sup> et al. performed a study on the use of a MFC with and without an external capacitor. The MFC was continuously operated when working without external capacitor and it was operated in a batch-mode with external capacitor. This study showed that more energy could be harvested when the MFC was operated with external capacitor. Another study on the use of external capacitors with an MFC has been performed by Kim<sup>30</sup> et al.. They used 4 MFCs and 8 capacitors to build a stack. The capacitors were charged in parallel and discharged in series. They also observed an increase in the peak power production of the MFCs when used with a capacitor. Use of an internal capacitor in an MFC however has not been tested before.

Goal of this research is the integration of a capacitive electrode with the bioanode. Such an integrated system would not require the use of an external capacitor. Microorganisms are expected to grow on the capacitive electrode and thereby to transfer the produced electrons into the capacitive electrode.

In terms of costs and material use, the integrated system has advantages compared to a system with an external capacitor, because there is no need for an additional spacer or electrolyte. The membrane, which is already present in the MFC to separate anodic and cathodic compartment, is used as a separator (spacer) for the capacitor. The wastewater, which is used to feed the microorganisms in the anodic compartment, is used as electrolyte. Furthermore, this integrated system requires only one electrode for the capacitor.

The feasibility to grow microorganisms on the capacitive electrode was studied and performance and energy storage were compared with performance and energy storage of a noncapacitive bioanode.

## 2.2 Materials and methods

### 2.2.1 Electrochemical cell setup.

Four identical cells, which were similar to cells used in recent published work<sup>31</sup>, were used in our experiments. The two compartments were separated by a cation exchange membrane. The electrode of each compartment was situated opposite of the membrane. A plain graphite plate electrode (Müller & Rössner GmbH, Troisdorf, Germany) was used as cathode. As anode, two different types of electrode were used; a noncapacitive (plain graphite plate) electrode and a capacitive electrode, consisting of a current collector (plain graphite plate electrode) coated with a capacitive layer. Anode, cathode and membrane had a projected surface area of 22 cm<sup>2</sup>.

### 2.2.2 Electrode preparation and analysis.

The capacitive layer that was coated on the current collector consisted of a mixture of activated carbon powder and a polymer solution. The polymer solution was a mixture of NMP (N-methyl-2-pyrrolidone, Boom, Meppel, The Netherlands) and PVDF (Polyvinylidene fluoride, Kynar, Arkema, Amersfoort, The Netherlands). After mixing the two components, the mixture was kept in an oven at 50°C for at least 4 days, where it formed a homogeneous solution and was de-aerated. The polymer solution was placed in a ball mill grinder (PM 100, Retsch, Haan, Germany) together with activated carbon powder (DLC Super 30, Norit, Amersfoort, The Netherlands) and extra NMP, as solvent. Mixing was done at 450 RPM for 30 minutes to ensure homogeneity of the mixture. After grinding, the capacitive paint was kept in an oven at 50°C for 24 h for de-aeration.

Before coating the capacitive layer on the electrode, the current collector was roughened with sandpaper, rinsed with distilled water and blow-dried with pressurized air. Capacitive paint was coated on the current collector at a thickness

of 500  $\mu\text{m}$  using a casting knife (stainless steel, 500  $\mu\text{m}$ ). Finally, the coated current collector was placed in an oven at 50  $^{\circ}\text{C}$  for 48 h for drying.

A small fraction of the capacitive paint was coated on a glass plate at the same thickness of 500  $\mu\text{m}$  to investigate specific surface area. Gas-Adsorption-Analysis was carried out to determine the specific surface area ( $\text{m}^2/\text{g}$ ) using the BET-adsorption model according to<sup>32</sup>.

Atomic Force Microscope (NanoScope IIIa, Veeco, Santa Barbara, California) was used to determine the roughness of each electrode surface. The AFM - scan was performed on 2.5  $\text{mm}^2$  of each electrode surface. Pore-size distribution on the surface of each electrode was analyzed with a Scanning Electron Microscope (JEOL Technics Ltd., Tokyo, Japan). AFM-pictures and SEM-pictures were captured for three different positions on each electrode surface to get a representative overview.

### **2.2.3 Operation and Measurements.**

Catholyte of the MFCs consisted of 100 mM ferricyanide solution. Anolyte consisted of 10 mM sodium acetate solution and 10 mM phosphate buffer solution. Additional supplies fed to the anolyte were 10 mL/L of macronutrient solution containing 4.31 g/L  $\text{NH}_4\text{Cl}$ , 5.37 g/L  $\text{MgSO}_4 \cdot 7\text{H}_2\text{O}$  and 4.31 g/L  $\text{CaCl}_2 \cdot 2\text{H}_2\text{O}$ , 1mL/L of micronutrient solution and 1mL/L of vitamin solution as described in<sup>14</sup>. Anolyte was continuously supplied at an inflow rate of 1.3 mL/min. Both anolyte and catholyte were circulated over the respective compartments at a flow rate of 100mL/min. Anolyte was inoculated with effluent from another active MFC run on acetate<sup>10</sup>. Temperature of all cells was controlled at 30 $^{\circ}\text{C}$  using a water bath (K10, Thermo scientific, Geel, Belgium). Cells were operated at controlled anode potential with a potentiostat (N-stat, Ivium Technologies, Eindhoven, The Netherlands). Anode potential was set to -0.400 V (vs. Ag/AgCl+ 0.2V vs. NHE), Pro Sense, Oosterhout, The Netherlands) as optimal working potential (determined during earlier experiments) for the microorganisms on the anode<sup>33</sup>. The pH in the

anode compartment was constantly measured by a pH-electrode (Liquisys, Endress + Hauser, Naarden, The Netherlands). During MFC operation, voltage and current were constantly measured and anode potential was controlled unless stated otherwise. The cells were run for 150 days at a controlled potential of -0.400V. During the 150 days of operation, performance was analyzed on each cell by polarization curves and charge-discharge experiments. The polarization curves were measured at day 75, day 106 and at day 145 of the MFC operation, in between the polarization curves the charge-discharge experiments were measured.

All electrochemical measurements were conducted with the same potentiostat as indicated before. Polarization curves were performed to determine current output as a function of anode potential. During the polarization curve anode potential was varied in the range from -0.450 V to -0.250 V in steps of 0.050 V. The anode potential was kept at each value for 10 min to reach a stable current output. Stable current density for each anode potential was taken from the average of stable current output from the last minute at each potential.

During charge-discharge experiments, control of anode potential was alternated with open circuit conditions. Open circuit condition was used as the charging period for the cells. During the discharging period the cells were operated at a set anode potential of -0.300 V. This potential was chosen according to the highest current density from the noncapacitive electrode from polarization curves. For charge-discharge experiments, different sets of charge and discharge periods have been performed, which were consecutively repeated for 15 times. As a first charge-discharge experiment, 10 minutes (charging) and 20 minutes (discharging) was chosen and compared with 20 minutes (charging) and 10 minutes (discharging) to investigate whether the charging or discharging period needs to be longer. Afterwards, the charging period and the discharging period were varied. It was investigated, whether longer charging and discharging periods would influence the stable operation of the electrodes during the cycling experiments (open circuit

and control of the anode potential). For this purpose charging periods of 30 and 60 minutes were chosen and discharging periods of 60 minutes, 90 minutes and 120 minutes. All periods which were used for charging and discharging of the cells are in Table 2.1.

Table 2.1: Schedule for the charge-discharge experiments

		Charging Period (min)				
		5	10	20	30	60
Discharging Period (min)	10	x	nd	x	nd	nd
	20	x	x	nd	nd	nd
	60	nd	nd	nd	x	nd
	90	nd	nd	nd	nd	x
	120	nd	nd	nd	nd	x
	x	Determined				
nd	Not determined					

#### 2.2.4 Calculations.

During experiments, three situations can be distinguished: Steady State current output, charging and discharging. The origin of the current during each situation is further described in figure 1a. The measured current ( $i_m$  in A) is the current that flows from the anode to the cathode and therefore can be measured for both the noncapacitive and the capacitive electrode. The produced current ( $i_p$  in A) is

defined as current produced by the microorganisms and stored on the electrode during the charging period.

Steady state current output is reached during the last minute at each potential of the Polarization curves, where produced current is equal to measured current ( $i_p = i_m$ ).

During the charging period, when the electric circuit is open, measured current is zero and produced current is stored as charge on the capacitive electrode

$$i_m = 0; i_p = \frac{dQ_s}{dt} \quad (2.1)$$

, where  $Q_s$  is the stored charge (C).

During the discharge period, measured current is equal to produced current plus stored charge (see Figure 2.1b).

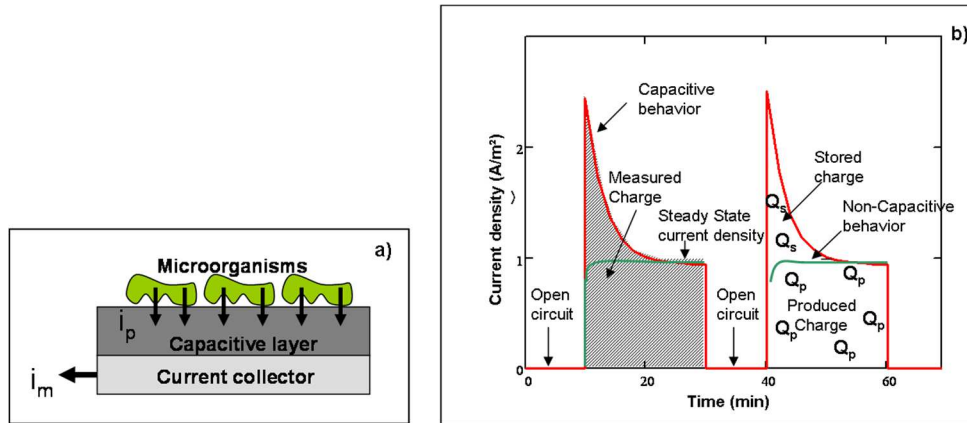


Figure 2.1 (a) Current distribution between microorganisms and the electrode, showing the origin of the measured and the produced current. (b) Theoretical discharge graph, giving the measured charge as shaded area underneath the current density graph. The measured charge can be split into the stored charge (area of the peak above the noncapacitive behavior line) and the produced charge (area underneath the noncapacitive behavior-line).

$$i_m = i_p + \frac{dQ_s}{dt} \quad (2.2)$$

Because it is impossible to distinguish between the amount of produced current and stored charge, further calculations are made to determine the amount of measured charge. Measured charge ( $Q_m$  in C) is the integral of the current curve from the charge-discharge experiment (shaded area in Figure 2.1b)

$$Q_m = \int_0^{t_o} i_m dt \quad (2.3a)$$

Substituting the measured current in (2.3a) leads to:

$$Q_m = \int_{t_c}^{t_o} (i_p + \frac{dQ_s}{dt}) dt \quad (2.3b)$$

$$Q_m = i_p(t_o - t_c) + \Delta Q_s \quad (2.3c)$$

where  $t_o$  is the overall time of the charge-discharge cycle (s) and  $t_c$  is the charging time (s). The expected charge is calculated as

$$Q_{cont,d} = i_s t_d \quad (2.4)$$

, where  $Q_{cont,d}$  is the expected charge (C),  $i_s$  is the steady state current (A) from the noncapacitive electrode taken from the polarization curves at an anode potential of -0.300 V and  $t_d$  is the discharge time ( $t_d = t_o - t_c$ ) (s).

To assess the effectiveness of each electrode the charge recovery ( $\eta_{rec}$  in C) is introduced:

$$\eta_{rec} = \frac{\sum Q_{m,k}}{n * Q_{cont,d,k}} \quad (2.5)$$

The charge recovery relates the measured charge from each experiment to the expected charge for each experiment.  $Q_{cont,d}$  is the expected charge (C),  $n$  is the number of cycles and  $\sum Q_{m,k}$  is the sum of the measured charge of each cycle (cumulative total charge) (C). Charge recovery can reach three different states: (a)

$\eta_{rec} \leq 1$ , (b)  $\eta_{rec} = 1$ , and (c)  $\eta_{rec} \geq 1$ . When charge recovery is smaller than 1,

measured charge is lower than the expected charge. When charge recovery is equal to 1, measured charge is equal to the expected charge and when charge recovery is bigger than 1, measured charge is bigger than the expected charge.

## **2.3 Results and discussion**

The difference in performance of the capacitive and noncapacitive electrode was determined using different techniques. First pore-size distribution was determined using SEM and AFM. Then, electrochemical properties were determined by recording potential scans and finally charge-discharge behavior of both electrodes was investigated.

### **2.3.1 Characterization of the capacitive electrode.**

Pore-size distribution was analyzed using AFM and SEM. SEM-pictures of the capacitive electrode are in Figure 2.2. Top view of the capacitive electrode is in Figure 2.2a and cross-sectional view of the capacitive electrode is in Figure 2b. Both figures show that carbon particles and polymer binder are well mixed. The SEM-pictures showed a pore-size distribution of 5  $\mu\text{m}$  on the electrode surface. The cross-sectional view showed that the depth of the pores of the capacitive electrode ranged from 5 to 10  $\mu\text{m}$ . The noncapacitive electrode had a pore-size distribution of 2  $\mu\text{m}$  on the electrode surface. AFM images confirm the typical pore-size distribution found in the SEM images. Pictures obtained from the AFM-Analysis are in the Appendix to Chapter 2 (p.120). The capacitive electrode was coated with 500  $\mu\text{m}$ , due to evaporation of the solvent during the drying process the electrode shrank down to a thickness of 220  $\mu\text{m}$ . BET-Analysis of the capacitive electrode revealed a specific surface area of 1081  $\text{m}^2/\text{g}$ . Both SEM-pictures and AFM-pictures show that the capacitive electrode has a rougher electrode surface than the noncapacitive electrode.

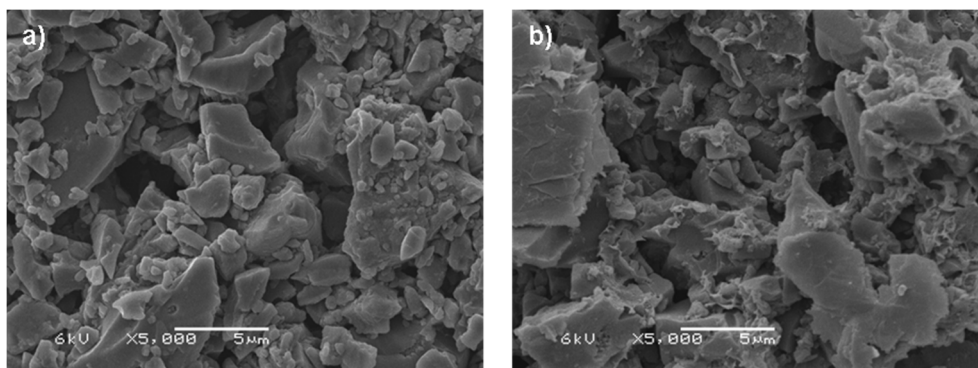


Figure 2.2: (a) SEM picture showing the top view of the capacitive electrode. (b) SEM-picture showing the cross-sectional view of the capacitive electrode.

### 2.3.2 Electrochemical characterization of the biofilm.

Electrochemical characterization of the biofilm was done by polarization curves. The obtained polarization curves are in Figure 2.3. The noncapacitive electrode reached a maximum current density of  $0.79 \pm 0.03 \text{ A/m}^2$  at an anode potential of  $-0.300 \text{ V}$ . Even though the anode potential was further increased to  $-0.250 \text{ V}$ , the current density decreased to  $0.77 \pm 0.03 \text{ A/m}^2$ . The capacitive electrode had a current density increase throughout the whole anode potential range. The capacitive electrode reached a maximum current density of  $1.02 \pm 0.04 \text{ A/m}^2$  at an anode potential of  $-0.250 \text{ V}$ . A negative current was observed for the capacitive electrode at an anode potential of  $-0.450 \text{ V}$  even after maintaining this potential for 20 min. The capacitive electrode performed better than the noncapacitive electrode in most of the applied anode potentials. This difference in performance could be due to the difference in roughness of the electrodes, because the surface of the capacitive electrode has an increased roughness compared with the noncapacitive electrode (see Characterization of the Capacitive Electrode).

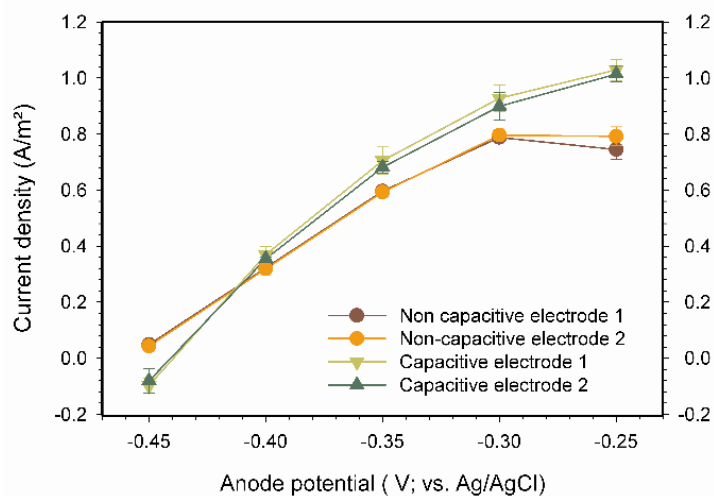


Figure 2.3: Polarization curves obtained from the different electrodes in an anode potential range of -0.450 V to -0.250 V. There are clear differences in performance between the noncapacitive electrode and the capacitive electrode. The capacitive electrode reached a higher current density output of up to 1.02 A/m<sup>2</sup> compared with the current density output of 0.79 A/m<sup>2</sup> of the noncapacitive electrode.

### 2.3.3 Charge-Discharge experiments.

During charge-discharge experiments the cells were controlled at open circuit, alternated with control of the anode potential at -0.300 V. The electrodes are charged when the electric circuit is open and they are discharged when the anode potential is controlled. This charging-discharging was done at 12 different intervals to investigate possible time effects (table 1). The potential behavior and the current density behavior for the charging (10 minutes) and discharging (20 minutes) are in Figure 2.4a and Figure 2.4b. These figures are representative for all charge-discharge experiments. Figures for the other charge-discharge experiments are available in the Appendix to Chapter 2.

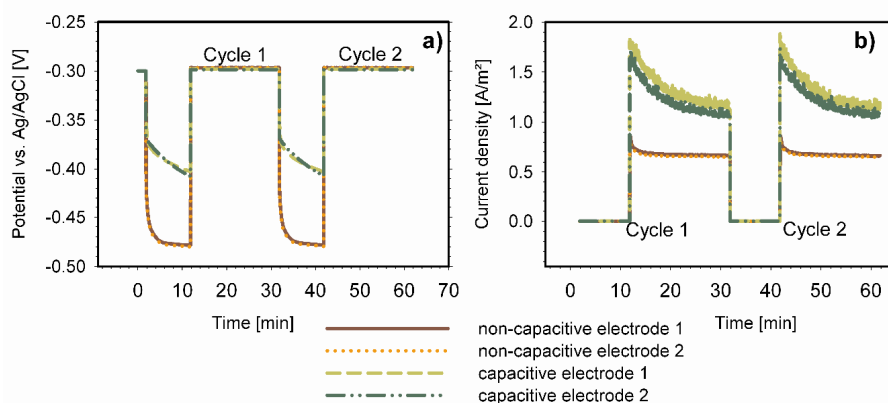


Figure 2.4 Typical potential (a) and current density (b) behavior for two cycles of a charge-discharge experiment with 10 minutes of charging and 20 minutes of discharging.

### 2.3.3.1 Potential behavior.

The typical potential behavior of the charge-discharge experiment is in Figure 2.4 a. After the electric circuit was opened the initial potential drop from the noncapacitive electrode was around 0.110 V, whereas the initial potential drop from the capacitive electrode was 0.070 V. The potential from the noncapacitive electrode decreased to the final value of -0.480V, the open circuit potential. The Potential from the capacitive electrode dropped to a potential value of around -0.410V till the charging period ended. The potential from the capacitive electrode dropped slower than the potential from the noncapacitive electrode. The noncapacitive electrode showed an immediate potential drop to potentials lower than -0.450 V. Because this potential is comparable to open circuit potential, this potential implies that the produced current is zero. Looking at the Polarization curves confirms that the produced current at these potentials is zero. In case of the capacitive electrode the overall potential drop was smaller than that of the noncapacitive electrode, therefore the produced current  $i_p$  was bigger then zero. This difference in potential behavior is due to the fact that electrons produced by

the microorganisms are stored in the capacitive electrode. The capacitive electrode has a rougher surface than the noncapacitive electrode. Through this rougher surface the double-layer capacitance of the capacitive electrode is increased compared with the double-layer capacitance of the noncapacitive electrode. The capacitive electrode therefore reaches a different final potential compared with the noncapacitive electrode. The smaller potential drop behavior of the capacitive electrode compared with the noncapacitive electrode demonstrated that the capacitive electrode is able to store charge.

#### 2.3.3.2 Current density behavior.

The typical current density behavior of the noncapacitive and capacitive electrode is in Figure 2.4 b. All electrodes had a peak in current density after the electric circuit was closed. After this peak, current density of each electrode decreased towards a stable current density. The height of this peak is related to the amount of charge that was stored according to equation (2.3). Presence of a peak in the current density indicates that more charge was produced during the charging period, than during continuous operation.

The noncapacitive electrode had a peak of  $0.9 \text{ A/m}^2$  throughout each time interval. The height of the peak in current density of the noncapacitive electrode was in accordance with the potential drop during the charging period. The noncapacitive electrode had a quick drop in potential, which showed that only a small amount of charge was stored. Afterwards the current density converged towards a stable value of  $0.7 \text{ A/m}^2$  during each interval. The capacitive electrode had a higher peak current density of  $1.7 \text{ A/m}^2$  during each interval compared to the noncapacitive electrode. This indicates that the amount of stored charge was larger for the capacitive electrode compared with the noncapacitive electrode. Stable current density output of the capacitive electrode was  $1.15 \text{ A/m}^2$ .

The noncapacitive electrode reached the stable current density output which was comparable with the polarization curves in figure 3. Only a small amount of charge

was stored on the noncapacitive electrode. Uría<sup>34</sup> et al. showed that a small amount of charge can be stored in the biofilm, which might be happening in case of the noncapacitive electrode.

The capacitive electrode performed better during the charge-discharge experiments (1.15 A/m<sup>2</sup>) than it was expected from the polarization curves (0.93 A/m<sup>2</sup>). Part of this better performance can be linked to the rougher surface of the capacitive electrode. But another part of performance increase might be explained by the fact that storage of charge occurred. During the charging period electrons are stored inside the electrode and the produced protons accumulate in the biofilm. During the discharging period the electrons are released from the anode to the cathode and the accumulated protons are transported from the biofilm to the bulk solution. Since the protons are most likely transported out of the biofilm through the protonation of the conjugate base of the buffer<sup>35</sup>, immediate release of all stored protons (at closure of the electric circuit) would lead to an increase in buffer-capacity at the biofilm and this would enable a high current density output.

Performance of each electrode was also compared according to average current density reached during cycling between open electric circuit and potential control. This average current density during the cycled experiment (open circuit + closed circuit) was compared with the current density of constant operation. The current density value for constant operation was taken from the polarization curves at an anode potential of -0.300 V. The noncapacitive electrode reached a current density of 0.79 A/m<sup>2</sup> during the polarization curves. During the charge-discharge experiment the average current density was 0.41 A/m<sup>2</sup>, this was 0.38 A/m<sup>2</sup> lower than during constant operation. The capacitive electrode reached a current density of 0.93 A/m<sup>2</sup> during the polarization curves. During the charge-discharge experiments the average current density was 0.76 A/m<sup>2</sup>, this was only 0.17 A/m<sup>2</sup> lower than during continuous operation. This shows that an internal capacitor inside an MFC improves the relative performance compared with an MFC without

internal storage capacity at discontinuous operation, which is in accordance with the work by Dewan<sup>24</sup> et. al.

The capacitive electrode was able to produce 0.2 kWh/g (of activated carbon powder), which is comparable to other electrochemical capacitors<sup>23</sup>. This performance might be improved by choosing for a different PVDF-solution or a different activated carbon powder. Also the thickness of the capacitive electrode, which was casted with 500  $\mu\text{m}$ , might have an influence on its performance.

### 2.3.4 Cumulative Total Charge.

Cumulative total charge during each experimental interval was calculated according to equation (2.3) to gain further insights into storage capacity, stability and time effects of each electrode. The graph of cumulative total charge is in Figure 2.5a and b.

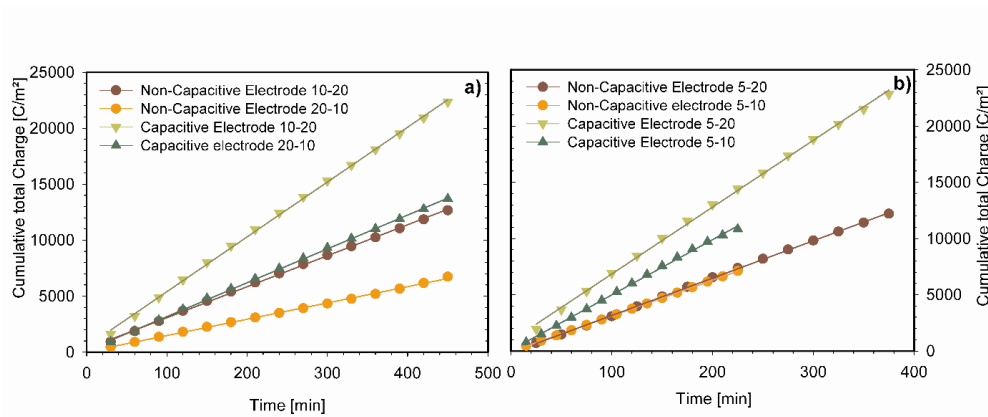


Figure 2.5: (a) the cumulative total charge from the charge-discharge experiments, with a charging time of 10 minutes and discharging time of 20 minutes, is compared with the charge-discharge experiments, with a charging time of 20 minutes and a discharging time of 10. (b) The cumulative total charge from the charge-discharge experiments, with 5 minutes of charging time and 20 minutes of discharging time, is compared with the charge-discharge experiments, with 5 minutes of charging time and 10 minutes of discharging time.

Under cycling conditions (open electric circuit and control of the anode potential) the stable operation of each electrode was tested. Therefore each defined charge-discharge cycle has been repeated consecutively 15 times. The slope of each graph

in Figure 2.5a and b represents the amount of measured charge for each single charge-discharge cycle. The amount of measured charge remained stable over each charge-discharge experiment for both electrodes; hence the noncapacitive and the capacitive bioanode are both able to cope with the cycling.

The effect of charging time and discharging time on the amount of cumulative total charge was investigated by performing experiments with different time settings. During the first set of charge-discharge experiments it was investigated, whether the charging or the discharging of the electrode would take longer. The graphs of the cumulative total charge in Figure 2.5 reveal that the discharging of the electrode takes longer than the charging. The discharging process of the electrodes is slower, than the charging process. Therefore a long discharge time is required to enable the electrodes to release all the charge that was produced during the preceding charging period. Furthermore these experiments showed that the capacitive electrode is able to produce more charge, than the noncapacitive electrode.

After these shorter charge-discharge experiments, the charging and discharging times have been elongated in further experiments. The charging time was elongated up to 60 minutes and the discharging time up to 120 minutes. This elongation of the discharging times has been done to test, whether the MFC can be used as a system for distributed energy generation. Schoenung<sup>36</sup> et al. defined a discharge time range of 0.5h till 4h as requirement for a suitable distributed energy generation system. A distributed energy generation system reaching this discharge time ranges can be used in the existing electrical grids for peaks in electricity requirement and load leveling. In Table 2.2 is the comparison of the cumulative total charge for all experiments.

Table 2.2 Cumulative total charge of each experiment for the noncapacitive and the capacitive electrode.

Experiment		10-20	20-10	5-20	5-10	30-60	60-90	60-120	
		min	min	min	min	min	min	min	
<b>Non-capacitive Electrode</b>		$Q_m(C/m^2)$	12665	6739	12195	7112	33743	59673	80895
<b>Capacitive Electrode</b>		$Q_m(C/m^2)$	22345	13688	22831	10819	56809	79750	128160

The cumulative total charge in table 2 shows that the capacitive electrode was able to produce more charge than the noncapacitive electrode during each charge-discharge experiment. The graphs of the cumulative total charge for these experiments can be found in the Appendix to Chapter 2.

The comparison of the ability to store charge of the noncapacitive electrode and the capacitive electrode was quantified through the charge recovery according to equation (2.4). The charge recovery is in Table 2.3.

Table 2.3 Charge recovery for the noncapacitive electrode and the capacitive electrode during each charge-discharge experiment.

Experiment		10-20	20-10	5-20	5-10	30-60	60-90	60-120	Average	
		min	min	min	min	min	min	min		
<b>Non-capacitive Electrode</b>		$\eta_{rec}$	0.870	0.874	0.894	0.368	0.791	0.933	0.948	0.811
<b>Capacitive Electrode</b>		$\eta_{rec}$	1.571	1.925	1.606	1.522	1.332	1.246	1.502	1.529

The charge recovery of the noncapacitive electrode was lower than 1 for most of the charge-discharge experiments. Thus, the measured charge of the noncapacitive electrode is lower than the expected charge. The charge recovery shows that in average the noncapacitive electrode produced 18.9% less charge than expected. During the charge-discharge experiment with 5 minutes of charging and 10 minutes of discharging the noncapacitive electrode performed less than the average and achieved a charge recovery of only 37%. In this experiment, the open circuit condition is held for one third of the whole charge-discharge cycle. The microorganisms delivered the electrons to the electrode with some delay after the electric circuit was closed; this caused the small charge recovery. In the charge-discharge experiments with 60 minutes (charging) and 90 minutes and 120 minutes (discharging) the noncapacitive electrode is reaching charge recoveries which are close to 1. This good performance could be due to the long working periods at the set anode potential. The electrodes are able to reach stable conditions.

The capacitive electrode performed better during all experiments and has higher values for the charge recovery compared with the noncapacitive electrode. For all experiments the charge recovery is higher than 1. In average the capacitive electrode produced 52.9% more charge than expected. From this 52.9% charge recovery around 18% can be assigned to improved performance of the capacitive electrode already measured during the polarization curves, where the noncapacitive electrode only achieved a current density of 0.79 A/m<sup>2</sup> and the capacitive electrode achieved 0.93 A/m<sup>2</sup>. The remaining 35% of improved charge recovery are due to actual storage of charge taking place in the capacitive electrode as indicated in Figure 2.1b. This indicates that the integrated storage system with the capacitive electrode inserted into the anode compartment of an MFC is successful.

### **2.3.5 Perspectives.**

A system consisting of a capacitive electrode inside of an MFC was compared to a system with a noncapacitive electrode. The capacitive system outperformed the noncapacitive system throughout each experiment. The capacitive electrode enabled the on-demand release of stored electrons. With the capacitive electrode we already have managed to receive 0.2 kWh/g (of activated carbon powder). This amount of electricity storage can be improved in the future by changing composition and thickness of the capacitive electrode. Also charging and discharging periods need to be further improved to reach the required discharging time of 4 hours for the distributed energy generation.

With a capacitive electrode it is possible to use the microbial fuel cell simultaneously for production and storage of renewable energy. This offers new possibilities for application of the MFC.

### **Acknowledgements**

This work was performed in the TTIW-cooperation framework of Wetsus, Centre of Excellence for Sustainable Water Technology ([www.wetsus.nl](http://www.wetsus.nl)). Wetsus is funded by the Dutch Ministry of Economic Affairs, the European Union European Regional Development Fund, the Province of Fryslân, the city of Leeuwarden and by the EZ-KOMPAS Program of the “Samenwerkingsverband Noord-Nederland”. The authors like to thank the participants of the research theme “Bio-energy” for the fruitful discussions and their financial support. Special thanks go out to Annemiek ter Heijne and Philipp Kuntke for critical reading of this paper and to Michel Saakes for the support in the lab.



## Chapter 3

# Influence of the thickness of the capacitive layer on the performance of bioanodes in Microbial Fuel Cells

This chapter has been published as:

Deeke, A., Sleutels, T. H. J. A., Heijne, A. Ter, Hamelers, H. V. M., & Buisman, C. J. N. (2013). Influence of the thickness of the capacitive layer on the performance of bioanodes in Microbial Fuel Cells. *Journal of Power Sources*, 243(0), 611-616. doi:<http://dx.doi.org/10.1016/j.jpowsour.2013.05.195>

## Abstract

Earlier it was shown, that it is possible to operate a Microbial Fuel Cell with an integrated capacitive bioanode with a thickness of 0.5 mm and thereby to increase the power output. The integrated capacitive bioanode enabled storage of electricity produced by microorganisms directly inside an MFC. To increase the performance of this integrated storage system even more; the thickness of the capacitive electrode was varied: 0.2 mm, 0.5 mm and 1.5 mm. Each of these capacitive electrodes was tested in the MFC setup during polarization curves and charge-discharge experiments for the steady-state current density and the maximum charge recovery.

The capacitive electrode with a thickness of 0.2 mm outperformed the other electrodes in all experiments: it reached a maximum current density of  $2.53 \text{ Am}^{-2}$  during polarization curves, and was able to store a cumulative total charge of  $96013 \text{ Cm}^{-2}$  during charge-discharge experiments. The highest relative charge recovery for this electrode was 1.4, which means that 40 % more current can be gained from this capacitive electrode during intermittent operation compared to continuous operation of a noncapacitive electrode. Surprisingly it was possible to increase the performance of the MFC through decrease of the thickness of the capacitive electrode.

### 3.1 Introduction

Energy production from renewable sources receives more and more attention due to the depletion of fossil fuels and the increasing pollution of the atmosphere. Most of this attention is focused on solar and wind energy<sup>25</sup>. But there are also an increasing number of researchers looking at possibilities to use biomass as a renewable energy source<sup>26</sup>. One type of biomass, which is not yet used in the most efficient way, is wastewater. So far, most wastewater treatment plants spend energy to remove the organic compounds contained in wastewater. But recently there has been developed a more efficient technology: the Microbial Fuel Cell (MFC). In MFCs the organic compounds of the wastewater are directly converted into electricity<sup>27</sup>. An MFC consists of an anode compartment and a cathode compartment, which are usually separated by a membrane<sup>19</sup>. Both compartments contain an electrode; the anode and cathode. On the anode grow electrochemically active microorganisms which convert the organic matter from wastewater into protons, electrons and carbon dioxide. Positively charged ions migrate through the membrane (in case of a cation exchange membrane) to the cathodic compartment and the electrons are transported through an external circuit to the cathode. At this cathode the protons and electrons react with oxygen to form water<sup>28</sup>.

The MFC is thereby presenting a way of simultaneously treating wastewater and producing electricity. However, the wastewater needs to be treated continuously and the energy which is produced by the MFC might not be consumed continuously. To match the production and demand of this electricity, storage of the electricity would be necessary<sup>20</sup>. Two different techniques have been investigated for the storage of electricity from MFCs: external and internal capacitors<sup>24,30,37-39</sup>. Dewan<sup>24</sup> et al. and Kim<sup>30</sup> et al., Grondin<sup>37</sup> et al., Liang<sup>38</sup> et al. and Hatzell<sup>39</sup> et al. showed that using a Bio Electrochemical System (BES) with an external capacitor can improve the power output compared to continuous

operation of the BES without capacitor. Another way of increasing the power output of MFCs was shown by Deeke<sup>40</sup> et al.. They operated the MFC with a capacitor integrated in the anode compartment, and also found an increase in power output. Until now, however, it is not known which parameters determine the performance of the MFC with a capacitor.

Several studies in the field of electricity storage in capacitors have shown that the specific capacitance is, amongst others, depending on the thickness of the active material of the electrodes<sup>41,42</sup>. Emmenegger<sup>41</sup> et al. compared the specific capacitance of electrodes used in electrochemical double-layer capacitors, which were made of Activated Carbon Powder (ACP) in 6 different thicknesses varying from 0.1mm to 0.8mm. They found an increase in the specific capacitance, when increasing the thickness of the active material. Tsay<sup>42</sup> et al. tested four different thicknesses for their supercapacitor electrodes: 0.05mm, 0.1mm, 0.2mm and 0.3mm. They found an optimum in the specific capacitance for their electrodes at a thickness of 0.1mm.

To further improve the performance of MFCs with an internal capacitive bioanode, we compared three different thicknesses for the capacitive layers: 0.2mm, 0.5mm and 1.5mm. The performance of the layers with different thickness was analyzed using polarization curves and charge-discharge experiments to see the steady-state current density and the maximum charge recovery in a two chamber MFC.

## **3.2 Materials and methods**

### **3.2.1 Electrochemical cell setup.**

In this study, six identical cells were used to characterize the performance of the different capacitive layers. The six cells were similar to the ones used in the proof of concept study of the internal capacitive bioanode<sup>40</sup>. The cells consisted of two flow channels of each 33 mL for the anodic and cathodic compartment. The flow channels were separated by a Cation Exchange Membrane (Ralex, Mega, Straz pod

Ralskem, Czech Republic) and on both sides of the membrane the electrodes (Müller & Rössner GmbH, Troisdorf, Germany) were placed. The cathode electrode was a noncapacitive (plain graphite plate) electrode and the anode was a current collector (plain graphite plate) covered with the capacitive layer. Anode, cathode and membrane had a projected surface area of 22cm<sup>2</sup> each.

### **3.2.2 Electrode Preparation.**

The capacitive layers were prepared by mixing a pre-mixed PVDF-solution; 200mL NMP (N-methyl-2-pyrrolidone, Boom, Meppel, The Netherlands) and 44.1 g PVDF (Polyvinylidene fluoride 2, Kynar, Arkema, Amersfoort, The Netherlands) with 25.2 g of Activated Carbon Powder (ACP, DLC Super 30, Norit, Amersfoort, The Netherlands). A scheme of the preparation of the capacitive electrodes is in Figure 3.1.

This solution was placed in a ball-mill grinder (PM 100, Retsch, Haan, Germany) and mixed at 450 rpm for 30 minutes. Afterwards the capacitive paint was kept in an oven for 24 h at 50 °C for de-aeration. The capacitive paint was casted in three different thicknesses on the current collector using a casting knife. The thicknesses of the tested electrodes were, 0.2mm, 0.5 mm and 1.5 mm. Each electrode was casted in triplicate.

Each capacitive electrode was analyzed using several techniques: BET-Analysis, AFM and SEM pictures. The specific surface area of the capacitive electrodes was determined using the BET-Analysis<sup>32</sup>. The roughness of each capacitive electrode was determined using atomic force microscope (AFM, Nanoscope IIIa, Veeco, Santa Barbara, CA, USA). The AFM-scan was performed on 1mm<sup>2</sup> of the surface area. The roughness of the scanned surface area was determined using the AFM<sup>43</sup> as the arithmetic average  $R_a$  of the absolute roughness values of the surface of each capacitive layer. The pore-size distribution on the surface was determined using SEM (Scanning Electron Microscope, JEOL Technics Ltd., Tokyo, Japan). AFM-

scans and SEM-pictures were taken on three different positions of each capacitive electrode to get a representative overview.

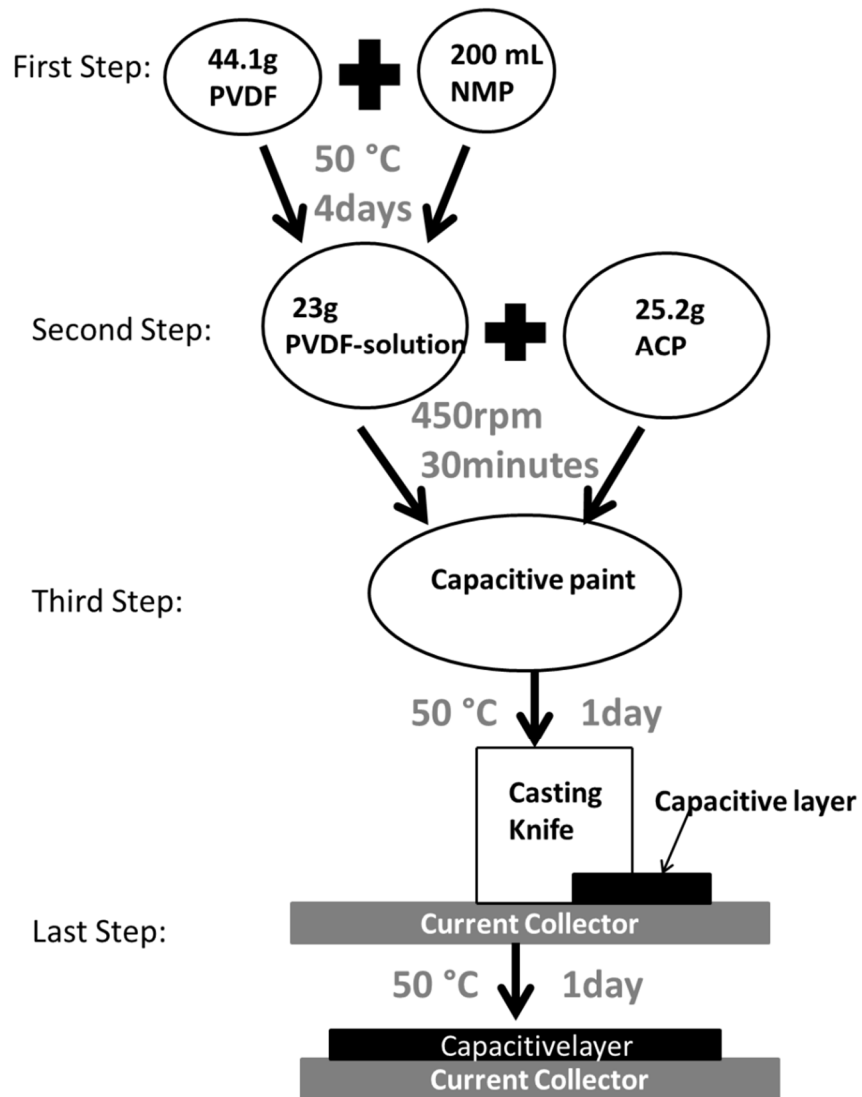


Figure 3.1: Preparation of the capacitive layers from the beginning till the end

### 3.2.3 Operation and Measurements.

The MFCs were fed with synthetic wastewater containing 10mM of sodium acetate and 10mM of phosphate buffer. New influent was supplied at a rate of 1.3 mL/min and recirculated over a storage vessel with a rate of 100 mL/min using peristaltic pumps (Master Flex, Cole Parmer, Vernon Hills, IL, USA). A Vitamin solution, Micro- and Macronutrients were added to the anolyte with 1mL/L, 1mL/L and 10mL/L. The composition of the Nutrient-solutions can be found in<sup>14</sup>. The catholyte was a 10mM potassiumferricyanide solution, which was supplied to the MFCs at a rate of 100 mL/min. The temperature of each cell was controlled at 30 °C with a water bath (K10, Thermo scientific, Geel, Belgium). The pH in the anode compartment was constantly measured using a pH- electrode (Liquisys, Endress + Hauser, Naarden, The Netherlands).

The cells were operated at a controlled anode potential with a potentiostat (N-stat, Ivium Technologies, Eindhoven, The Netherlands). The anode potential was set to -0.400 V (vs. Ag/AgCl+ 0.2V vs. NHE), Pro Sense, Oosterhout, The Netherlands)(demonstrated as an optimal working potential for the microorganisms during earlier research<sup>33</sup>) unless stated otherwise. Current and anode potential were measured constantly.

The cells were operated for 120 days, during these days of operation polarization curves and charge-discharge experiments were performed. All capacitive layers were tested in duplicate.

Polarization curves were performed to determine the maximum current density output of the capacitive electrodes. The polarization curves were recorded at day 32, 76 and 120 of operation. During the polarization curves the anode potential was varied from -0.450V to -0.250V in steps of 0.050V. Each potential was held for 10 min till the cell reached a stable current output. The current density output for each potential was taken from the average for the last minute at each potential.

During the charge-discharge experiments; periods of operation at open circuit conditions (charging) were alternated with periods of operation at a set anode potential (discharging) of -0.300V (this potential was chosen according to the maximum current density of the noncapacitive electrode<sup>40</sup>). The periods for charging and discharging were varied to determine the maximum charge capacity of the capacitive electrodes. The different charge and discharge periods which have been used are in Table 3.1.

Table 3.1: Charge and Discharge times (min) used during the experiments

<b>Ratio charging time [min] total experiment time [min]<sup>-1</sup></b>		
<b>0.5</b>	<b>0.67</b>	<b>various</b>
10 - 10	5 - 10	5 - 20
15 - 15	10 - 20	60 - 90
20 - 20	30 - 60	90 - 120
30 - 30	60 - 120	90 - 150
60 - 60	n.d.	120 - 180

n.d.: not determined

### 3.2.4 Calculations.

The current density was calculated from the measured current divided by the surface area of the anode as  $i=I/A$  in  $\text{Am}^{-2}$ .

To evaluate the performance of each capacitive electrode during the charge-discharge experiments the cumulative total charge was calculated. The cumulative total charge is represented by the surface area of the current density-curve of a charge-discharge experiment. Therefore the cumulative total charge can be calculated as

**Equation 3.1** 
$$Q_m = \int i_m dt$$

, where  $Q_m$  is the charge measured during the discharge period (measured charge) and  $i_m$  is the current measured during the discharge period. The measured charge consists of two different parts: the current which is produced and retrieved directly from the bio-electrode and the stored charge, which was delivered from the microorganisms to the capacitive electrode during the charging period. This means that the measured charge can also be expressed as;

**Equation 3.2** 
$$Q_m = i_p(t_o - t_c) + \Delta Q_s$$

, where  $i_p$  is the current produced by the microorganisms,  $t_o$  is the overall time of the charge-discharge experiment,  $t_c$  is the charging time and  $Q_s$  is the charge stored during the charging period.

To evaluate the efficiency of these capacitive electrodes the cumulative total charge of each experiment is related to the charge, which could have been extracted from a noncapacitive electrode during continuous operation. The charge for continuous operation is calculated according to;  $Q_{cont} = i_{nc} * t_o$ , where  $Q_{cont}$  is the charge of continuous operation,  $i_{nc}$  is the current measured for the noncapacitive electrode at an anode potential of -0.300 V (1.74 mA) and  $t_o$  is the overall charge-discharge time. Relating the measured charge to the continuous charge leads to the charge recovery according to:

**Equation 3.3** 
$$\eta_{rec} = Q_m * Q_{cont}^{-1}$$

When the charge recovery is larger than 1, it is more effective to operate the capacitive electrode in the charge-discharge mode, than the noncapacitive electrode in continuous mode. When it is equal to 1, than the charge-discharge operation of the capacitive electrode is just as effective as the continuous operation of the noncapacitive electrode. When the charge recovery is smaller than 1, it would have been more effective to operate a noncapacitive electrode in continuous mode.

### 3.3 Results and discussion

#### 3.3.1 Electrochemical characterization of the bioanode

The bioanode was characterized by recording a polarization curve at day 32, 76 and 120 for each of the six cells. For each capacitive layer, the average current density of two cells during these three polarization curves can be found in Figure 3.2. For each capacitive electrode, the current density increased throughout the whole range of measured anode potentials. The capacitive electrode with a thickness of 1.5mm reached a maximum current density of 1.86 Am<sup>-2</sup> at an anode potential of -0.250 V. The capacitive electrode with a thickness of 0.5 mm reached a maximum current density of 1.96 Am<sup>-2</sup> and overall the highest current density was achieved by the capacitive electrode with a thickness of 0.2 mm and its maximum current density was 2.53 Am<sup>-2</sup>. All capacitive bioanodes showed very similar performance between the duplicates and also in the beginning, middle and end of operation, what means that they are really stable in their current density output.

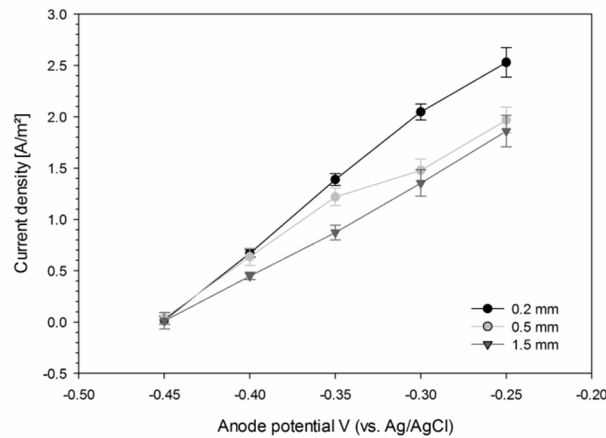


Figure 3.2: Polarization curves obtained for the different capacitive electrodes for the anode potential range from -0.450 V to -0.250 V. The thickness of the electrode has a clear influence on the performance of each capacitive electrode with 0.2mm showing the best performance.

### 3.3.2 Characterization of the capacitive layers

The capacitive electrodes were characterized for their surface properties using the BET-Analysis. Through the BET-Analysis the specific surface area of each electrode was determined. The results are in Table 3.2.

Table 3.2: Specific surface area for each capacitive electrode

Norit DLC Super 30			
	0.2 mm	0.5 mm	1.5 mm
Specific surface area [ $\text{m}^2\text{g}^{-1}$ ]	$942 \pm 16.2$	$795 \pm 20.4$	$742 \pm 37.0$
Surface roughness $R_a$ [nm]	67.2	57	52.9

The BET-results show that with increasing thickness, the specific surface area of the capacitive electrode decreases. With the AFM the roughness of these capacitive electrodes was determined. The roughness is shown as the arithmetic average  $R_a$  in Table 3.2. The roughness of the capacitive layers also decreased with increasing thickness. The SEM-pictures, which were taken from these capacitive layers showed an even distribution of ACP and PVDF throughout the whole layer. No differences between the three different capacitive layers could be detected from the SEM-pictures.

### 3.3.3 Charge-Discharge Experiments

During the charge-discharge experiments, a period with open circuit (charging) was alternated with a period in which the anode potential was controlled at an

anode potential of  $-0.300$  V (discharging). The periods for charging and discharging were varied in different ratios between charging and discharging, according to the times given in Table 3.1. Representative graphs for the cumulative total charge (charging (60 min) and discharging (60 min)), calculated according to Equation 3.2 are shown in Figure 3.3.

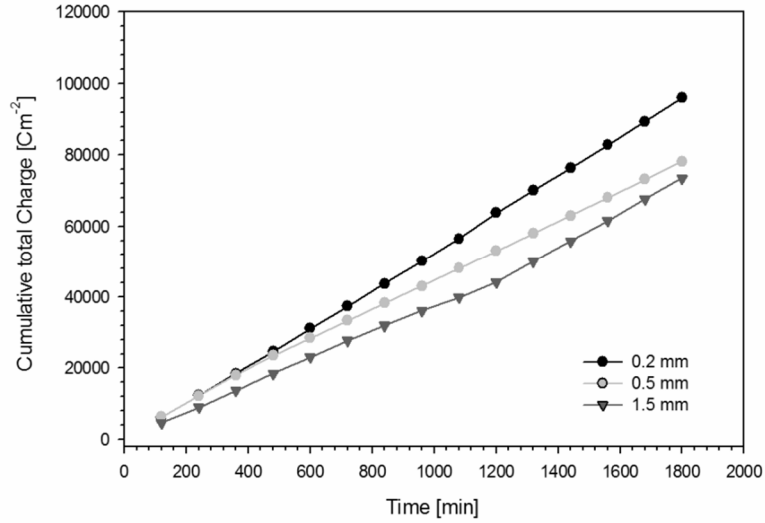


Figure 3.3: Cumulative Total Charge of the capacitive electrodes during the charge–discharge experiment (60–60min). This experiment shows the representative trend in behavior of the capacitive electrodes for all charge–discharge experiments.

Clearly, the capacitive electrodes performed very stable during the alternating conditions of the charge–discharge experiment: each charge/discharge step results in a similar increase in total charge, which is shown by a linear increase of the cumulative total charge in time. Furthermore, in accordance with the observations in the polarization curves, the capacitive electrode with a thickness of 0.2 mm performed best during this representative experiment. This capacitive electrode reached a cumulative total charge of  $96013$  Cm<sup>2</sup>. The capacitive electrode with a

thickness of 0.5 mm was the second best ( $78215 \text{ Cm}^{-2}$ ) and the capacitive electrode with a thickness of 1.5 mm was the least performing electrode ( $73481 \text{ Cm}^{-2}$ ).

### 3.3.4 Relative Charge Recovery

The relative charge recovery was calculated for each charge-discharge experiment according to Equation 3.3. This relative charge recovery indicates the performance of the capacitive electrode during one charge-discharge cycle compared to the performance of a noncapacitive electrode during continuous operation in the same time. The relative charge recovery for the charge-discharge experiments with a ratio of 0.5 for the charging time vs. total cycle time is shown in Figure 3.4.

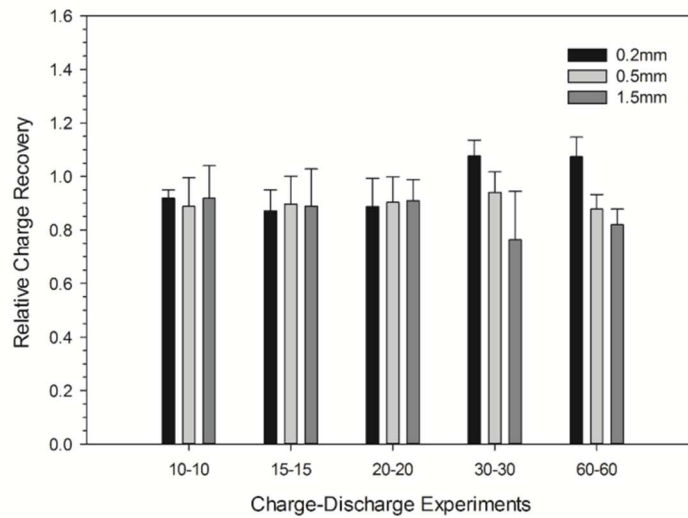


Figure 3.4: The relative charge recoveries for each capacitive electrode during the charge-discharge experiments with the 0.5 ratio of charging time compared to the total cycle time.

During the experiments with a shorter total cycle time, the capacitive electrode with a thickness of 1.5 mm had a higher relative charge recovery than the other capacitive electrodes. The relative charge recovery was close to 1, which means that it is as efficient to operate this capacitive electrode in the cycling mode with periods of an open electric circuit, than to operate a noncapacitive electrode

continuously. Furthermore, the relative charge recovery of the capacitive electrode with a thickness of 1.5mm decreased when the total cycle time increased. During the experiments with 20 minutes of charging and 20 minutes of discharging all the capacitive electrodes achieved the same relative charge recovery of 0.95. For the experiments with a longer total cycle time, the capacitive electrode with a thickness of 0.2mm was outperforming the other capacitive electrodes (and the continuous operation of a noncapacitive electrode as well) as its relative charge recovery was as high as 1.15. For the 0.2mm capacitive electrode, the relative charge recovery was increasing with increasing total experiment time. The relative charge recovery for the experiments with a ratio of charging time vs. total cycle time of 0.67 is in Figure 3.5.

The capacitive electrode with a thickness of 0.2 mm outperformed the other two electrodes throughout all these experiments, its relative charge recovery being larger than or equal to 1 throughout all these experiments. The highest relative charge recovery achieved by this electrode was 1.32. The relative charge recovery for the charge-discharge experiments with various ratios between charging and total cycle time is shown in Figure 3.6.

During all these experiments the capacitive electrode with a thickness of 0.2 mm again outperformed the other two electrodes, its relative charge recovery being larger than 1 during all these experiments. The maximum relative charge recovery was 1.35.

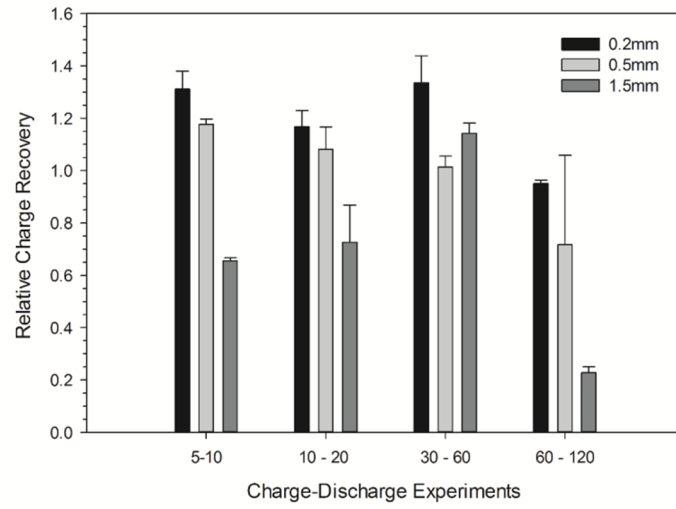


Figure 3.5: The relative charge recovery of the capacitive electrodes during the charge-discharge Experiments with the ratio of 0.67 for charging time compared to the total cycle time.

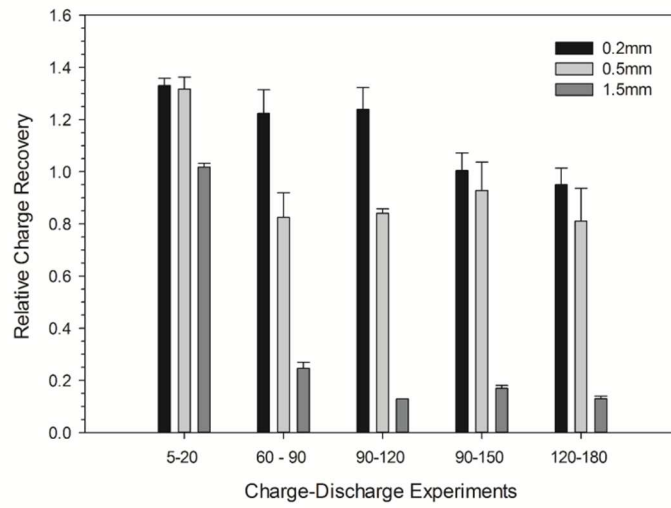


Figure 3.6: The relative charge recovery of the capacitive electrodes during the charge-discharge experiments with various ratios of charging time compared to total cycle time.

### 3.3.5 Discussion

The effect of the thickness of the capacitive electrode on bioanode performance was determined during polarization curves and charge-discharge experiments. The capacitive electrodes had thicknesses of 0.2 mm, 0.5 mm and 1.5 mm. It was found that the electrode thickness clearly affected bioanode performance. During the polarization curves, the capacitive electrode with a thickness of 0.2 mm performed better than the other two thicker capacitive electrodes. Interestingly, performance decreased with increasing thickness of the capacitive layer, which is different from literature<sup>41</sup> where they found an increase in performance with increasing thickness of the electrode. The same relationship was found for the specific surface area of the capacitive electrodes in the BET-Analysis and for the average roughness of the capacitive layer surface in the AFM-pictures. The specific surface area decreased with increasing thickness of the capacitive electrode, giving the highest specific surface area of  $942 \text{ m}^2\text{g}^{-1}$  and the highest roughness of 67.2 nm for the capacitive electrode with a thickness of 0.2 mm. Therefore, it can be expected that the capacitive electrode with 0.2 mm thickness is the most efficient, since a higher specific surface area and a rougher surface structure offers more space for the growth of microorganisms. This is in accordance with the polarization curves (Figure 3.2), where the capacitive electrode with a thickness of 0.2mm achieved the highest current density.

During charge-discharge experiments and their related relative charge recoveries part of the difference can be related to the difference in specific surface area, although some small fluctuations can be seen in Figure 3.4, Figure 3.5 and Figure 3.6. The part of the difference in performance, which cannot be related to the specific surface area, might be due to the difference in internal resistance in the capacitive electrodes. It is expected that with increasing thickness of the capacitive layer the transport resistance (resistance for transport of ions through the pores) is

increasing<sup>10</sup>. Therefore the ions are transported much easier through the capacitive layer with a thickness of 0.2mm compared to the capacitive layer with a thickness of 1.5mm. This might be the reason why the capacitive electrode with a thickness of 1.5mm is achieving lower current densities during the long charge-discharge cycles compared to the continuous operation in the polarization curves. The capacitive electrode with a thickness of 1.5 mm experienced some instability in the performance during the long charge-discharge cycles. With increasing charge-discharge cycle times this effect got stronger which is also reflected in the relative charge recovery of this electrode which was lower (see Figure 3.5 and Figure 3.6) than during shorter experiment cycle times.

The capacitive electrode with a thickness of 0.5 mm performed stable throughout both the polarization curves and the charge-discharge experiments. It was the most stable operating electrode. The capacitive electrode with a thickness of 0.2 mm performed best throughout most of the experiments, but its performance was fluctuating (see Figure 3.6). Overall, during most of the charge-discharge experiments, the capacitive electrode with a thickness of 0.2 mm achieved the best relative charge recovery. The achieved relative charge recoveries were close to or larger than 1, which means that, depending on the charge-discharge cycling time, the 0.2 mm capacitive electrode produced more charge than the noncapacitive electrode at continuous operation.

The highest achieved relative charge recovery was 1.4, meaning a 40% better performance compared to the noncapacitive electrode. In the previous study<sup>40</sup> the charge recovery was 52% higher than the noncapacitive electrode. But in that study the measured charge ( $Q_m$ ) was only related to the charge expected from the noncapacitive electrode during the discharging period  $t_d$  and not from the total experimental time  $t_o$  (see equation 2.3c). Recalculating the earlier found charge recovery increase of 52% to the relative charge recovery, would lead to an increase

of only 4%. Therefore the performance of the capacitive electrode has been increased by 36%, by decreasing its thickness from 0.5mm to 0.2mm.

### **3.4 Conclusion**

The influence of the thickness of the capacitive layer on the performance of these capacitive bioanodes was investigated in an MFC. Polarization curves, charge-discharge experiments and the relative charge recovery showed that the total current density and the amount of stored charge and therefore the performance increased in the order: capacitive layer 1.5mm < capacitive layer 0.5mm < capacitive layer 0.2mm. This increase in performance is similar to the increase in specific surface area, but this is not the only factor affecting the performance. It is assumed that the transport resistance is increasing with increasing thickness of the capacitive layer and therefore limiting the current output of the thicker electrodes. Further studies might deliver more insights on the factors which are affecting the power output of the capacitive bioanodes. Also variations in the properties of the capacitive layer, like the type of activated carbon powder and the type of binder, might lead to further increase in bioanode performance.

### **Acknowledgements**

This work was performed in the TTIW-cooperation framework of Wetsus, Centre of Excellence for Sustainable Water Technology ([www.wetsus.nl](http://www.wetsus.nl)). Wetsus is funded by the Dutch Ministry of Economic Affairs, the European Union European Regional Development Fund, the Province of Fryslân, the city of Leeuwarden and by the EZ-KOMPAS Program of the "Samenwerkingsverband Noord-Nederland". The authors like to thank the participants of the research theme "Resource Recovery" for the fruitful discussions and their financial support.

## Chapter 4

# **Influence of PVDF content on the performance of Capacitive Bioanodes in Microbial Fuel Cells**

This chapter is submitted as:

Deeke, A., Sleutels, T. H. J. A., Hamelers, H. V. M., & Buisman, C. J. N. (2014).  
Influence of PVDF content on the performance of Capacitive Bioanodes in  
Microbial Fuel Cells.

## Abstract

Capacitive bioanodes have been demonstrated as a promising anode in Microbial Fuel Cells (MFCs) for increased current density generation and electricity storage. A capacitive bioanode is produced by casting a mixture of activated carbon powder and the binder PVDF (Polyvinylidene fluoride) on a current collector. The influence of PVDF content of capacitive electrodes on bioanode performance was investigated. Six capacitive electrodes were made with PVDF contents of 2, 4, 10, 14, 21, and 46%. In the polarization curves, the capacitive electrode with the lowest PVDF content (2%) performed best, reaching a maximum current density of 2.4 A/m<sup>2</sup>. When expressed per gram of activated carbon, the electrode with the highest PVDF content of 46% reached the highest current density of 37 mA/g<sub>AC</sub>. In charge-discharge mode, the capacitive bioanode with 21% PVDF achieved the highest relative charge recovery of 1.8, producing 1.8 times more electricity than a non-capacitive electrode in continuous mode.

## 4.1 Introduction

Due to the depletion of fossil fuels, their extensive emissions of carbon dioxide and fine dust when combusted, and the consequences on the climate, more attention is devoted to the research on electricity production from renewable resources<sup>25</sup>. Biomass is one of these renewable resources<sup>26</sup>. Microbial Fuel Cells (MFCs) are a recently developed technology for the production of renewable electricity from biomass. In MFCs, organic material (biomass) from wastewater is oxidized at an electrode into protons, carbon dioxide and electrons by electrochemically active microorganisms<sup>28</sup>, while the electrons are used for a reduction reaction at the cathode. In this way, biomass is converted directly into electricity. The most standard way for operating MFCs is continuous harvesting of electricity; however, the electricity can also be harvested intermittently<sup>37</sup>. Intermittent harvesting can be done using a capacitor, which creates the possibility of electricity storage. Capacitors have been tested in combination with MFCs in two different ways so far: as a capacitor integrated in the anode itself<sup>40,44</sup>, and connected to the external circuit<sup>24,30,38,39</sup>.

Dewan et. al<sup>24</sup> operated an MFC with an external capacitor and they showed that with external storage and intermittent electricity harvesting, 111% more electricity was produced in the MFC compared to a system without a capacitor that continuously harvested electricity. Kim et al.<sup>30</sup> used several MFCs in series or in parallel connected to an external capacitor. They also found that more electricity was produced, in this case 29%, when harvested intermittently compared to continuously. With a capacitor integrated in the anode of an MFC, Deeke et al.<sup>40,44</sup> showed that 53% more electricity was produced in intermittent mode compared to continuous operation.

The bioanode with integrated capacitor of Deeke et al.<sup>40</sup> consisted of a current collector (anode) with a capacitive layer. This capacitive electrode was

produced by casting a mixture of the electrode material, 86% of activated carbon (AC) powder, and 14% of PVDF (Polyvinylidene fluoride) onto a current collector. Addition of PVDF to the activated carbon powder is necessary to bind the particles together and to attach the layer to the current collector. While PVDF is required as a binder, it has the disadvantage that it is a non-conductive material. By addition of PVDF to the activated carbon powder, part of the electrode surface area of the capacitive layer becomes non-conductive, reducing the conductive surface area available for the electrochemically active microorganisms. We therefore expect an increase in PVDF content to lead to a decrease in bioanode performance.

The objective of this study was to study the effect of PVDF content on the performance of capacitive bioanodes. Capacitive electrodes with 6 different PVDF contents were produced and tested: 2%, 4%, 10%, 14%, 21% and 46%. These capacitive electrodes have been analyzed for their specific surface area and charge-discharge behavior and for their performance as bioanodes in MFCs via polarization curves and charge-discharge experiments.

## **4.2 Experimental section**

### **4.2.1 Electrochemical cell setup.**

Six identical cells were used for this study. The cells were made of PMMA in a design described earlier<sup>31</sup>. The anode and cathode compartment each had a flow channel with a volume of 33ml. Anode and cathode compartment were separated by a proton exchange membrane (Ralex, Mega, Straz pod Ralskem, Czech Republic). The anode, cathode and membrane all had a projected surface area of 22cm<sup>2</sup>. The electrodes both were a plain graphite plate electrode (Müller & Rössner GmbH, Troisdorf, Germany). In case of the anode, the graphite plate electrode was used as a current collector and it was coated with a capacitive layer.

#### 4.2.2 Electrode preparation and analysis.

For the preparation of the capacitive layer first a PVDF-solution was made. This PVDF-solution was made of 44.1g of PVDF-powder (PVDF<sub>900</sub>, Polyvinylidene fluoride, Kynar, Arkema, Amersfoort, The Netherlands) and 200g of NMP (N-methyl-2-pyrrolidone, Boom, Meppel, The Netherlands). To achieve a homogeneous mixture the PVDF-solution was kept in an oven at 50°C for at least 4 days. The PVDF-solution was mixed in a ball mill grinder (PM 100, Retsch, Haan, Germany), together with the ACP (Activated Carbon Powder, DLC Super 50, Norit, *Amersfoort*, The Netherlands) and extra NMP, as a solvent, according to the recipe in <sup>40</sup>.

---

Table 4.1. Characteristics of the capacitive electrodes

---

<i>PVDF content (weight %)</i>	<i>Activated carbon powder (weight %)</i>	<i>Amount of acticated carbon (g<sub>AC</sub>/m<sup>2</sup>)</i>
2	98	156
4	96	155
10	90	153
14	86	152
21	79	137
46	54	107

---

After the mixing in the ball mill grinder, the paste was kept in an oven at 50°C for 24 hours for de-aeration. Afterwards the paste was coated onto the plain graphite plate at a thickness of 500µm with a casting knife (stainless steel,

500 $\mu$ m). The coated graphite plate was kept in an oven at 50°C for 2 days for drying. The characteristics of the capacitive electrodes are shown in Table 4.1. The amount of activated carbon on each electrode was determined by weighing the electrode before and after casting the activated layer on the current collector.

Surface properties of the capacitive electrodes. The surface properties of the electrodes were analyzed using Scanning Electron Microscopy (SEM, JEOL Technics Ltd., Tokyo, Japan) according to <sup>45,46</sup>, and gas-adsorption-analysis using the BET-model <sup>32</sup> according to <sup>47</sup>.

#### **4.2.3 Operation and Measurements**

Fresh anolyte was constantly supplied to the anodic compartment at a rate of 1.3 mL/min and it was recirculated over a storage vessel of 500 mL with a flow rate of 100 mL/min. The anolyte consisted of a 10mM acetate-solution supplied with additional vitamins, micro- and macronutrients according to<sup>48</sup>. A 10 mM Ferricyanide-solution, which was circulated at a flow rate of 100 mL/min, was used as the catholyte to avoid external influences on the anode performance. The temperature of the cells was kept constant at 30 °C using a water bath (K10, Thermo scientific, Geel, Belgium).

The MFCs were inoculated with effluent from another MFC operated on acetate<sup>49</sup>. After inoculation the cells were operated at a controlled anode potential of -0.400 V ((vs. Ag/AgCl, + 0.2V vs. NHE), Pro Sense, Oosterhout, The Netherlands). The anode potential was controlled by a potentiostat (n-stat, Ivium Technologies, Eindhoven, The Netherlands). The current and the anode potential were recorded constantly.

Each cell was operated in two runs. After the first run, the cell was opened and the capacitive bioanode was replaced with a new electrode with the same capacitive layer. All experiments were repeated in the second run. (Bio-

)Electrochemical characterization of the electrodes was done with three different methods: (i) polarization curves of anode potential vs current, (ii) charge-discharge-experiments and (iii) galvanostatic charge-discharge experiments on the capacitive electrode without biofilm. Polarization curves were measured three times during one run for both replicates. These three measurements occurred in a time period of about 2 weeks. Polarization curves were measured using a potential range from -0.45 V to -0.25 V in steps of 0.05 V. Each anode potential was kept constant for 10 minutes. The value for the current for each anode potential was calculated from the average current achieved during the last minute for each potential. Each potential thus had 6 data points (2 cells with 3 polarization curves). Charge-discharge experiments were performed to determine the storage capacity of each electrode. The charge-discharge experiments were performed by charging at open electric circuit (zero current) and discharging at -0.300V (vs Ag/AgCl), with different sets of charge and discharge times (Table 4.2).

Table 4.2. Sets of charge/discharge times used

<i>Charge:Discharge</i>	<i>Charge:Discharge</i>	<i>Charge:Discharge</i>
<i>1:1</i>	<i>1:2</i>	<i>other ratios</i>
10:10 min	5:10min	5:20 min
15:15 min	10:20 min	60:90 min
20:20 min	30:60 min	90:120 min
30:30 min	60:120 min	90:150 min
60:60 min		120:180 min

Prior to inoculation, the capacitance of each capacitive electrode (without biofilm) was evaluated using galvanostatic charge-discharge experiments. The galvanostatic charge-discharge experiments were performed at five different current densities according to <sup>50</sup>: 0.045A/m<sup>2</sup>, 0.45A/m<sup>2</sup>, 2.27A/m<sup>2</sup>, 4.54A/m<sup>2</sup> and 11.36A/m<sup>2</sup>. The capacitive electrodes were charged at each current density for 300s and then discharged at the same current density for 300s by reversing the current. Each experiment was performed in duplicate.

#### 4.2.4 Calculations

The current density was calculated from the current through;  $i = I/A$  in A/m<sup>2</sup>. From the current density in A/m<sup>2</sup> the current density in mA/g<sub>AC</sub> was calculated to be able to compare the different capacitive layers, through  $j = i/m$ , where  $m$  is the g<sub>AC</sub>/m<sup>2</sup> of each capacitive electrode. The measured charge  $Q_m$  (in C) was calculated as the integral of the area underneath the current density graph (mA/g<sub>AC</sub>) for each charge-discharge experiment in C/g<sub>AC</sub>. To evaluate the performance of each capacitive electrode the charge recovery was calculated as  $\eta_{rec} = \Sigma Q_m / Q_{cont,d}$ . Where  $\Sigma Q_m$  is the cumulative total charge of each respective charge-discharge experiment (in C) and  $Q_{cont,d}$  is the expected charge (in C), based on the current produced by a noncapacitive bioanode at the same potential of -0.3 V vs Ag/AgCl, being 0.79 A/m<sup>2</sup> <sup>51</sup>.

### 4.3 Results and Discussion

#### 4.3.1 Characterization of bioanode performance

Polarization curves, showing the current density as function of the anode potential, were recorded to compare the performance of the capacitive bioanodes with six different PVDF contents. The polarization curves of all capacitive bioanodes showed an increase in current density with increasing anode potential (Figure 4.1A). Each point and its standard deviation was

calculated over 6 measurements: the polarization tests were performed for 2 separate cells with the same capacitive electrode, and each cell was characterized at three different times within a period of about 2 weeks. The capacitive electrode with 2% PVDF achieved the highest current density of 2.4 A/m<sup>2</sup>, whereas the capacitive electrode with 14% PVDF had the lowest current density. There was no clear relationship between the PVDF content and bioanode performance in the polarization curves: the capacitive bioanodes with the highest PVDF content (21%, 46%) and the lowest PVDF content (2%, 4%) showed similar performance that was higher than the capacitive bioanodes with 10% and 14% PVDF. Because each capacitive electrode contained a different amount of electrode material (activated carbon) as shown in Table 4.1, the performance of the capacitive bioanodes can be better compared when normalizing the current to the amount of activated carbon (in g<sub>AC</sub>) used for each capacitive electrode (Figure 4.1B).

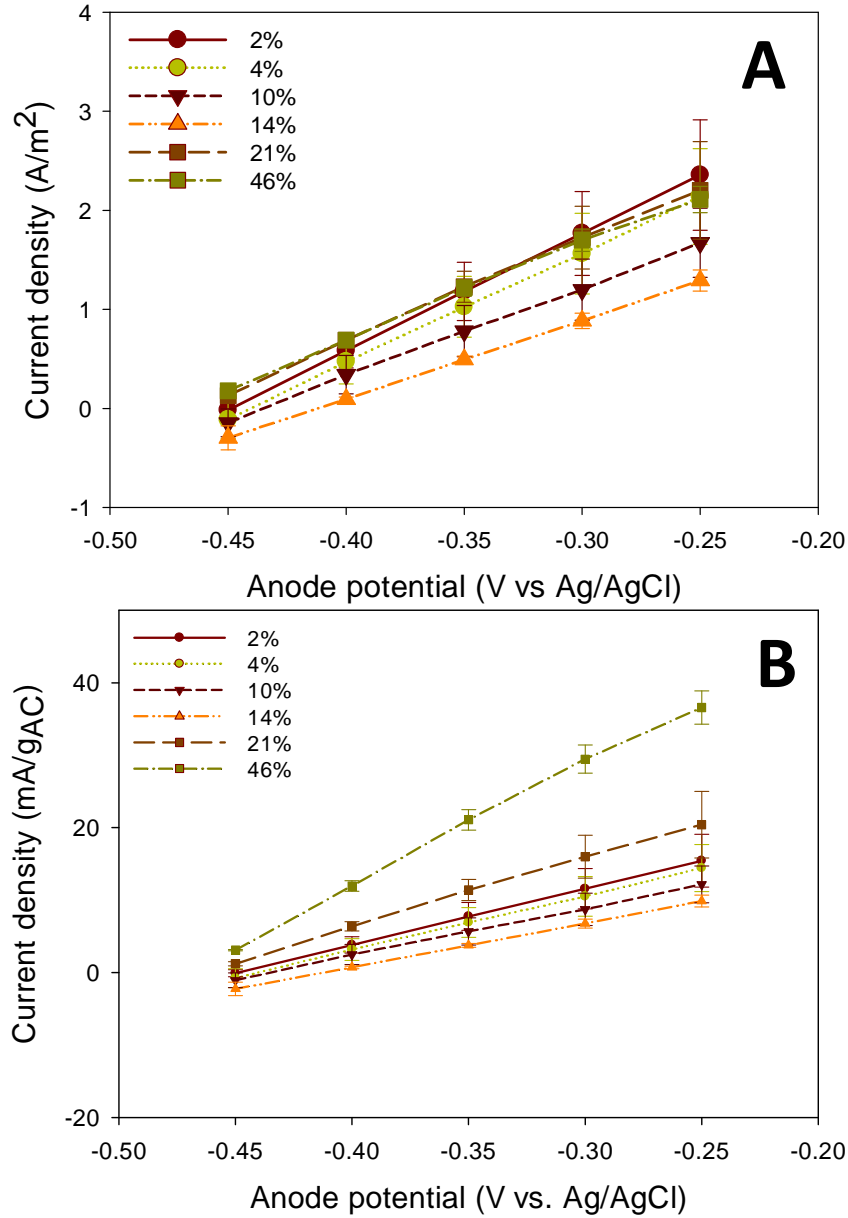


Figure 4.1: The polarization curves of the capacitive electrodes expressed in  $A/m^2$  (A, top) and  $mA/g_{AC}$  (B, bottom). The highest current density of  $2.4 A/m^2$  was measured for the capacitive electrode with 2% PVDF. The lowest current density of  $1.3 A/m^2$  was measured for the capacitive electrode with 14% PVDF. The average and standard deviations are calculated over 6 measurements for each data point.

The polarization curves with the current density expressed in A/g<sub>AC</sub> also showed an increase in current density with increasing anode potential. The maximum current of 37 mA/g<sub>AC</sub> was measured for the capacitive bioanode with 46% PVDF at an anode potential of -0.250 V, whereas the capacitive electrode with 14% PVDF again had the lowest current of 9.9 mA/g<sub>AC</sub>. Notably, the performance of the six different capacitive bio-anodes was quite stable and reproducible, both between the duplicates and in the course of three weeks. This stabilizing effect of the capacitive layer was also observed in previous studies<sup>[5,6]</sup>

To show the effect of PVDF content on bioanode performance, the current (mA/g<sub>AC</sub>) at each PVDF content at an anode potential of -0.3 V vs Ag/AgCl (from Figure 4.1A) is shown in Figure 4.2 .

The capacitive electrode with 14% PVDF had the lowest current per gram of AC, while both decreasing and increasing PVDF content resulted in higher currents. Moreover, the current density of the capacitive bioanode with 46% PVDF is several times higher than the current of the capacitive bioanode with 2% PVDF. This result is unexpected, because our hypothesis was that PVDF, when used in quantities higher than needed for effective binding of activated carbon, has a negative effect on the performance of the capacitive electrodes, since it is a non-conductive material. A possible explanation for PVDF actually enhancing bioanode performance could be that PVDF is also used as a membrane for protein binding <sup>[11,12]</sup>. This could mean that the electrochemically active microorganisms actually prefer to grow on the PVDF-covered part of the electrode, as long as they can make an electrical connection to the activated carbon to release the electrons extracted from acetate.

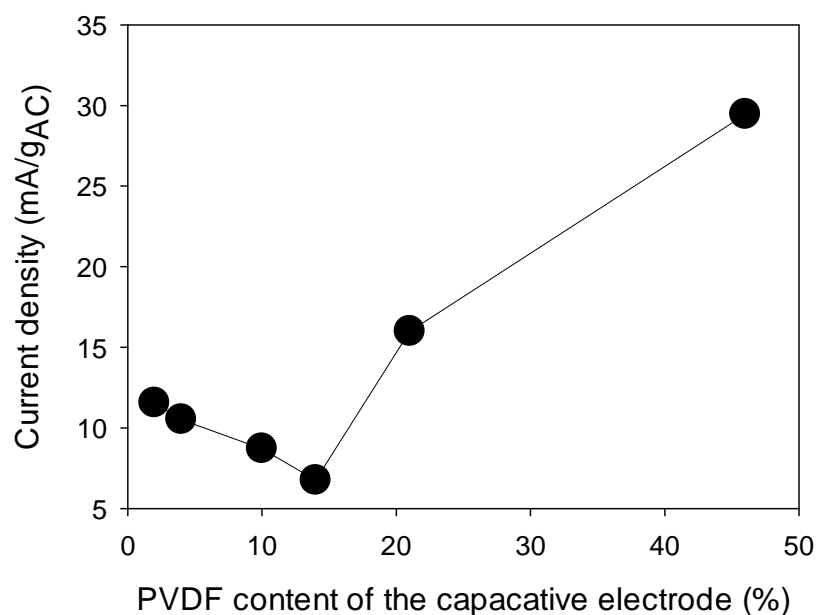


Figure 4.2: Current density of the capacitive electrodes with the different PVDF contents at -0.3 V anode potential vs. Ag/AgCl.

#### 4.3.2 Relative Charge Recovery

The relative charge recovery was calculated as the total charge recovered during the charge-discharge experiments (in  $C/m^2$ ), divided by the total charge recovered by a noncapacitive bioanode (in  $C/m^2$ ), which produced  $0.79 A/m^2$  continuously at the same anode potential<sup>51</sup>. A relative charge recovery higher than one therefore indicates that the total charge recovered with a capacitive bioanode during a full charge-discharge cycle is higher than the charge recovered with a noncapacitive bioanode in continuous mode during the same time period. The relative charge recovery for the 6 capacitive electrodes is shown in Figure 4.3. Different ratios between charging and discharging time were studied. Figure 4.3A shows the relative charge recovery for the charge-discharge experiments with the same charge and discharge time (1:1). Throughout all these experiments the capacitive bioanode with 21%

PVDF achieved the highest relative charge recovery between 1.3 and 1.4, while the capacitive bioanode with 14% had the lowest relative charge recovery of 0.8 or lower. Figure 4.3B shows the relative charge-recovery for experiments with a charge/discharge time of 1:2. Again, the capacitive bioanode with 21% PVDF achieved the highest recovery in all but one of the experiments. The highest relative charge recovery measured was 1.8, at 60 min charging and 120 min discharging, which means 1.8 times as much electricity can be produced when operating this capacitive bioanode intermittently, compared to operating a noncapacitive bioanode continuously. Figure 4.3C shows the relative charge recovery for the charge-discharge experiments with different ratios between charge/discharge times. Again, the highest relative charge recovery of maximum 1.6 was found for capacitive bioanode with 21% PVDF. In most of the experiments, the relative charge recovery of the capacitive bioanodes with intermediate PVDF content (10% and 14%) was considerably lower than the relative charge recovery of the capacitive bioanodes with low (2% and 4%) and high (21% and 46%) PVDF content. This is in line with the results found in the polarization curves (Figure 4.1). It is interesting to note that even though the capacitive bioanode with 21% PVDF contained the second lowest amount of activated carbon (Table 4.2, experimental section), this electrode had a higher relative charge recovery than the capacitive bioanodes with more activated carbon.

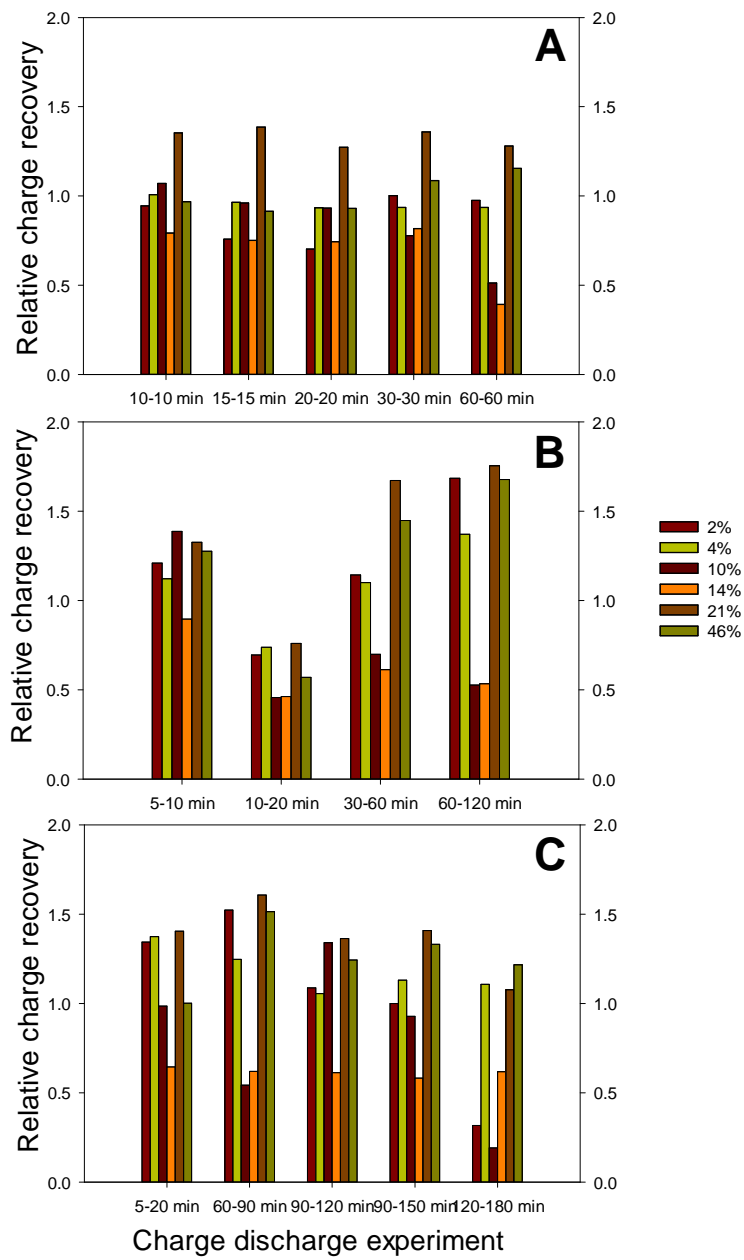


Figure 4.3: Relative charge recovery of the different capacitive electrodes giving the highest charge recovery for the capacitive electrode with a PVDF-content of 21%.

### 4.3.3 Surface properties of the electrodes without biofilm

The capacitive layer on the electrodes, without biofilm, was characterized using SEM and BET-analysis. Figure 4.4 shows the SEM-pictures of two capacitive electrodes: (a) the capacitive electrode with the lowest PVDF content of 2% and (b) the capacitive electrode with the highest PVDF content of 46%.

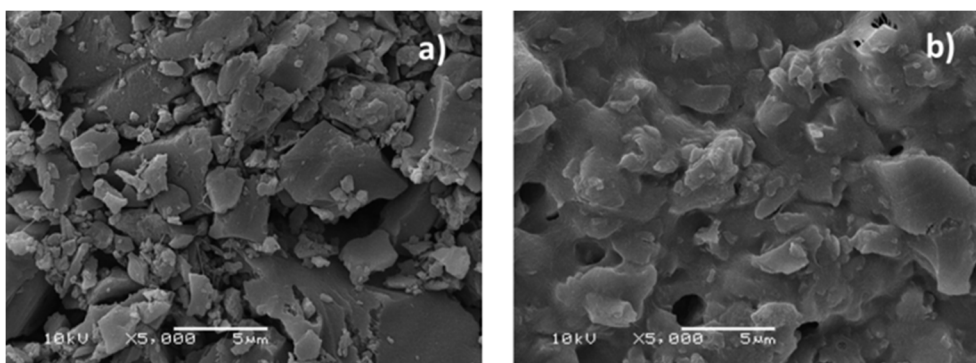


Figure 4.4: SEM-Picture of the capacitive electrodes with different PVDF-contents: a) 2%PVDF, b) 46% PVDF. The capacitive electrode with 2% PVDF shows mainly activated carbon particles, while the capacitive electrode with 46% PVDF shows particles bound together by PVDF.

The surface of the capacitive electrode with 2% PVDF (Figure 4.4a) mainly shows activated carbon particles, while the PVDF can barely be observed. Figure 4.4b) on the other hand, shows the surface of the capacitive electrode with 46% PVDF. The surface of this capacitive electrode clearly shows activated carbon particles covered with and bound together by PVDF. This indicates that the specific surface decreases with increasing PVDF-content. This trend was confirmed by BET-Analysis (Table 4.3). The capacitive electrode with 2% PVDF had the highest specific surface area of 1109 m<sup>2</sup>/g, whereas the capacitive electrode with 46% PVDF had the lowest specific surface area of 581m<sup>2</sup>/g. The differences in specific surface area, however, do not explain the differences in performance between the different capacitive

layers that we found in the polarization tests and in the charge-discharge experiments. In this respect, it is important to note that this specific surface area includes all pores of all sizes, many of which might not be accessible to microorganisms.

Table 4.3: Specific surface area for each capacitive electrode based on BET-analysis

<b>PVDF-content</b>	2%	4%	10%	14%	21%	46%
<b>Area (m<sup>2</sup>/g)</b>	1109	984	971	952	824	581

#### 4.3.4 Electrochemical behavior of the capacitive electrodes without biofilm

The different capacitive electrodes were analyzed for their electrochemical behavior without biofilm using galvanostatic charge-discharge experiments. Figure 4.5 shows the results for the galvanostatic charge-discharge experiment performed at a current density of 5 A/m<sup>2</sup>. This result is representative for the results obtained at the other current densities. First the capacitive electrodes were charged with a current density of 5 A/m<sup>2</sup> for 300 s, then the direction of the current was changed and the capacitive electrodes were discharged at 5 A/m<sup>2</sup> for 300s. The surface area below the charging curve shows for the capacitance of each capacitive electrode. The larger the surface area, the higher the capacitance of this specific capacitive electrode. The highest capacitance was measured for the capacitive electrode with 2% PVDF. This is in line with the results of the polarization curves where this bioanode showed the highest performance (Figure 4.1).

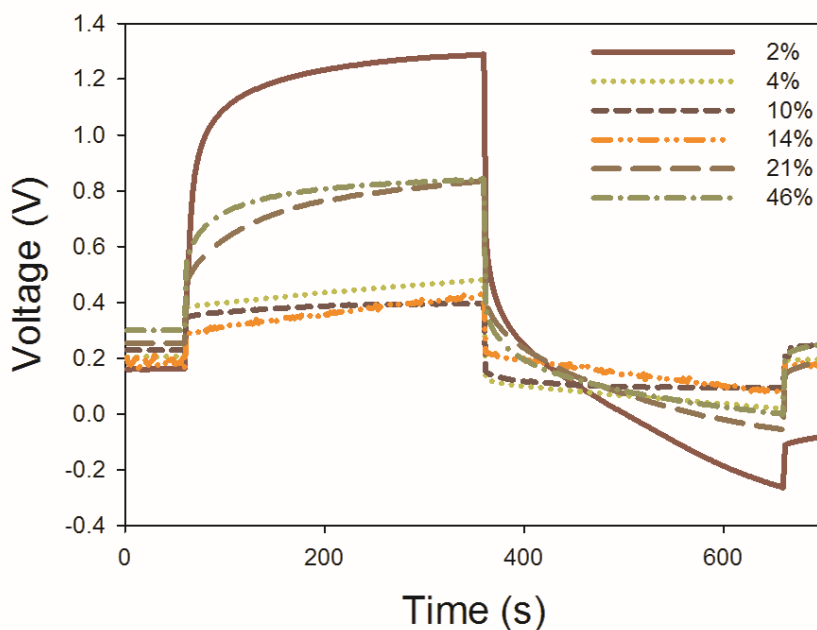


Figure 4.5 The charging curves measured during the galvanostatic charge-discharge experiments of the capacitive electrodes without biofilm. The highest capacitance was measured for the capacitive electrode with 2% PVDF. The lowest capacitance was measured for the electrode with 14% PVDF.

Based on the BET-analysis and the electrochemical behavior of the capacitive electrodes without biofilm, the capacitive electrode with 2% PVDF is expected to produce the highest current density, since it has the largest specific surface area of all electrodes. However, in the charge-discharge experiments (Figure 4.3), the highest charge recovery was found for the capacitive bioanodes with 21% and 46% PVDF, and not for the capacitive bioanode with 2% PVDF. This is surprising, because the electrodes with high PVDF content have the lowest specific surface area (Table 4.3). The lower performance of the electrode with 2% PVDF compared to the electrodes with 21% and 46% PVDF is also apparent from the polarization curves (Figure 4.1). An increase in PVDF-content was expected to give a decrease in performance because the amount of capacitive

particles is lower, but, when the current density was normalized for the amount of activated carbon on each electrode (Figure 4.2), we observed no direct correlation between the PVDF content and the current. It seems that PVDF actually enhances the performance of the capacitive bioanodes. Our hypothesis was that PVDF, when used in quantities higher than needed for effective binding of activated carbon, has a negative effect on the performance of the capacitive electrodes, since it is a non-conductive material. A possible explanation for PVDF actually enhancing bioanode performance could be that PVDF is also used as a membrane for protein binding<sup>52,53</sup>. This could mean that the electrochemically active microorganisms actually prefer to grow on the PVDF-covered part of the electrode, at least as long as they can make an electrical connection to the activated carbon to be able to release their electrons.

#### **4.4 Conclusions**

We studied the effect of PVDF content on the performance of capacitive bioanodes. It was expected that a low PVDF-content would give a higher performance than a high PVDF-content because of the higher electrode surface area. On the contrary, low PVDF content resulted in low performance, while high PVDF content resulted in high performance, also when corrected for the amount of activated carbon. During the charge-discharge experiments the capacitive bioanode with 21% PVDF achieved the highest relative charge recovery of 1.8, meaning that it produced 1.8 times more electricity than a noncapacitive bioanode operated in continuous mode.

### **Acknowledgements**

This work was performed in the TTIW-cooperation framework of Wetsus, Centre of Excellence for Sustainable Water Technology ([www.wetsus.nl](http://www.wetsus.nl)). Wetsus is funded by the Dutch Ministry of Economic Affairs, the European Union European Regional Development Fund, the Province of Fryslân, the city of Leeuwarden and by the EZ-KOMPAS Program of the “Samenwerkingsverband Noord-Nederland”. The authors like to thank the participants of the research theme “Resource Recovery” for the fruitful discussions and their financial support.



## Chapter 5

# **The fluidized capacitive bioanode as a novel reactor concept for enhanced performance of the microbial fuel cell**

This chapter has been submitted as:

Deeke, A.; Sleutels, T. H. J. A.; Heijne, A. Ter; Donkers, T. F. W. Hamelers, H. V. M.; Buisman, C. J. N. The fluidized capacitive bioanode as a novel reactor concept for enhanced performance of the microbial fuel cell. *Environmental Science and Technology*

## Abstract

The use of granular electrodes in Microbial Fuel Cells (MFCs) is attractive because granules provide a cost-effective way to create a high electrode surface area, which is essential to achieve high current and power densities. Here, we show a novel reactor design based on capacitive granules: the fluidized capacitive bioanode. Activated carbon granules are colonized by electrochemically active microorganisms, which extract electrons from acetate and store the electrons. Electricity is harvested from the AC granules in an external discharge cell. We show a proof-of-principle of the fluidized capacitive system with a total anode volume of 2 L. After a start-up period of 100 days, the current increased from 0.56 A/m<sup>2</sup> with 100 g AC granules, to 0.99 A/m<sup>2</sup> with 150 g AC granules, to 1.3 A/m<sup>2</sup> with 200 g AC granules. Contact between moving AC granules and current collector was confirmed in a control experiment without biofilm and was likely the reason for current production in the fluidized capacitive system with biofilm. SEM images confirmed that a biofilm was present on the AC granules after operation in the fluidized capacitive system. Although current densities reported here need further improvement, the high surface area of the AC granules in combination with external discharge offers new and promising opportunities for scaling up MFCs.

## 5.1 Introduction

With the increase in world population and the resulting increase in energy consumption, together with the need to keep our planet healthy, the search is on for renewable energy production technologies. One of these technologies is the Microbial Fuel Cell (MFC), in which electrochemically active microorganisms convert the chemical energy in biodegradable organics into electrical energy, so that electricity is directly recovered from wastewater. In the past decade, many crucial elements in the MFC have been studied, from electrode materials <sup>11</sup>, to membranes <sup>17,54,55</sup>, reactor design <sup>33,56,57</sup>, microbial communities <sup>58</sup>, electron transfer mechanisms <sup>59,60</sup>, mass transport <sup>18</sup>, start-up strategies <sup>61,62</sup>, types of wastewater <sup>63-65</sup>, alternative cathode reactions <sup>15,66,67</sup>, and scaling up <sup>68,69</sup>.

An important parameter for operation of Microbial Fuel Cells (MFCs) is the power output, which expresses the rate at which energy is recovered from wastewater. During the past decade, the research on MFCs has intensified considerably, and the highest reported power densities increased from 0.01W/m<sup>2</sup> in 2002 <sup>70,71</sup> up to 3.1 W/m<sup>2</sup> in 2009 <sup>72</sup> (Figure 5.1). At the same time, we see in the past few years, reported power densities seem to have stagnated around 2-3 W/m<sup>2</sup>. This power density is still too low to be competitive with one of the competing technologies: anaerobic digestion, in which an energy recovery of 1,000 W/m<sup>3</sup> can be achieved <sup>73,74</sup>.

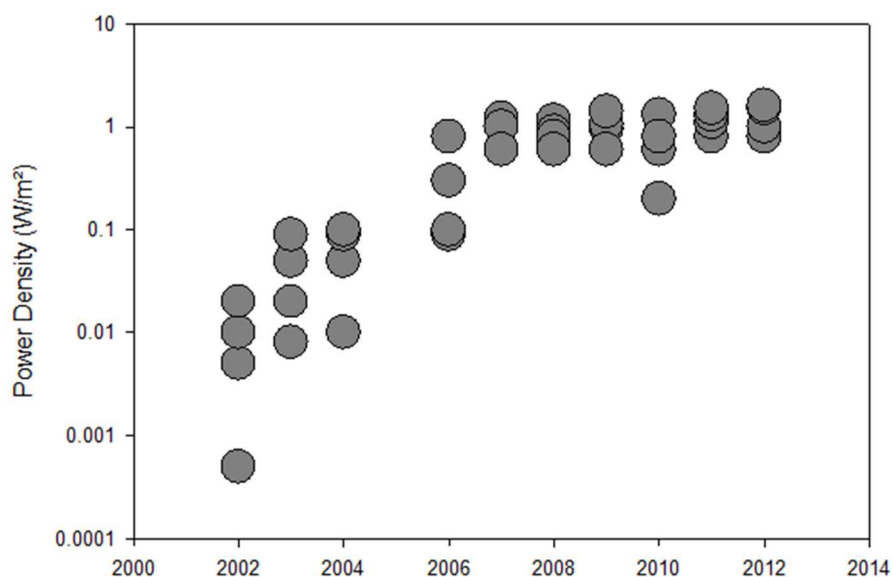


Figure 5.1: Development of reported power densities in literature over the past decade.

Although these power densities have been demonstrated at lab-scale, the question is how and if these systems will show the same performance when operated at a larger scale. In a recent review <sup>75</sup>, the tubular and flat plate designs that have been tested on larger scale (reactors larger than 1L) are discussed. The main limitations in these scaled-up systems are related to a high internal resistance, caused by electrode spacing or limited conductivity of the electrodes, especially when granular materials are used in a tubular design.

Granular materials are attractive because they provide a cost-effective way to create a high electrode surface area, which is essential to achieve high current and power densities. Granular materials, usually in the form of graphite or activated carbon, have mostly been used in a fixed bed reactor, in which the electric current was harvested via a current collector, which is a graphite rod <sup>76</sup> or a Ti-wire or mesh <sup>77</sup>. To enhance mass transport, it was demonstrated that electricity could be generated in an anaerobic fluidized bed MFC, where the active carbon particles could flow freely in the anaerobic column so that better mixing could be achieved

<sup>78</sup>. In this setup, the electricity was also harvested in-situ via a graphite rod inserted in the column. Both granular activated carbon, and graphite granules were tested, and it was shown that with the use of a mediator (neutral red), a power density up to 1.1 W/m<sup>2</sup> could be produced <sup>78</sup>.

Another approach is to integrate capacitive materials in the bioanode of an MFC<sup>40</sup>. When a capacitive activated carbon layer was cast onto an electrode, it was shown that 53% more charge could be recovered compared to a noncapacitive flat plate electrode. The thickness of the capacitive layer was shown to affect the current and power density<sup>44</sup>. Recently, Liu et al <sup>79</sup> have shown that electricity could be harvested intermittently from capacitive particles that were charged by exoelectrogenic biofilms inside a 7 mL anode chamber and discharged at a current collector integrated in the anode chamber. Mixing of the particles resulted in improved performance compared to a fixed bed setup.

The objective of this study was to study a new reactor concept where AC granules are charged in a charging column, and the electricity is harvested in an external electrochemical cell instead of in-situ in the anaerobic reactor. We tested this fluidized capacitive system with a total anolyte volume of 2.1 L and we analyzed the performance of this system in terms of current density, COD removal, and coulombic efficiency.

## **5.2 Materials and methods**

### **5.2.1 System setup**

The principle of the fluidized capacitive system is shown in Figure 5.2. The setup consisted of a charging column (2.08 L) and a discharge cell (0.022 L), with a total anode volume of 2.1 L.

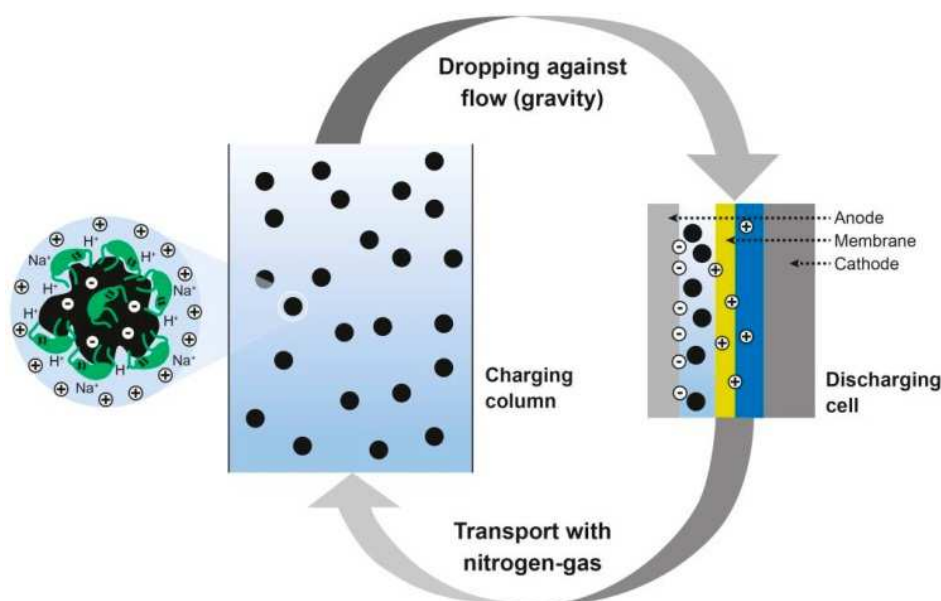


Figure 5.2: The working principle of the fluidized capacitive system. AC granules are charged by electrochemically active microorganisms in the charging column. Electricity is harvested in the discharging cell. AC granules are recirculated through the system driven by a nitrogen gas flow.

In the charging column, the AC granules are transported upward by a flow of nitrogen gas. After the upward transport, the granules settle via the discharge cell, that consists of a current collector (anode) and a cathode, both flat graphite plates (Müller & Rössner GmbH, Troisdorf, Germany) of 11 cm<sup>2</sup> surface area. Both electrodes are separated by two plates with a flow channel, similar to the ones used in<sup>31</sup>, but smaller. The flow channel had a contact area of the electrodes of 11 cm<sup>2</sup> and a thickness of 2 cm, resulting in 22 mL anode and cathode compartment volume in the discharge cell. A cation exchange membrane (Ralex, Mega, Straz pod Ralskem, Czech Republic) was used to separate anode and cathode compartment. Total circulation volume of the cathode was 1.02 L, consisting of the discharge cathode compartment of 22mL plus a storage vessel of 1L.

### 5.2.2 Electrode preparation and analysis

The anode granules consisted of activated carbon (AC) granules (bulk density: 510 kg/m<sup>3</sup>, GAC 1620, Norit, Amersfoort, The Netherlands). 100 g (dry weight) of the AC granules were soaked in tap-water prior to inoculation. The granules were first placed in a flat plate cell and inoculated with effluent of another MFC operated on acetate<sup>49</sup> to achieve biofilm growth on the granules. The load used for the flat-plate cell was 500Ω. After 2 weeks, the flat-plate cell was opened and the granules were transferred into the fluidized bed reactor. On day 130 and 180, an additional 50g of pre-inoculated granules were added from the flat plate cell to the fluidized bed reactor, resulting in a final amount of 200g AC granules.

### 5.2.3 Operation and Measurements

The fluidized capacitive anode was continuously fed with 5.2 mL/min of fresh medium and the anolyte and catholyte were recirculated at a rate of 500mL/min. The HRT of the medium in the anode compartment was 6.7 h. The influent to the fluidized capacitive anode was a mixture of 10 mM sodium acetate with a 10 mM phosphate buffer solution. Additionally, 10 mL/L of a macronutrient, 1 mL/L of a micronutrient and 1 mL/L of a vitamin solution was supplied to the anolyte<sup>17</sup>. The catholyte (discharging cell) consisted of a 10 mM ferricyanide solution. The charging column was constantly flushed with nitrogen gas at a rate of 0.9 L/h from the bottom to the top to drive the upward transport of the AC granules. The average granule recirculation rate was 45 s, meaning that it took each granule in average 45s to pass one time through the reactor. The current collector was constantly controlled at a potential of -0.300V vs. Ag/AgCl (+0.2V vs. NHE, Pro Sense, Oosterhout, The Netherlands). This anode potential was chosen based on performance of capacitive bioanodes during charge-discharge experiments in an earlier study<sup>51</sup>. The anode potential was controlled with a potentiostat (n-stat, Ivium Technologies, Eindhoven, The Netherlands). The pH of the anolyte was constantly measured using a pH-electrode (Liquisys, Endress + Hauser, Naarden, The Netherlands). Voltage and current were constantly recorded.

Before inoculation, control experiments were performed without particles in the fluidized reactor and with 50g of non-inoculated granules in the fluidized bed reactor to study contact between the AC granules and current collector. The anolyte and catholyte were the same as used during the rest of the experiment. The potential of anode current collector was controlled in three steps: first two charging steps at an anode potential of -0.3 V vs Ag/AgCl during 30 s and -0.5 V vs Ag/AgCl during 30 s, then one discharging step at an anode potential of -0.1 V vs Ag/AgCl for 300 s. The same procedure was repeated after addition of 50 g AC granules to the anode compartment.

#### **5.2.4 Analyses and calculations**

During the first 112 days of operation the COD of the anode compartment was monitored in the influent and in the effluent of the cell. From these measurements the COD-removal rate and the coulombic efficiency were determined. The COD was measured using a standard test kit (Nr 414, Hach Lange, Tiel, The Netherlands).

The specific surface area of the AC granules was determined using BET-Analysis according to <sup>51</sup>. Before and during the experiment, the AC granules were analyzed using SEM (Scanning Electron Microscope, JEOL Technics Ltd., Tokyo, Japan) <sup>46</sup>. Using SEM, the surface of several AC granules was analyzed to obtain a representative overview. After 112 days of operation, a few granules were taken from the active fluidized capacitive anode, and after fixation <sup>45</sup>, were analyzed in the same way.

The current density was calculated from the produced current through;  $i = I/A$  in A/m<sup>2</sup>, where A is the projected surface area of the anode, cathode or membrane (0.0011 m<sup>2</sup>).

The COD removal of the fluidized bed anode was determined between day 55 and 112. The COD removal efficiency (rCOD in %) was calculated according to:

$$rCOD = \frac{(COD_{in} - COD_{out})}{COD_{in}}$$

where  $COD_{in}$  is the concentration of COD (mol/L) measured in the inflow of the fluidized bed anode and  $COD_{out}$  is the concentration of COD (mol/L) measured in the outflow of the fluidized bed anode.

With the COD removal and the average current density (A/m<sup>2</sup>), the coulombic efficiency (CE) was calculated according to:

$$CE = \frac{M_{O_2} \times I}{n \times F \times Q \times \Delta COD}$$

where  $M_{O_2}$  is the molecular weight of oxygen (32 g/mol),  $I$  is the average current,  $n = 4$  is the number of electrons exchanged per mole of oxygen,  $F$  is the Faraday constant (96485 C/mol),  $Q$  is the volumetric influent rate (L/s) and  $\Delta COD$  is the difference in COD between the influent and the effluent (g/L).

### 5.3 Results and discussion

In this work, we studied a novel reactor system in which AC granules are used in a fluidized reactor to store electrons derived from wastewater by electrochemically active microorganisms, and in which the electricity is harvested in an external discharge cell.

#### 5.3.1 Increase in current production with increasing loading of AC particles

During the first 100 days after addition of 100g pre-inoculated AC granules in the system, current density in the discharge cell (at -0.3V vs Ag/AgCl) was around 0.17 A/m<sup>2</sup>. After 100 days, an increase in current density was observed to 0.56 A/m<sup>2</sup>. After addition of another 50 g AC granules, the current density first decreased but then gradually increased to 0.99 A/m<sup>2</sup>. After addition of again 50 g AC granules, a further increase to 1.3 A/m<sup>2</sup> was observed on day 218. This increase in current density with increasing loading of pre-inoculated AC granules indicates that the electrochemically active microorganisms on the AC granules are able to store electrons that are harvested in the discharge cell. It is possible, though, that

part of the current was produced by electrochemically active microorganisms attached to the current collector (anode) of the discharge cell. To study the possible contribution of a biofilm on the current collector to current production, we performed another experiment in which we operated the discharge cell as a Microbial Fuel Cell (MFC), without AC granules. After inoculating the anolyte with electrochemically active microorganisms and controlling the anode potential of the discharge cell at  $-0.3\text{ V vs Ag/AgCl}$ , the bioanode produced a maximum current of  $2.7\text{ A/m}^2$  after two weeks. After addition of  $50\text{ g}$  non-inoculated granules to the anolyte, that were recirculated via the discharge cell, the current gradually decreased to  $0.51\text{ A/m}^2$  after 21 hours (data not shown). Thus, during continuous flow of AC granules along the electrode, most of the biofilm activity on the anode current collector stops. Although biofilm formation on the current collector is possible and can contribute to the total current, it seems that the AC granules remove the biofilm when they come in contact with the current collector. In Figure 5.3, therefore, part of the current may originate from the current collector itself, but it is likely that most of the current originates from the electrochemically active microorganisms on the AC granules, because we measured an increase in current density with increasing loading of AC granules, and we confirmed that the recirculation of AC granules in the system results in reduced current density.

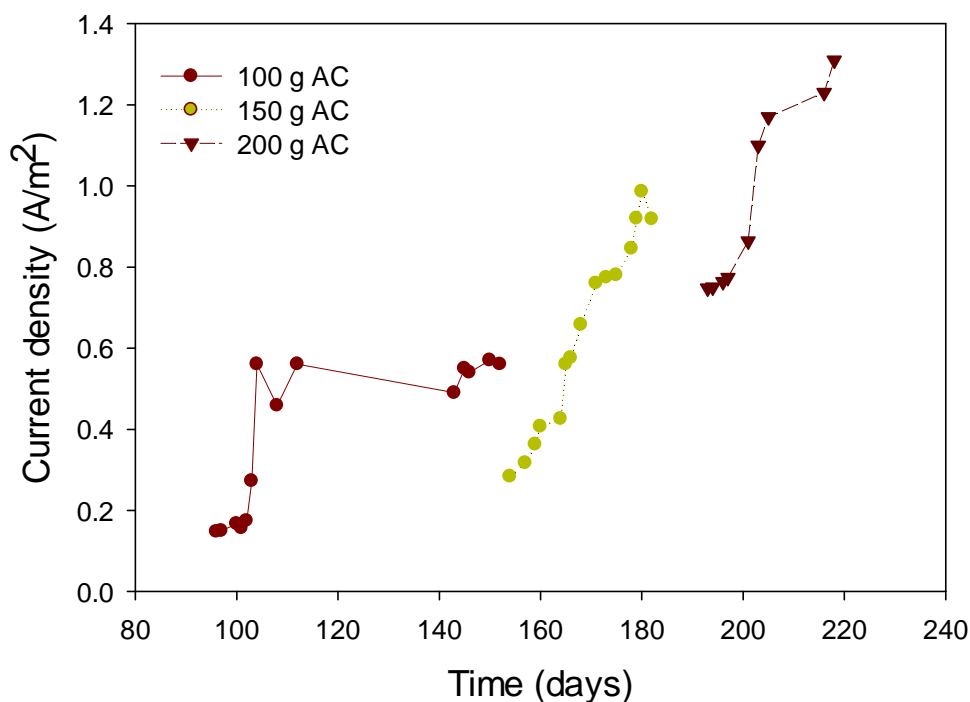


Figure 5.3: The development of the current density of the fluidized bed anode. The current density increased from 0.18A/m<sup>2</sup> at day 96 to 1.3 A/m<sup>2</sup> at day 218. During the experimental period the AC granule loading was increased from 100g at the start, to 150g on day 153, to 200g on day 185.

To monitor the microbial activity during start-up of the fluidized capacitive anode, the COD removal was measured and coulombic efficiency was determined between day 51 and 112. From day 51 to day 105, the current density was stable around 0.17 A/m<sup>2</sup>, and thereafter an exponential increase in current was observed to 0.56 A/m<sup>2</sup>. The COD removal efficiency increases in time from 20-40% in the beginning to 65-72% in the days that a sharp increase in current density was found. The coulombic efficiency increased as well, from 7% on day 51 to 27 % on day 112. This reflects that the electrochemically active microorganisms indeed became more active during the last weeks before the increase in current was observed. Still, large

part of the substrate was not converted into electrons, indicating loss of substrate to either biomass growth or methanogens.

### **5.3.2 Role of AC granules in current production**

To study in more detail if the AC granules indeed contributed to transfer of electrons, we tested if the granules made electrical contact with the current collector. An abiotic charge-discharge experiment was performed in the system, on the current collector alone and with 50 g AC granules using the standard anolyte medium, but without inoculation. We tested two charging steps at -0.3 and -0.5 V vs Ag/AgCl, where electrons were transferred from current collector to AC granules, followed by one discharging step at -0.1 V vs Ag/AgCl, where electrons were transferred from AC granules to current collector. The charging current is represented by a positive current, the discharging current is represented by a negative current. The results are shown in Figure 5.4 and summarized in Table 5.1. At -0.1 V vs Ag/AgCl, the current collector alone showed a small peak, after which the current quickly dropped to almost zero. At -0.3 V vs Ag/AgCl, a similar trend was observed but current stayed slightly higher. At -0.5 V vs Ag/AgCl, a discharge peak can be seen where the electrons were transported from the charged AC granules to the current collector. When repeating the test with 50 g AC granules, we see a similar pattern, but with a considerable higher current density at each potential, indicating that the AC granules do exchange electrons with the current collector. This effect was more pronounced for the charging steps than for the discharging steps, which is also reflected in the total transferred charge (Table 5.1). For the current collector alone, in the three cycles, 61-100 % of the electrons that were transferred during charging, were recovered in the discharge step. For the current collector with 50 g AC granules, the percentage of charge recovered in the discharge step was lower, between 12 and 16%. These results show that it is possible to charge and discharge the AC granules on the current collector in this fluidized capacitive system, although part of the electrons charged on the particles

were not recovered in the discharge step. It is at this point not clear why only part of the electrons were recovered when using 50 g AC granules. Explanations could be that the discharge time is not sufficiently long, that too few particles have been charged during the charging step, or that the driving force for discharge (at -0.1 V vs Ag/AgCl) was too low. While the results show that electron transfer between AC granules and current collector does occur, the results do not show what the mechanism of charge storage is in the actual MFC system. Are the electrons stored inside the AC granules, or can they also be stored in the biofilm <sup>80</sup>? Where the charge is stored, and how this influences the performance of a fluidized capacitive bioanode, is an aspect that needs further study.

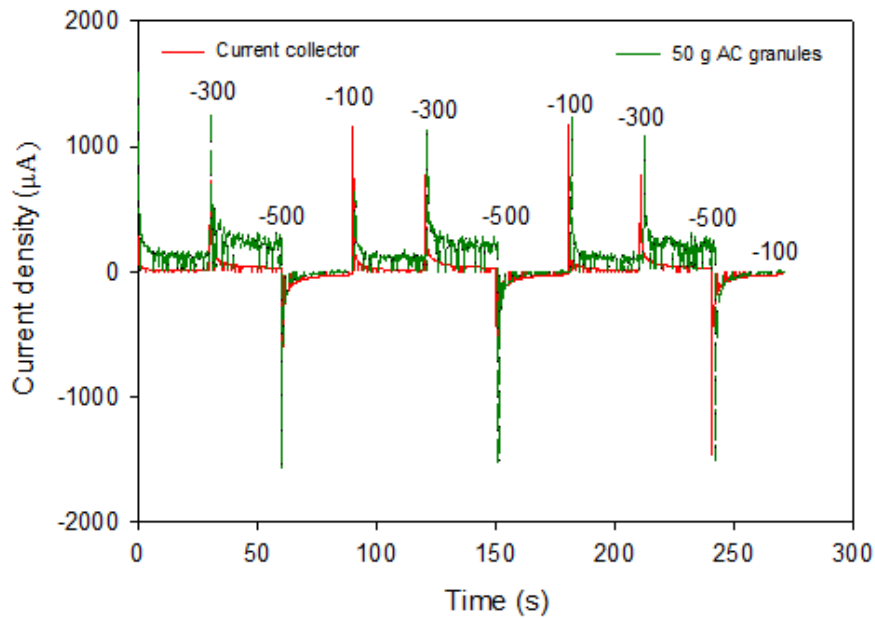


Figure 5.4: Charge-discharge behaviour of the current collector and the current collector with 50g AC granules. The current and stored charge with 50g AC granules is higher than for the current collector alone, indicating that charge is transferred between current collector and AC granules.

Table 5.1: Overview of the transferred charge for the current collector alone and for the current collector with 50g AC granules that are recirculated via the charging column at different potentials.

Potential (mV vs Ag/AgCl)	Transferred charge (mC)	
	Current collector	50 g AC particles
Cycle 1		
-300 (charge step 1)	0.43	4.54
-500 (charge step 2)	1.75	7.94
<i>Total charging</i>	2.18	12.48
-100 (discharge)	-2.29	-1.52
% of charge recovered	105	12
Cycle 2		
-300 (charge step 1)	1.05	3.68
-500 (charge step 2)	1.82	6.99
<i>Total charging</i>	2.87	10.67
-100 (discharge)	-1.76	-1.50
% of charge recovered	61	14
Cycle 3		
-300 (charge step 1)	1.01	3.73
-500 (charge step 2)	1.89	6.61
<i>Total charging</i>	2.90	10.34
-100 (discharge)	-2.17	-1.72
% of charge recovered	75	17

### 5.3.3 Granules are covered with a biofilm

The AC granules were characterized using the BET-Analysis. During this BET-Analysis, a specific surface area of  $1989.4 \pm 236.2 \text{ m}^2/\text{g}$  was measured, which is a typical value for AC granules<sup>81</sup>.

To study if the AC granules were colonized by microorganisms, the granules were analyzed by Scanning Electron Microscopy (SEM) before and after operation in the fluidized capacitive system. Figure 5.5A shows the surface of a non-colonized AC granule. Figure 5.5B shows the surface of a particle after operation as used for the fluidized anode.

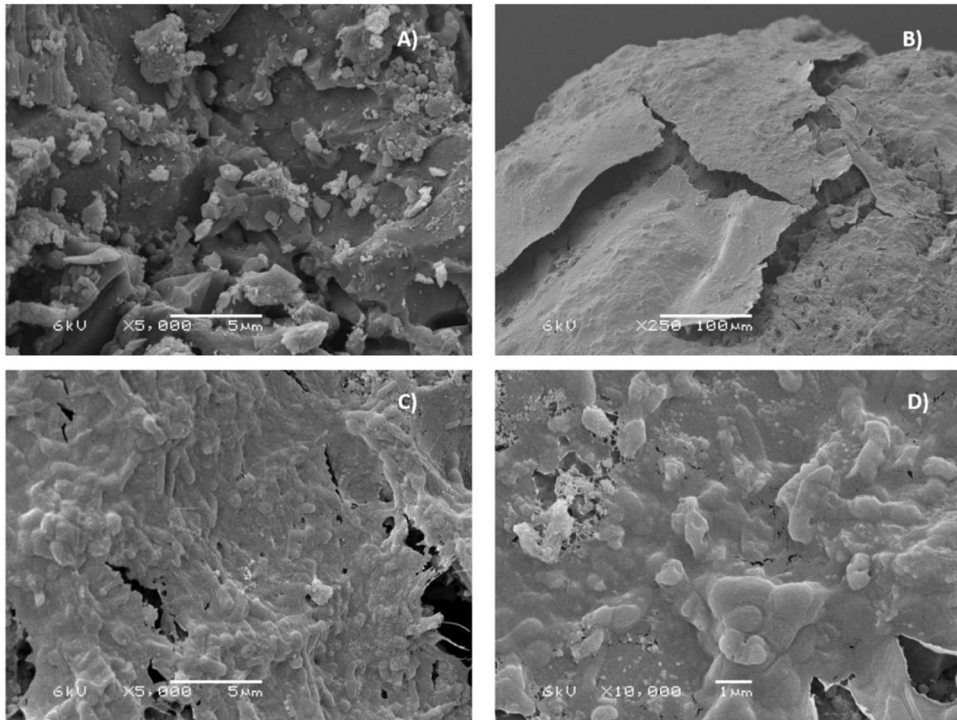


Figure 5.5: SEM-Picture of the AC granules used in this study. A) Surface structure of the granule before use, B) surface structure of the granule covered with biofilm after operation in the fluidized capacitive anode. C) and D) also show the surface of the granule covered with a biofilm after operation in the fluidized capacitive anode at different magnifications.

The surface is completely covered with a biofilm that seems packed together and attached to the particle. Figure 5.5C and D show the biofilm on the AC granules in more detail and show that indeed microorganisms are present on the AC granules. Whereas the granule before operation shows a rough surface area, the granule after operation has a much more smooth area with microorganisms clearly visible.

### 5.3.4 Discussion and perspectives

We show a proof-of-principle of the fluidized capacitive anode, where AC granules with electrochemically active microorganisms are charged in a charging column, and electricity is harvested in an external discharge cell. Advantages of the fluidized capacitive anode compared to standardized MFC set-ups are that a high

electrode surface can be achieved in a cost-effective way, that ohmic losses during discharge are minimized, and that the system is well-mixed so that mass transport limitations at the bioanode are reduced.

A high electrode surface area can be achieved with the AC granules, while the discharge cell can be of relatively small size. When high currents can be achieved in the discharge cell, this may offer an economically attractive alternative for scaling up microbial electrochemical systems as the need for the expensive constituents of such a cell (membranes, cathodes with catalyst) are reduced.

The second advantage is that, when charged, the AC granules will be surrounded by cations in the electrical double layer. In this way, the generally low conductivity of the wastewater does not pose a major limitation in the charging step. During discharge, these cations are also released, leading to locally high conductivity and therefore minimal ohmic losses in the discharge cell, compared to MFC designs where wastewater is directly converted into electricity and not stored in AC granules.

Because the granules are fluidized, the diffusion layers of acetate towards the biofilm, and protons away from the biofilm, are minimized, and mass transfer is increased. An important issue to address in later study is that, for practical application, mixing should be achieved with minimum energy (gas sparging).

The maximum current density achieved in this fluidized capacitive system was 1.3 A/m<sup>2</sup>. This current density is in the same range, but slightly lower than the current achieved by a bioanode on a flat electrode, up to 4.5 A/m<sup>2</sup> at -0.3 V vs Ag/AgCl<sup>31</sup>. In a system with fluidized anode particles that were discharged in-situ, current densities reported reached up to 2.4 A/m<sup>2</sup> at -0.4 V vs Ag/AgCl<sup>79</sup>. In fact, electroactive microorganisms on the current collector may even have contributed to the current density, though AC granules touching the current collector seem to prevent biofilm formation on the current collector. Visual inspection of the current collector at the end of the experiment showed that the surface was slightly eroded

by the AC granules, but that also there were small zones where a biofilm could be formed. Similarly, the biofilm may also detach from the AC granules when touching the current collector, an aspect that we have not studied in more detail here. In addition to enhancing biofilm attachment to the AC granules, several other strategies, like increased particle loading rate, and optimizing retention and cycling times, need to be explored to show the feasibility and applicability of this novel reactor concept for MFCs.

### **Acknowledgements**

This work was performed in the TTIW-cooperation framework of Wetsus, Centre of Excellence for Sustainable Water Technology ([www.wetsus.nl](http://www.wetsus.nl)). Wetsus is funded by the Dutch Ministry of Economic Affairs, the European Union European Regional Development Fund, the Province of Fryslân, the city of Leeuwarden and by the EZ-KOMPAS Program of the “Samenwerkingsverband Noord-Nederland”. The authors like to thank the participants of the research theme “Resource Recovery” for the fruitful discussions and their financial support. Also the authors would like to thank Jan Tuinstra and Razan Rosli for the support in the lab.



# Chapter 6

## Discussion and Outlook

## 6.1 Introduction

This thesis deals with integration of capacitive energy storage with a bioanode. Integration of capacitive storage with a bioanode opens up two new applications of the MFC: (i) temporary storage of electrical energy to match supply of renewable energy with consumption and (ii) use of fluidized bed bioanode that allows the use of large-scale reactors without the drawback of a high internal resistance.

The integration of capacitive electricity storage with the bioanode is done through the insertion of a capacitive layer into the anode compartment. The capacitive layer is made of a mixture of activated carbon powder and PVDF binder. The microorganisms grow on the capacitive layer, which is the anode electrode and the electrons can be stored directly in the capacitive layer, see Figure 6.1.

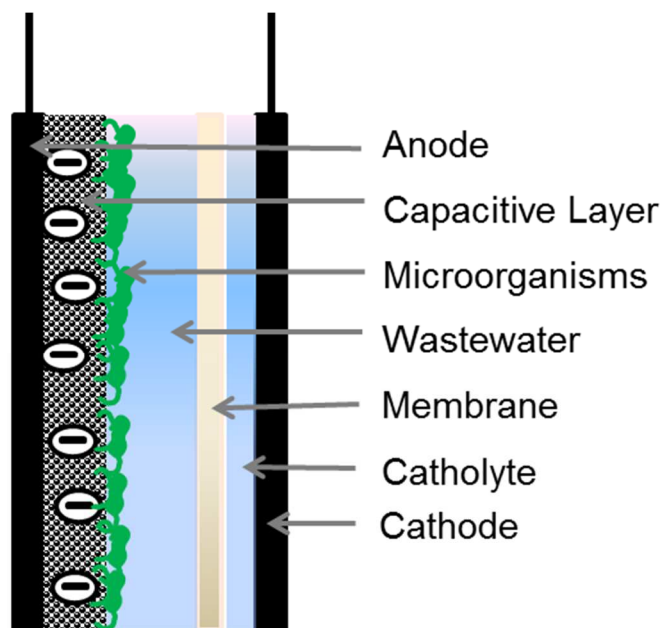


Figure 6.1: The principal of bioelectrochemical charging in case of the capacitive electrode

The capacitive bioanode can be operated in different modes. It is possible to use it as conventional bioanode during polarization curves for constant electricity

production, but it can also be used as capacitive electrode for electricity storage (charging and discharging). During charging the external electric circuit is open (zero current) and the electrons produced by the microorganisms are stored in the capacitive layer. Upon discharging, the electric circuit is closed, and the anode potential was controlled at  $-0.300\text{V}$  (vs.  $\text{Ag}/\text{AgCl}$ ). Looking at the current density plot of the charge-discharge graph (see Figure 6.2) this means that there is zero current during the charging period and at the beginning of the discharging period there is first a peak in current density.

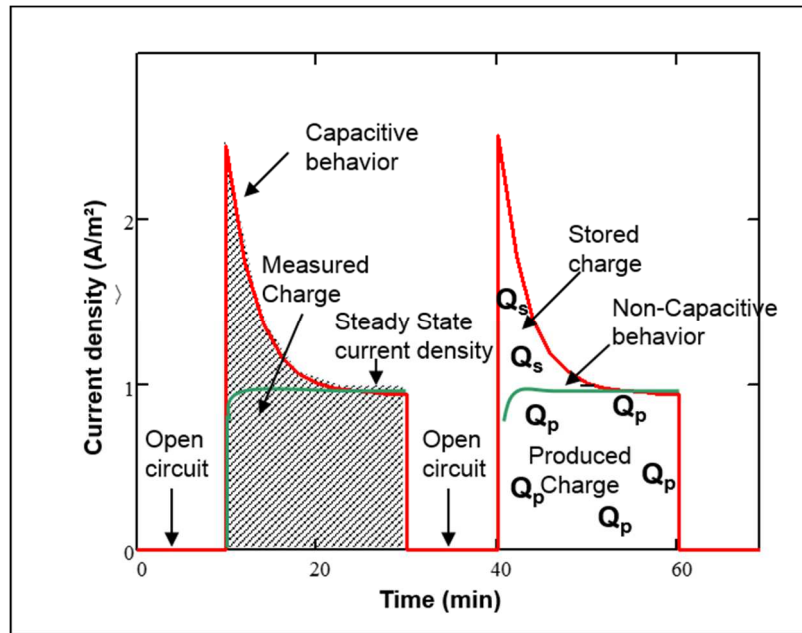


Figure 6.2: Charge distribution measured during a charge-discharge experiment

This peak indicates that electrons were stored in the previous charging period. After this peak the current density levels off towards the constant current density (same current density as during polarization curves is expected). After that the current has levelled off, the charging and discharging cycle can be repeated again.

The concept of electricity storage combined with the operation of an MFC was also studied by other groups across the world. Table 6.1 gives an overview of all studies which were performed during the period of this thesis (2009 -2014).

Initially, an external capacitor was used, we were the first to use an integrated capacitive bioanode. Afterwards mainly the route of integrated capacitors has been used.

To enable the new applications for MFCs the following steps were undertaken in this research: (i) it was studied whether a biofilm can function under repeatedly changing conditions of charging and discharging, (ii) effect of thickness and binder content were studied, (iii) operational choice of charge and discharge times were studied to assess the suitability for energy storage and finally (iv) a proof-of-principle of a fluidized bed bioanode is given.

Table 6.1: Results of the research efforts on the electricity storage in Microbial Fuel Cells

Intermittent operation	Reactor design	Electricity Storage	Anode Material	Maximum power density (W/m <sup>2</sup> )	Reference
Yes	flat-plate MFC	external	graphite plate	0.02	Dewan et al. 2009
No	stacked	external	graphite brush	0.50	Hatzell et al. 2012
Yes	flat-plate MFC	external	graphite plate	0.03	Liang et al. 2011
Yes	flat-plate MFC	internal	graphite plate with capacitive layer	0.51	Deeke et al. 2012
Yes	flat-plate MFC	internal	graphite plate with capacitive layer	1.26	Deeke et al. 2013
Yes	tubular MFC	internal	Carbon veil electrode with extra AC	1.35	Fradler et al. 2014
Yes	tubular MFC	internal	loofah sponge carbon with extra AC	1.11	Yong et al. 2014
Yes	flat-plate MFC	internal	graphite plate with capacitive layer	1.53	Deeke et al. 2014
Yes	fluidized bed MFC	internal	activated carbon granules	0.65	Deeke et al. 2014
Yes	fluidized bed MFC	internal	activated carbon granules	0.95	Liu et al. 2014

## 6.2 Can biofilms withstand charge-discharge cycles

During the proof-of-principle experiments (Chapter 2) for the first time a capacitive electrode was integrated with the bioanode of an MFC. The performance of this capacitive bioanode was tested by measuring polarization curves and via charge-discharge experiments.

The polarization curve showed that the capacitive bioanode outperformed the noncapacitive bioanode. This capacitive electrode reached a maximum current density of  $1.02\text{A}/\text{m}^2$  ( $0.51\text{ W}/\text{m}^2$ ), whereas the noncapacitive bioanode only achieved a maximum current density of  $0.79\text{ A}/\text{m}^2$  ( $0.4\text{ W}/\text{m}^2$ ). During the charge-discharge experiments the capacitive electrode also outperformed the noncapacitive bioanode. The constant current density towards the end of the discharging period of the charge-discharge experiments was higher than the maximum current density reported during the polarization curves obtained of the same capacitive electrode. ( $1.25\text{A}/\text{m}^2$  during charge-discharge experiment,  $1.02\text{A}/\text{m}^2$  during polarization curve). This means that the capacitive electrode is performing even better during the changing conditions of the charging and discharging than during the constant conditions of the polarization curves. This improved performance might be due to i) a better selection of the microorganisms and ii) release of buffer during the discharge period. The better performance of microorganisms during the changing conditions of charging and discharging was also found during the work done with external capacitors (<sup>24,38,39</sup>, Table 6.1). But the increase in current 1.53 (this work) was even higher than those found during the previous work 1.11 (Dewan et al., 2009) on external storage. This extra increase in performance might be due to the extra buffering capacity which is created upon discharging through the release of the cations, which were stored in the double layer of the capacitive electrode.

### 6.3 Effect of binder and thickness

After the successful first experiments from Chapter 2 it was time to improve this flat-plate capacitive electrode. Therefore we looked at several material parameters to find the optimal composition. First we varied the thickness of the capacitive electrode in 3 different thicknesses of 0.2 mm, 0.5 mm and 1.5 mm and second, we varied the PVDF-content of the capacitive layer in six different concentrations of: 2%, 4%, 10%, 14%, 21% and 46%. The capacitive electrode which was used for the proof-of-principle experiments had a thickness of 0.5mm and a PVDF-content of 14%. The performance of this capacitive electrode could be improved by lowering the thickness to 0.2mm and increasing the PVDF-content to 21%. In contrast to what was expected the thickness of the capacitive electrode needed to be smaller than the one previously used, 0.2mm instead of 0.5mm. The capacitive electrode with 0.2 mm thickness achieved a current density of 2.53 A/m<sup>2</sup>, whereas the capacitive electrode with a thickness of 0.5mm only achieved a current density of 1.2 A/m<sup>2</sup>. This might be due to poor colonization of the deeper layers of the capacitive layer by the microorganisms. Since this capacitive layer was used in a flat-plate MFC, the microorganisms were only able to colonize the top of the capacitive layer. Furthermore the capacitive layer might have suffered from poor conductivity between the AC powder particles when the thickness increases. This was also found in research on the use of capacitive layers in supercapacitors<sup>23</sup>. The hypothesis at the beginning of the study for Chapter 4 was that an increasing amount of PVDF-content would lower the performance of the MFC as it is a nonconductive material. This nonconductive material is expected to fill the space on the surface of the AC powder particles, which is necessary for the colonization of the microorganisms. But during the polarization curves and the charge-discharge experiments the capacitive electrode with a PVDF-content of 21% actually outperformed all the other electrodes. This electrode achieved a current density of 2.3A/m<sup>2</sup>, whereas the capacitive electrode with a PVDF-content of 14 %

achieved a current density of  $1.02\text{A}/\text{m}^2$ . Next to the characteristic of being a nonconductive material, the PVDF binder also has the positive characteristic of being a protein binder. This means that the PVDF actually does not take up the space on the surface of AC powder particles which is needed for the microorganisms, but it is offering a more attractive surface for the microorganisms to grow on. As long as the microorganisms are still able to form an electrical connection to the AC powder particles (capacitive electrode with 46% PVDF is performing less than the capacitive electrode with 21% PVDF).

During the experiments performed with the different material properties of the capacitive electrodes the storage capacity was actually increased from  $840\text{C}/\text{g}_{\text{AC}}$  for the capacitive electrode (14% PVDF, 0.5mm) used in Chapter 2, to  $1395\text{C}/\text{g}_{\text{AC}}$  for the best capacitive electrode (14% PVDF, 0.2mm) of Chapter 3, and finally to  $1567\text{C}/\text{g}_{\text{AC}}$  for the best capacitive electrode (21%PVDF, 0.5mm) of Chapter 4.

#### **6.4 Charge and discharge times**

Next to the study of the effect of material on the performance of the capacitive electrodes we also looked into the effect of the charging and discharging times. The aim was to determine how long the microorganisms can withstand the changing conditions of charging and discharging. Not only was the overall experimental time varied, but also the charging time and discharging time itself.

First it was determined, whether the charging time needs to be longer or shorter or equal to the discharging time. At first, charge-discharge experiments were performed with 10 min of charging and 20 min of discharging and the opposite experiment with 20min of charging and 10 min of discharging. Here the capacitive electrodes generally achieved better performances during the charge-discharge experiments, where the discharging time is longer than the charging time. Afterwards 15 different sets of charging and discharging times were tested, where the discharging time was longer than the charging time in each case.

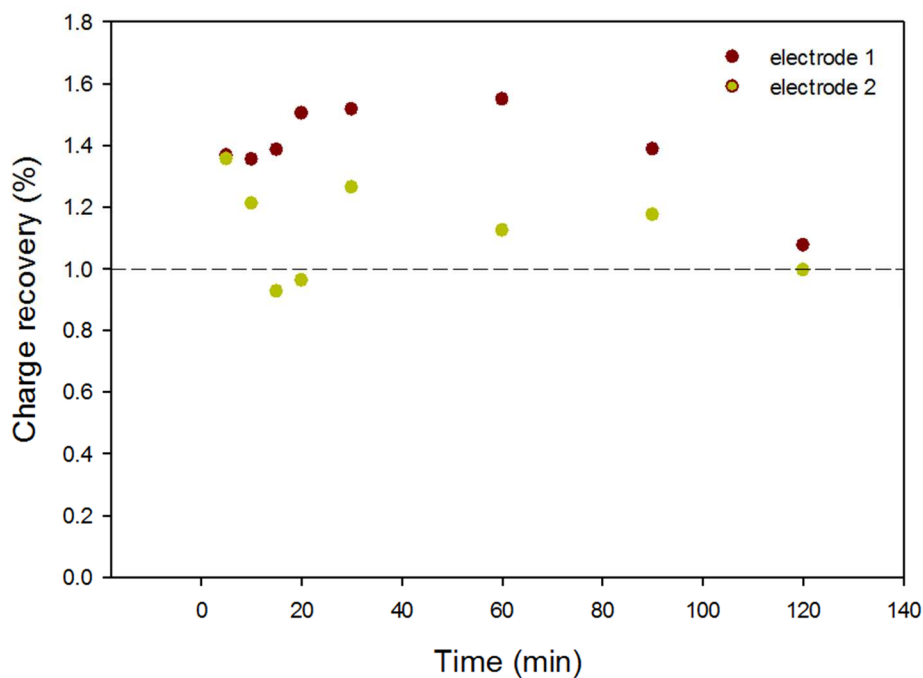


Figure 6.3: Charge Recovery dependent on the different charging times. Electrode 1 (red) is the best performing capacitive electrode from chapter 4 and electrode 2 (green) is the best performing electrode from chapter 3.

From the charge-discharge experiments the stored charge was calculated and related to the continuous operation of a noncapacitive electrode in the charge recovery (see Equation 1.7). Figure 6.3 shows the dependency of the charge recovery of two different capacitive electrodes on the different charging times. The green dots represent the best performing capacitive electrode of chapter 3 and the red dots represent the best performing capacitive electrode of chapter 4. The development of the charge recovery is specific for each type of capacitive electrode (thickness, PVDF-content), but in general each capacitive electrode has its optimal charging and discharging time. But during almost all experiments the charge recovery of the capacitive electrode is larger than 1. This means that during all the

experiments with a charge recovery of 1 or larger, it was more efficient to use the capacitive electrode under the changing conditions of the charge-discharge experiments, than to use the noncapacitive electrode in constant operation. It actually worked much better, since charge recoveries around 1.6 were achieved, this means by operating the capacitive electrode under the changing conditions 60% of extra charge was obtained. The longest charge-discharge experiments which were performed during the studies is with 120 min charging and 180 min of discharging. These times already qualify the capacitive MFC system for distributed energy generation without reducing the energy production whatsoever (<sup>36</sup>, Table 6.2).

Table 6.2: Requirements for specific energy storage systems

<b>Storage system for short duration</b>		
Distributed energy generation	0.5 - 5 MW	1 hour
Renewable matching (intermittent)	100kW - 1MW	Several min - 1 hour
Back-up Energy system	1 - 2kW	~ 2 hours

## 6.5 Performance of fluidized bed anode

Next to the realization of the electricity storage in the flat-plate MFCs we also worked on a proof-of-principle for a fluidized bed anode. The capacitive fluidized anode consisted of activated carbon granules which are fluidized in the charging column under the influence of a nitrogen flow. The charging column is connected to a small discharge cell in the flat-plate design. The fluidized bed anode enables the use of expensive membrane and cathode materials, since the size of the discharging cell is small compared to the size of the anode compartment. During

the proof-of-principle experiments three different amounts of activated carbon granules were used, namely 100g, 150g and 200g. These particles were discharging every travel cycle through the reactor by making contact with the current collector in the discharge cell and the maximum achieved current densities in this system were 100g - 0.56A/m<sup>2</sup>, 150g - 0.99A/m<sup>2</sup> and 200g - 1.3 A/m<sup>2</sup>. This also translates into a small increase in the storage capacity of the particles from 0.11C/g<sub>AC</sub> for 100g of activated carbon granules to 0.13C/g<sub>AC</sub> for 200g of activated carbon granules. Compared to the storage capacity of 22C/g<sub>AC</sub> (3294C/m<sup>2</sup>, 151g<sub>AC</sub>/m<sup>2</sup>) which was achieved with the flat-plate capacitive electrodes during a charge-discharge experiments with 1min of charging and 2 min of discharging this is still 100 times lower. This shows there is still huge improvement possible on for example: operational conditions, capacitance of the material, pore structure, and biofilm growth. During this study the total reactor volume of the anode compartment was 2L and the maximum amount of activated carbon granules used in the anode compartment was only 200g. Considering the specific density of the AC granules (0.5g/cm<sup>3</sup>) this translates into a volume of 400mL filled with activated carbon granules. The void of the fluidized bed reactor can be calculated according to:

**Equation 7:** 
$$\Phi = V_v/V_T,$$

where  $\Phi$  is the void (empty fraction of the reactor),  $V_v$  is the volume of the void and  $V_T$  is the total reactor volume. With the volume of the void  $V_v = 2000\text{mL} - 400\text{mL} = 1600\text{mL}$  and the total volume being  $V_T = 2000\text{mL}$  this results in a void of 0.8. Typically a void from 0.4 to 0.6 is applied for fluidized systems. This means that the amount of granules can be increased up to a maximum of 600g. When the amount of activated carbon granules is increased to 600g the achieved current density will also increase further, which will improve the storage capacity of the system. Table 6.3 gives a comparison between the required surface areas of the

noncapacitive flat-plate MFC and the capacitive fluidized MFC. The required surface area refers to the surface area of membrane, cathode and current collector which are needed for 1 m<sup>3</sup> of reactor volume. The capacitive fluidized MFC only requires 0.55 m<sup>2</sup>/m<sup>3</sup>, whereas the flat-plate system requires 67 m<sup>2</sup>/m<sup>3</sup>. This means that more expensive materials can be used for the capacitive fluidized MFC, since the overall required surface area of these components is much smaller than in a noncapacitive flat-plate system. Also the necessary cathode surface area is smaller for the capacitive fluidized MFC than for the noncapacitive flat-plate MFC. The capacitive factor can still be improved by using more granules (as calculated before) or improvement of the reactor design.

Table 6.3: Comparison of the set-up factors from the noncapacitive flat-plate MFC and the capacitive fluidized MFC

	Noncapacitive flat-plate MFC	Capacitive Fluidized MFC
<b>Required surface (m<sup>2</sup>/m<sup>3</sup>)</b>	67	0.55
<b>Capacitive factor</b>	1	0.86 (100g) 1.52 (150g) 2 (200g)
<b>Needed cathode surface (m<sup>2</sup>)</b>	0.0022	0.0011

The surface of the activated carbon granules might not completely be colonized by the microorganisms due to the contact with the current collector and probably also

due to the shear forces in the liquid phase. This means there is still room for improvement of the capacitive fluidized anode. However the work reported in this thesis already proves that the integrated capacitive electrode is a promising technology for electricity storage inside the MFC.

## **6.6 Concluding remarks**

With the work done for this thesis we proved that the integrated storage system for the MFC is a) able to store electricity and b) to enhance the overall performance of the MFC. Next to testing the flat-plate capacitive electrode first steps in the development of the capacitive fluidized bed anode were taken. The system described here is able to convert wastewater with low conductivity and low COD concentrations into stored electricity which can be released on demand. The efficiency of this system can be improved a lot, so future research should focus on the choice of capacitive material, the operational conditions and the loading rates for example.



## Bibliography

- (1) Nye, M.; Whitmarsh, L.; Foxon, T. Sociopsychological perspectives on the active roles of domestic actors in transition to a lower carbon electricity economy. *Environ. Plan. A* **2010**, *42*, 697–714.
- (2) Fawcett, T.; Lane, K.; Boardman, B.; Banks, N.; Griffin, H.; Lipp, J.; Schiellerup, P.; Therivel, R.; Blok, K.; van Brummelen, M. *Lower carbon futures for European households*; Citeseer, 2000.
- (3) Von Borgstede, C.; Andersson, M.; Johnsson, F. Public attitudes to climate change and carbon mitigation – Implications for energy-associated behaviours. *Energy Policy* **2013**, *57*, 182–193.
- (4) Statistik, B. fuer. No Title  
<https://www.destatis.de/DE/ZahlenFakten/Wirtschaftsbereiche/Energie/Erzeugung/Tabellen/Bruttostromerzeugung.html>.
- (5) Logan, B. E.; Hamelers, B.; Rozendal, R.; Schroder, U.; Keller, J.; Freguia, S.; Aelterman, P.; Verstraete, W.; Rabaey, K. Microbial Fuel Cells: Methodology and Technology. *Environ. Sci. Technol.* **2006**, *40*, 5181–5192.
- (6) Lee, H.-S.; Torres, C. I.; Rittmann, B. E. Effects of Substrate Diffusion and Anode Potential on Kinetic Parameters for Anode-Respiring Bacteria. *Environ. Sci. Technol.* **2009**, *43*, 7571–7577.
- (7) Jiang, D.; Li, B. Granular activated carbon single-chamber microbial fuel cells (GAC-SCMFCs): A design suitable for large-scale wastewater treatment processes. *Biochem. Eng. J.* **2009**, *47*, 31–37.
- (8) Li, Z.; Zhang, X.; Zeng, Y.; Lei, L. Electricity production by an overflow-type wetted-wall microbial fuel cell. *Bioresour. Technol.* **2009**, *100*, 2551–2555.
- (9) Liu, J.; Lowy, D.; Baumann, R.; Tender, L. Influence of anode pretreatment on its microbial colonization. *J. Appl. Microbiol.* **2007**, *102*, 177–183.
- (10) Sleutels, T. H. J. A.; Lodder, R.; Hamelers, H. V. M.; Buisman, C. J. N. Improved performance of porous bio-anodes in microbial electrolysis cells by enhancing mass and charge transport. *Int. J. Hydrogen Energy* **2009**, *34*, 9655–9661.

- (11) Zhou, M.; Chi, M.; Luo, J.; He, H.; Jin, T. An overview of electrode materials in microbial fuel cells. *J. Power Sources* **196**, 4427–4435.
- (12) You, S.-J.; Ren, N.-Q.; Zhao, Q.-L.; Kiely, P. D.; Wang, J.-Y.; Yang, F.-L.; Fu, L.; Peng, L. Improving phosphate buffer-free cathode performance of microbial fuel cell based on biological nitrification. *Biosens. Bioelectron.* **2009**, *24*, 3698–3701.
- (13) Wang, B. Recent development of non-platinum catalysts for oxygen reduction reaction. *J. Power Sources* **2005**, *152*, 1–15.
- (14) Ter Heijne, A.; Hamelers, H. V. M.; Buisman, C. J. N. Microbial Fuel Cell Operation with Continuous Biological Ferrous Iron Oxidation of the Catholyte. *Environ. Sci. Technol.* **2007**, *41*, 4130–4134.
- (15) Rismani-Yazdi, H.; Carver, S. M.; Christy, A. D.; Tuovinen, O. H. Cathodic limitations in microbial fuel cells: An overview. *J. Power Sources* **2008**, *180*, 683–694.
- (16) Aldrovandi, A.; Marsili, E.; Stante, L.; Paganin, P.; Tabacchioni, S.; Giordano, A. Sustainable power production in a membrane-less and mediator-less synthetic wastewater microbial fuel cell. *Bioresour. Technol.* **2009**, *100*, 3252–3260.
- (17) Ter Heijne, A.; Hamelers, H. V. M.; de Wilde, V.; Rozendal, R. A.; Buisman, C. J. N. A Bipolar Membrane Combined with Ferric Iron Reduction as an Efficient Cathode System in Microbial Fuel Cells. *Environ. Sci. Technol.* **2006**, *40*, 5200–5205.
- (18) Sleutels, T. H. J. A.; Hamelers, H. V. M.; Buisman, C. J. N. Effect of mass and charge transport speed and direction in porous anodes on microbial electrolysis cell performance. *Bioresour. Technol.* **102**, 399–403.
- (19) Rozendal, R. A.; Hamelers, H. V. M.; Rabaey, K.; Keller, J.; Buisman, C. J. N. Towards practical implementation of bioelectrochemical wastewater treatment. *Trends Biotechnol.* **2008**, *26*, 450–459.
- (20) Pickard, W. F.; Shen, A. Q.; Hansing, N. J. Parking the power: Strategies and physical limitations for bulk energy storage in supply-demand matching on a grid whose input power is provided by intermittent sources. *Renew. Sustain. Energy Rev.* **2009**, *13*, 1934–1945.

- (21) Price, A. Electrical energy storage - a review of technology options. *Civ. Eng.* **2005**, *158*, 52–58.
- (22) Ibrahim, H.; Ilinca, A.; Perron, J. Energy storage systems--Characteristics and comparisons. *Renew. Sustain. Energy Rev.* **2008**, *12*, 1221–1250.
- (23) Hall, P. J.; Mirzaeian, M.; Fletcher, S. I.; Sillars, F. B.; Rennie, A. J. R.; Shitta-Bey, G. O.; Wilson, G.; Cruden, A.; Carter, R. Energy storage in electrochemical capacitors: designing functional materials to improve performance. *Energy Environ. Sci.* **2010**, *3*, 1238–1251.
- (24) Dewan, A.; Beyenal, H.; Lewandowski, Z. Intermittent Energy Harvesting Improves the Performance of Microbial Fuel Cells. *Environ. Sci. Technol.* **2009**, *43*, 4600–4605.
- (25) Moomaw, W. Renewable Energy and Climate Change An Overview. *IPCC Scoping Meet. Renew. Energy Sources - Proc.* **2008**, 3–32.
- (26) Berndes, G.; Hoogwijk, M.; van den Broek, R. The contribution of biomass in the future global energy supply: a review of 17 studies. *Biomass and Bioenergy* **2003**, *25*, 1–28.
- (27) Aelterman, P.; Rabaey, K.; Clauwaert, P.; Verstraete, W. Microbial Fuel Cells for wastewater treatment. *Water Sci. Technol.* **2006**, *54*, 9–15.
- (28) Logan, B. E.; Hamelers, B.; Rozendal, R.; Schröder, U.; Keller, J.; Freguia, S.; Aelterman, P.; Verstraete, W.; Rabaey, K. Microbial fuel cells: Methodology and technology. *Environ. Sci. Technol.* **2006**, *40*, 5181–5192.
- (29) Obreja, V. V. N. On the performance of supercapacitors with electrodes based on carbon nanotubes and carbon activated material--A review. *Phys. E Low-dimensional Syst. Nanostructures* **2008**, *40*, 2596–2605.
- (30) Kim, Y.; Hatzell, M. C.; Hutchinson, A. J.; Logan, B. E. Capturing power at higher voltages from arrays of microbial fuel cells without voltage reversal. *Energy Environ. Sci.* **2011**, *4*, 4662–4667.
- (31) Ter Heijne, A.; Hamelers, H. V. M.; Saakes, M.; Buisman, C. J. N. Performance of non-porous graphite and titanium-based anodes in microbial fuel cells. *Electrochim. Acta* **2008**, *53*, 5697–5703.

- (32) Atkins, P. W. *Physical Chemistry*; VCH Wiley Interscience: Weinheim, 1990; Vol. 1.
- (33) Logan, B. E.; Regan, J. M. Microbial Fuel Cells: Challenges and Applications. *Environ. Sci. Technol.* **2006**, *40*, 5172–5180.
- (34) Uría, N.; Muñoz Berbel, X.; Sánchez, O.; Muñoz, F. X.; Mas, J. Transient Storage of Electrical Charge in Biofilms of *Shewanella oneidensis* MR-1 Growing in a Microbial Fuel Cell. *Environ. Sci. Technol.* **2011**, *article in.*
- (35) Torres, C. I.; Kato Marcus, A.; Rittmann, B. E. Proton transport inside the biofilm limits electrical current generation by anode-respiring bacteria. *Biotechnol. Bioeng.* **2008**, *100*, 872–881.
- (36) Schoenung, S. M.; Hassenzuhl, W. V. *Long vs. Short-Term Energy Storage: Sensitivity Analysis*; Sandia National Laboratories, 2007.
- (37) Grondin, F.; Perrier, M.; Tartakovsky, B. Microbial fuel cell operation with intermittent connection of the electrical load. *J. Power Sources* **2012**, *208*, 18–23.
- (38) Liang, P.; Wu, W.; Wei, J.; Yuan, L.; Xia, X.; Huang, X. Alternate Charging and Discharging of Capacitor to Enhance the Electron Production of Bioelectrochemical Systems. *Environ. Sci. Technol.* **2011**, *45*, 6647–6653.
- (39) Hatzell, M. C.; Kim, Y.; Logan, B. E. Powering microbial electrolysis cells by capacitor circuits charged using microbial fuel cell. *J. Power Sources* **2013**, *229*, 198–202.
- (40) Deeke, A.; Sleutels, T. H. J. A.; Hamelers, H. V. M.; Buisman, C. J. N. Capacitive Bioanodes Enable Renewable Energy Storage in Microbial Fuel Cells. *Environ. Sci. Technol.* **2012**, *46*, 3554–3560.
- (41) Emmenegger, C.; Mauron, P.; Sudan, P.; Wenger, P.; Hermann, V.; Gallay, R.; Züttel, A. Investigation of electrochemical double-layer (ECDL) capacitors electrodes based on carbon nanotubes and activated carbon materials. *J. Power Sources* **2003**, *124*, 321–329.
- (42) Tsay, K.-C.; Zhang, L.; Zhang, J. Effects of electrode layer composition/thickness and electrolyte concentration on both specific

capacitance and energy density of supercapacitor. *Electrochim. Acta* **2012**, *60*, 428–436.

- (43) Haugstad, G. *Atomic Force Microscopy: Understanding Basic Modes and Advanced Applications*; Wiley, 2012.
- (44) Deeke, A.; Sleutels, T. H. J. A.; Heijne, A. Ter; Hamelers, H. V. M.; Buisman, C. J. N. Influence of the thickness of the capacitive layer on the performance of bioanodes in Microbial Fuel Cells. *J. Power Sources* **2013**, *243*, 611–616.
- (45) Dreszer, C.; Vrouwenvelder, J. S.; Paulitsch-Fuchs, A. H.; Zwijnenburg, A.; Kruithof, J. C.; Flemming, H.-C. Hydraulic resistance of biofilms. *J. Memb. Sci.* **2013**, *429*, 436–447.
- (46) Wagterveld, R. M.; Miedema, H.; Witkamp, G.-J. Effect of Ultrasonic Treatment on Early Growth during CaCO<sub>3</sub> Precipitation. *Cryst. Growth Des.* **2012**, *12*, 4403–4410.
- (47) Boels, L.; Keesman, K. J.; Witkamp, G.-J. Adsorption of Phosphonate Antiscalant from Reverse Osmosis Membrane Concentrate onto Granular Ferric Hydroxide. *Environ. Sci. Technol.* **2012**, *46*, 9638–9645.
- (48) Ter Heijne, A.; Hamelers, H. V. M.; Buisman, C. J. N. Microbial fuel cell operation with continuous biological ferrous iron oxidation of the catholyte. *Environ. Sci. Technol.* **2007**, *41*, 4130–4134.
- (49) Kuntke, P.; Geleji, M.; Bruning, H.; Zeeman, G.; Hamelers, H. V. M.; Buisman, C. J. N. Effects of ammonium concentration and charge exchange on ammonium recovery from high strength wastewater using a microbial fuel cell. *Bioresour. Technol.* **2011**, *102*, 4376–4382.
- (50) Sales, B. B.; Liu, F.; Schaetzle, O.; Buisman, C. J. N.; Hamelers, H. V. M. Electrochemical characterization of a supercapacitor flow cell for power production from salinity gradients. *Electrochim. Acta* **2012**, *86*, 298–304.
- (51) Deeke, A.; Sleutels, T. H. J. A.; Hamelers, H. V. M.; Buisman, C. J. N. Capacitive bioanodes enable renewable energy storage in microbial fuel cells. *Environ. Sci. Technol.* **2012**, *46*, 3554–3560.

- (52) Ahmad, A. L.; Ideris, N.; Ooi, B. S.; Low, S. C.; Ismail, A. Synthesis of polyvinylidene fluoride (PVDF) membranes for protein binding: Effect of casting thickness. *J. Appl. Polym. Sci.* **2013**, *128*, 3438–3445.
- (53) Tovey, E. R.; Baldo, B. A. Protein binding to nitrocellulose, nylon and PVDF membranes in immunoassays and electroblotting. *J. Biochem. Biophys. Methods* **1989**, *19*, 169–183.
- (54) Min, B.; Cheng, S.; Logan, B. E. Electricity generation using membrane and salt bridge microbial fuel cells. *Water Res.* **2005**, *39*, 1675–1686.
- (55) Kim, J. R.; Cheng, S.; Oh, S.-E.; Logan, B. E. Power generation using different cation, anion, and ultrafiltration membranes in microbial fuel cells. *Environ. Sci. Technol.* **2007**, *41*, 1004–1009.
- (56) Liu, H.; Ramnarayanan, R.; Logan, B. E. Production of electricity during wastewater treatment using a single chamber microbial fuel cell. *Environ. Sci. Technol.* **2004**, *38*, 2281–2285.
- (57) Rabaey, K.; Clauwaert, P.; Aelterman, P.; Verstraete, W. Tubular microbial fuel cells for efficient electricity generation. *Environ. Sci. Technol.* **2005**, *39*, 8077–8082.
- (58) Michaelidou, U.; Ter Heijne, A.; Euverink, G. J. W.; Hamelers, H. V. M.; Stams, A. J. M.; Geelhoed, J. S. Microbial communities and electrochemical performance of titanium-based anodic electrodes in a microbial Fuel Cell. *Appl. Environ. Microbiol.* **2011**, *77*, 1069–1075.
- (59) Schröder, U.; Schröder, U. Anodic electron transfer mechanisms in microbial fuel cells and their energy efficiency. *Phys. Chem. Chem. Phys.* **2007**, *9*, 2619.
- (60) Lovley, D. R. Microbial fuel cells: novel microbial physiologies and engineering approaches. *Curr. Opin. Biotechnol.* **2006**, *17*, 327–332.
- (61) Cheng, S. A.; Logan, B. E. Ammonia treatment of carbon cloth anodes to enhance power generation of microbial fuel cells. *Electrochem. Commun.* **2007**, *9*, 492–496.
- (62) Min, B.; Román, Ó. B.; Angelidaki, I. Importance of temperature and anodic medium composition on microbial fuel cell (MFC) performance. *Biotechnol. Lett.* **2008**, *30*, 1213–1218.

- (63) Aelterman, P.; Rabaey, K.; Clauwaert, P.; Verstraete, W. Microbial fuel cells for wastewater treatment. *Water Sci. Technol.* **2006**, *54*, 9–15.
- (64) Ahn, Y.; Logan, B. E. Effectiveness of domestic wastewater treatment using microbial fuel cells at ambient and mesophilic temperatures. *Bioresour. Technol.* **2006**, *101*, 469–475.
- (65) Cha, J.; Choi, S.; Yu, H.; Kim, H.; Kim, C. Directly applicable microbial fuel cells in aeration tank for wastewater treatment. *Bioelectrochemistry* **2006**, *78*, 72–79.
- (66) Heijne, A. T.; Liu, F.; Weijden, R. V. D.; Weijma, J.; Buisman, C. J. N.; Hamelers, H. V. M.; Ter Heijne, A. Copper recovery combined with electricity production in a microbial fuel cell. *Environ. Sci. Technol.* **2010**, *44*, 4376–4381.
- (67) Lefebvre, O.; Ooi, W. K.; Tang, Z.; Abdullah-Al-Mamun, M.; Chua, D. H. C.; Ng, H. Y. Optimization of a Pt-free cathode suitable for practical applications of microbial fuel cells. *Bioresour. Technol.* **2009**, *100*, 4907–4910.
- (68) Dekker, A.; Ter Heijne, A.; Saakes, M.; Hamelers, H. V. M.; Buisman, C. J. N. Analysis and improvement of a scaled-up and stacked microbial fuel cell. *Environ. Sci. Technol.* **2009**, *43*, 9038–9042.
- (69) Logan, B. E. Scaling up microbial fuel cells and other bioelectrochemical systems. *Appl. Microbiol. Biotechnol.* **2010**, *85*, 1665–1671.
- (70) Bond, D. R.; Lovley, D. R. Electricity production by *Geobacter sulfurreducens* attached to electrodes. *Appl. Environ. Microbiol.* **2003**, *69*, 1548–1555.
- (71) Park, D.; Zeikus, J. Impact of electrode composition on electricity generation in a single-compartment fuel cell using *Shewanella putrefaciens*. *Appl. Microbiol. Biotechnol.* **2002**, *59*, 58–61.
- (72) Borole, A. P.; Hamilton, C. Y.; Vishnivetskaya, T.; Leak, D.; Andras, C. Improving power production in acetate-fed microbial fuel cells via enrichment of exoelectrogenic organisms in flow-through systems. *Biochem. Eng. J.* **2009**, *48*, 71–80.
- (73) Arends, J.; Verstraete, W. 100 years of microbial electricity production: three concepts for the future. *Microb. Biotechnol.* **2012**, *5*, 333–346.

- (74) Ter Heijne, A.; Liu, F.; van Rijnsoever, L. S.; Saakes, M.; Hamelers, H. V. M.; Buisman, C. J. N. Performance of a scaled-up Microbial Fuel Cell with iron reduction as the cathode reaction. *J. Power Sources* **2011**, *In press*.
- (75) Janicek, A.; Fan, Y.; Liu, H. Design of microbial fuel cells for practical application: a review and analysis of scale-up studies. *Biofuels* **2014**, *5*, 79–92.
- (76) Clauwaert, P.; Van Der Ha, D.; Boon, N.; Verbeken, K.; Verhaege, M.; Rabaey, K.; Verstraete, W. Open air biocathode enables effective electricity generation with microbial fuel cells. *Environ. Sci. Technol.* **2007**, *41*, 7564–7569.
- (77) Sleutels, T. H. J. A. . b; Hamelers, H. V. M. .; Rozendal, R. A. .; Buisman, C. J. N. . b. Ion transport resistance in Microbial Electrolysis Cells with anion and cation exchange membranes. *Int. J. Hydrogen Energy* **2009**, *34*, 3612–3620.
- (78) Kong, W.; Guo, Q.; Wang, X.; Yue, X. Electricity Generation from Wastewater Using an Anaerobic Fluidized Bed Microbial Fuel Cell. *Ind. Eng. Chem. Res.* **2011**, *50*, 12225–12232.
- (79) Liu, J.; Zhang, F.; He, W.; Zhang, X.; Feng, Y.; Logan, B. E. Intermittent contact of fluidized anode particles containing exoelectrogenic biofilms for continuous power generation in microbial fuel cells. *J. Power Sources* **2014**, *261*, 278–284.
- (80) Freguia, S.; Rabaey, K.; Yuan, Z. G.; Keller, J. Electron and carbon balances in microbial fuel cells reveal temporary bacterial storage behavior during electricity generation. *Environ. Sci. Technol.* **2007**, *41*, 2915–2921.
- (81) Cao, Q.; Xie, K.-C.; Lv, Y.-K.; Bao, W.-R. Process effects on activated carbon with large specific surface area from corn cob. *Bioresour. Technol.* **2006**, *97*, 110–115.

# Appendix

## Appendix to Chapter 2

The AFM-picture is in Figure A1. The AFM revealed a maximum pore size of 2  $\mu\text{m}$  for the non-capacitive electrode and a maximum pore-size of 5  $\mu\text{m}$  for the capacitive electrode.

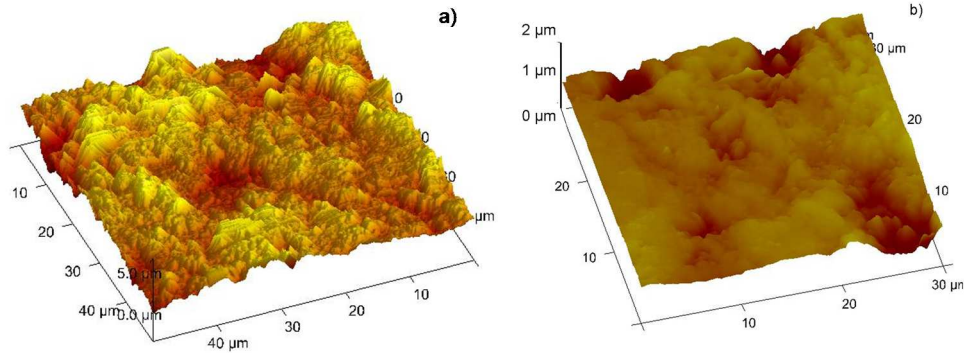


Figure A1: The top view of the capacitive electrode is in figure S1 a, and the top view of the non-capacitive electrode is in figure S1b.

In Figure A2 a and b are the potential behavior and the current density of the charge-discharge experiment with 5 minutes of charging and 20 minutes of discharging. The potential behavior and the current density behavior of the experiment with 10 minutes of charging and 20 minutes of discharging are in figure A2 c and d. The potential behavior and the current density behavior of the experiment with 20 minutes of charging and 10 minutes of discharging are in figure A2e and f and the potential behavior and the current density behavior of the experiment with 5 minutes of charging and 10 minutes of discharging are in Figure A2 g and h. The typical potential behavior of each electrode is in Figure A2 a, c, e and g. During the first charge-discharge experiment which is in Figure A2a the non-capacitive electrode experienced an immediate potential drop from -0.300 V down to -0.480 V when the cells were controlled at zero current.

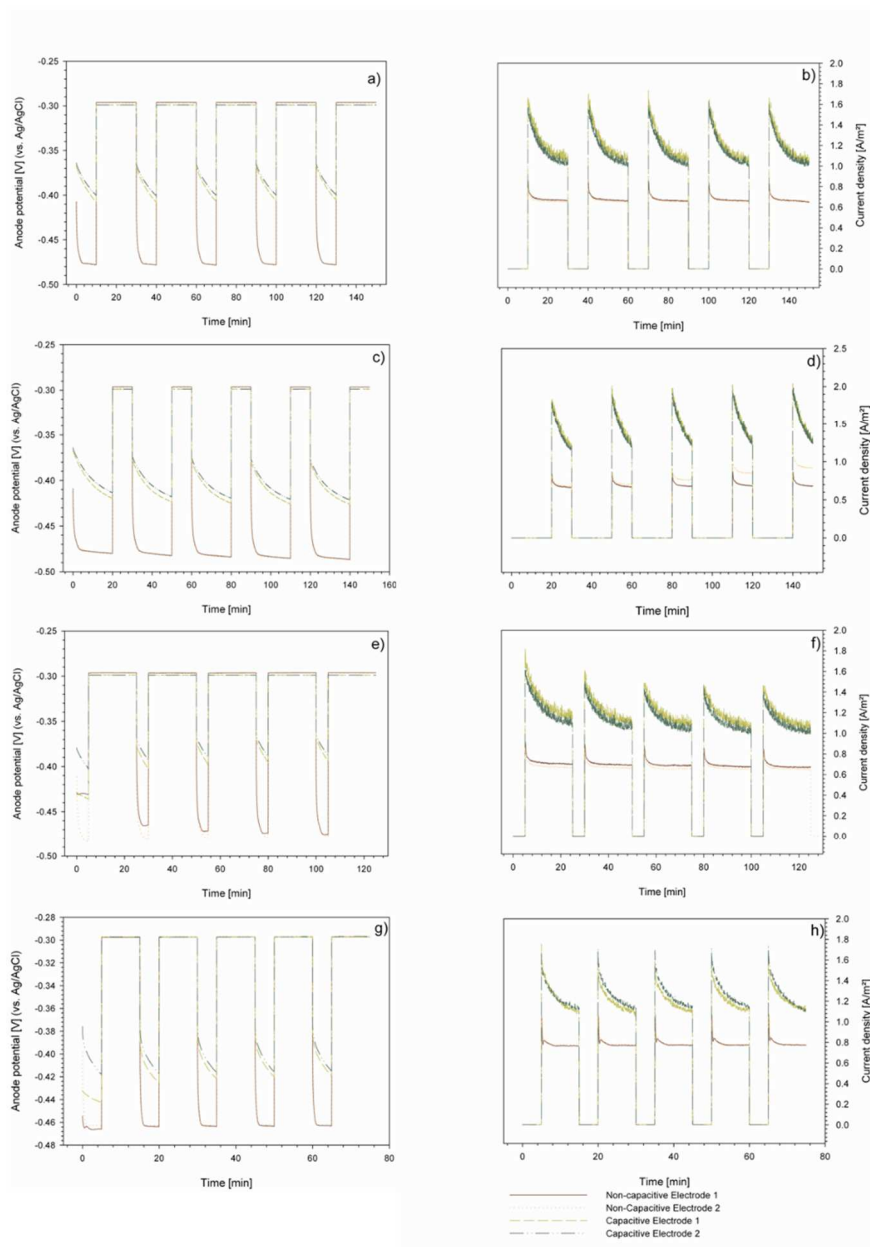
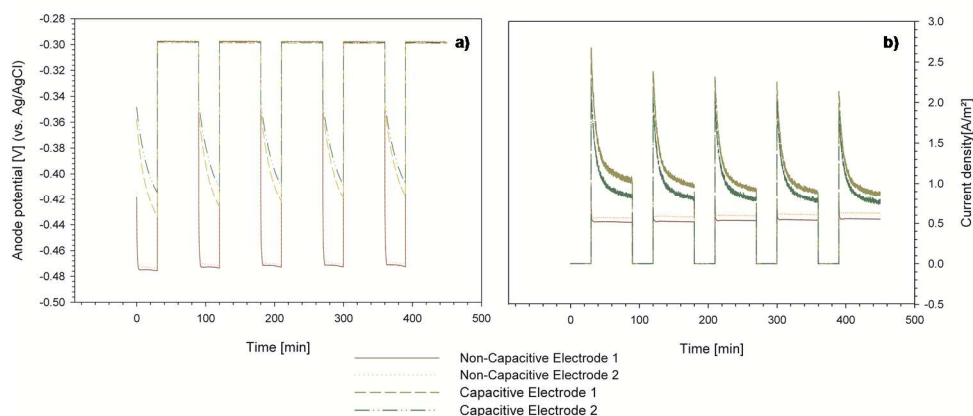


Figure A2: The charge-discharge graph showing in a), c), e) and g) the potential behavior of each experiment and in b), d), f) and h) showing the different current density behavior of each experiment.

The potential remained stable at -0.480V during both cycles. The capacitive electrode experienced a much smaller potential drop from -0.300V down to -0.410 V when the cells were controlled at zero current. The potential drop of the capacitive electrode remained stable over each cycle.

During the second set of the charge-discharge experiments which is in Figure A2c, the noncapacitive electrode experienced an immediate potential drop from -0.300 V down to -0.480V when the cells were controlled at zero current. The capacitive electrode had a potential drop from -0.300V down to -0.420 V in this experiment, which remained stable over each cycle. During the third set of the charge-discharge experiments, in Figure A2 e: the non-capacitive electrode had a potential drop from -0.300V down to -0.480 V when the cells were controlled at zero current, whereas the capacitive electrode had a potential drop from -0.300 V down to -0.400 V. During the fourth charge-discharge experiment shown in Figure A2 g the potential drop of the non-capacitive electrode was smaller from -0.300 V down to -0.460V. The capacitive electrode experienced a potential drop from -0.300 V down to -0.420 V.

The typical current density behavior is in Figure A2 b, d, f and h. The current density behavior of the non-capacitive and the capacitive electrode was the same throughout each set of the charge-discharge experiment in Figure A2 b, d, and f. The non-capacitive electrode had a small peak current density of 0.9 A/m<sup>2</sup> and reached a stable current density output of 0.7 A/m<sup>2</sup>. The capacitive electrode reached a higher peak current density of 1.6 A/m<sup>2</sup> through 1.9 A/m<sup>2</sup>, and the stable current density output during all experiments was 1.1 A/m<sup>2</sup> through 1.2 A/m<sup>2</sup>. Throughout the longer experiments the capacitive electrode was performing even better than expected.



**Figure A3:** The charge-discharge graph with 30 minutes of charging and 60 minutes of discharging. In a) is the anode potential behavior and in b) is the current density behavior.

In Figure A3 is the charge-discharge graph of the experiment with 30 minutes of charging and 60 minutes of discharging. In Figure A3a) is the typical behavior of the anode potential and in Figure A3b) the typical behavior of the current density. The non-capacitive electrode has a potential drop from -0.300 V to -0.470V, when the electrodes are switched to zero current. This potential remained stable through each cycle. During this experiment the first capacitive electrode had slight difference in behavior from the second capacitive electrode. The capacitive electrode 1 had a potential drop from -0.300 V to -0.420 V. The capacitive electrode 2 however, had a potential drop from -0.300 V to -0.410V. Those differences in potential remained stable throughout the whole experiment.

The current density behavior of the non-capacitive electrode has a small peak of 0.8 A/m<sup>2</sup> and a stable current density output of 0.7 A/m<sup>2</sup>. The current density behavior of the capacitive electrode has peak current density of 2.3 A/m<sup>2</sup> and a stable current density output of 0.9 A/m<sup>2</sup>. The stable current density output is what was expected from this electrode from the polarization curve. According to

the long charging period the capacitive electrode achieved a higher storage of charge and therefore the peak current density of the capacitive electrode is higher.

The anode potential and current density behavior of each electrode during the charge-discharge experiment with 60 minutes of charging and 90 minutes of discharging are in Figure A4.

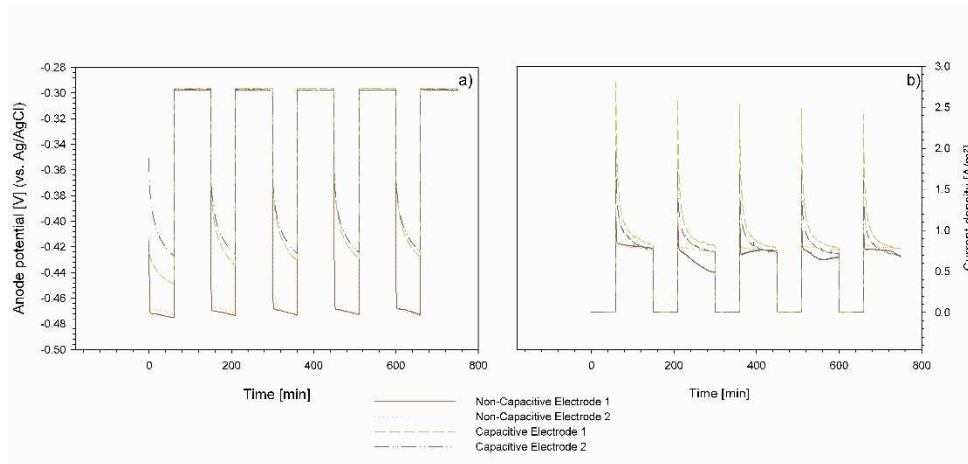


**Figure A4:** The charge-discharge graph with 60 minutes of charging and 90 minutes of discharging. In a) is the anode potential behavior and in b) is the current density behavior.

In Figure A4a) is the anode potential behavior of each electrode. The anode potential behavior of the non-capacitive electrode shows a potential drop from -0.300 V down to -0.470V. The capacitive electrode has an initial potential drop from 0.070V from -0.300 V to -0.370V. Afterwards the potential converged slowly to -0.430 V. During this experiment the capacitive electrode achieved a lower potential, this could be due to the longer charging period. For the current density behavior of the non-capacitive electrode, there is again a small peak in the current density of 0.9 A/m<sup>2</sup> and a stable current density output of 0.7 A/m<sup>2</sup>. During this experiment the non-capacitive electrode 1 experienced some instability. The capacitive electrode had a peak current density of 2.5 A/m<sup>2</sup> and a stable current density of 0.9 A/m<sup>2</sup>. The difference in current density was really small during this

experiment and this resulted also in a small difference of charge recovery, as can be seen in Table 2.3.

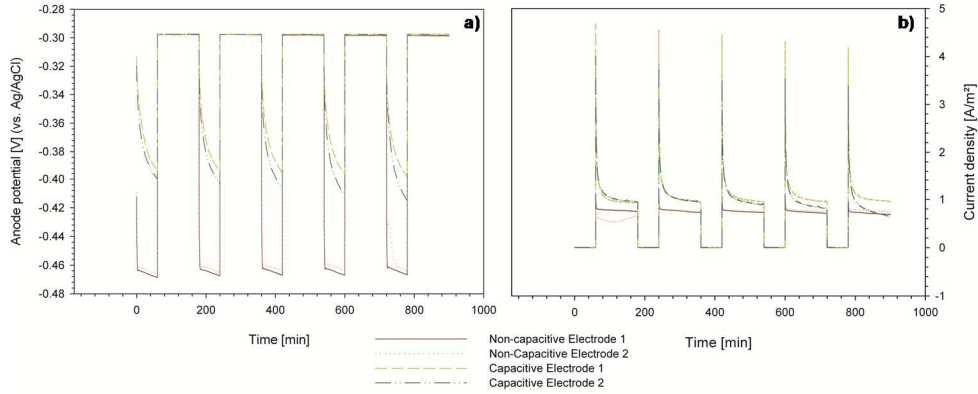


Figure A5: The charge-discharge graph with 60 minutes of charging and 120 minutes of discharging.

In Figure A5 are the anode potential behavior and the current density behavior of the non-capacitive and capacitive electrode during the charge-discharge experiment with 60 minutes of charging and 120 minutes of discharging. In Figure A5a) the anode potential behavior of each electrode is shown. The non-capacitive electrode had a potential drop from -0.300 V down to -0.470V. This was the same potential drop as measured during each other experiment. The capacitive electrode had an initial potential drop of 0.040 V down to -0.340V. From this the potential dropped slowly to the final value of -0.400 V. This anode potential is not as low as it was during all other experiments. The same can be found for the current density behavior in Figure A5b). The non-capacitive electrode had a small peak current density of 0.9 A/m<sup>2</sup> and a stable current density of 0.8 A/m<sup>2</sup>. This stable current density is reflecting the current density value which is expected according to the polarization curve. The capacitive electrode had a high peak current density of 4 A/m<sup>2</sup> and a stable current density of 1 A/m<sup>2</sup>. The stable current density of the capacitive electrode is also reflecting the value that would have been expected

from the polarization curve. During this experiment the electrodes are operating at a set anode potential for such a long time that they are able to achieve stable conditions again. Furthermore the difference between the current density of the non-capacitive electrode and the capacitive electrode was smaller which can be seen in the charge recovery of this experiment in Table 2.3.

The calculated cumulative total charge is shown in Figure A6 and Figure A7. In figure S6 is the cumulative total charge for the experiment with 30 minutes of charging and 60 minutes of discharging.

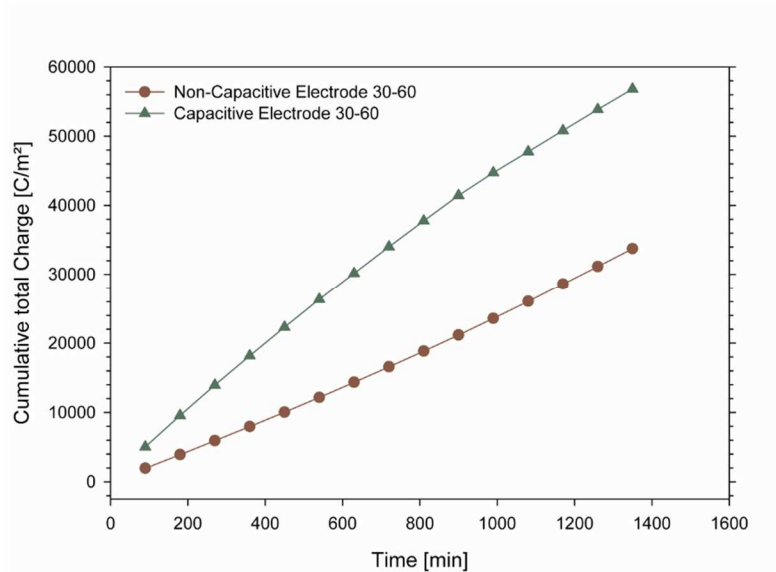


Figure A6: The cumulative total charge of the non-capacitive electrode and the capacitive electrode during the experiment with 30 minutes of charging time and 60 minutes of discharging time.

During this experiment the capacitive electrode was outperforming the non-capacitive electrode by far. The non-capacitive electrode was able to achieve a cumulative total charge of 33,743 C/m<sup>2</sup>, whereas the capacitive electrode was able to achieve a cumulative total charge of 56,809 C/m<sup>2</sup>. This difference in performance could already be seen in the current density behavior in Figure A3b). In Figure A7 is the cumulative total charge for the experiments with a charging period of 60 minutes and a discharging period of 90 minutes and of 120 minutes.

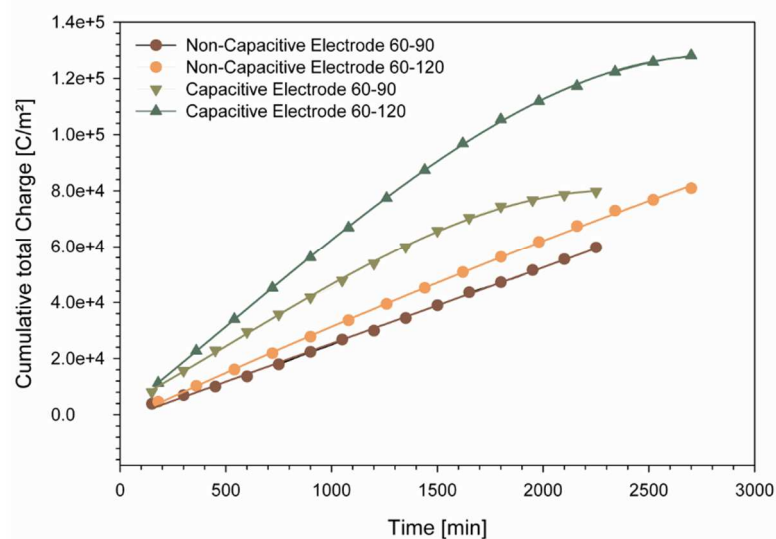


Figure A7: The cumulative total charge of the non-capacitive electrode and the capacitive electrode during the experiment with 60 minutes of charging time and 90 minutes of discharging time and the experiment with 60 minutes of charging time and 120 minutes of discharging time.

The capacitive electrode was still outperforming the non-capacitive electrode during these experiments. During the experiment with 60 minutes of the charging and 90 minutes of discharging the non-capacitive electrode achieved a cumulative total charge of 59,673 C/m<sup>2</sup> and the capacitive electrode achieved a cumulative total charge of 79,750 C/m<sup>2</sup>. The instability in the performance of the capacitive electrode which were shown in Figure A4b) are also visible in the graph of the cumulative total charge. During the experiment with 60 minutes of charging and 120 minutes of discharging the non-capacitive electrode achieved a cumulative total charge of 80,895 C/m<sup>2</sup> and the capacitive electrode achieved a cumulative total charge of 128,160 C/m<sup>2</sup>. The capacitive electrode was performing better during this experiment again compared to the experiment with 60 minutes of charging and 90 minutes of discharging. This can also be seen from the charge recoveries in Table 2.3.



## Summary

The energy supply and especially the electricity supply of today's society depends strongly on fossil fuels. But with the depletion of fossil fuels and the rising awareness of the environmental pollution by the use of these fossil fuels it is necessary to think about alternative possibilities. **Chapter 1** describes the current status of our primary energy use. From the 1970's to 2008 the world electricity use almost doubled and it is expected to increase even more, due to increasing wealth all over the world and the forthcoming change in lifestyle. Keeping in mind that the fossil fuel sources are depleting, the urge to look for renewable alternatives is increasing. Sun, wind, hydro and biomass are the renewable sources which are already in use today. However, for sun, wind and hydro-energy their discontinuous availability limits further development and therefore storage of the produced electricity is required. Another renewable electricity technology is the Microbial Fuel Cell. In the MFC organic compounds of wastewater can directly be converted into electrical energy. MFCs are one of the emerging technology of the past decade and many researchers have looked into improvement of current and power density. The development of the current and power density stagnated during the past few years and new impulses for future research are needed to bring this to practical application. Challenges which need to be overcome are limitations due to electrode spacing and electrolyte conductivity, electrode conductivity and required continuous treatment of wastewater. The continuous treatment of wastewater requires storage, either of the wastewater or of the electricity. Storage of electricity can be done by combining the operation of the MFC with a capacitor.

In **Chapter 2** an integrated system for storage of renewable electricity in an MFC was developed. The integrated storage was built by inserting a capacitive electrode in the anode compartment and thereby creating a capacitive bioanode. This capacitive bioanode was compared with a noncapacitive bioanode based on

performance during polarization curves and the storage capacity during charge-discharge experiments.

During polarization curves the capacitive electrode reached a maximum current density of  $1.02 \pm 0.04 \text{ A/m}^2$ , whereas the noncapacitive electrode reached a current density output of only  $0.79 \pm 0.03 \text{ A/m}^2$ , both at an anode potential of  $-0.300\text{V}$ (vs. Ag/AgCl). During the charge-discharge experiment with 5 minutes of charging and 20 min of discharging the capacitive electrode was able to store a total of  $22,831 \text{ C/m}^2$ , whereas the noncapacitive electrode was only able to store  $12,195 \text{ C/m}^2$ . Regarding the charge recovery of each electrode, the capacitive electrode was able to recover 52.9% more charge during each charge-discharge experiment compared to the noncapacitive electrode.

The capacitive electrode outperformed the noncapacitive electrode throughout each charge-discharge experiment. This chapter showed that when using the MFC with a capacitive bioanode the performance was improved and the electricity was stored.

The storage capacity of this first capacitive bioanode was further investigated during the studies for **Chapter 3** and **Chapter 4**. The capacitive layer of the capacitive bioanode was varied in its material parameters in order to determine the optimal composition. In **Chapter 3** different thicknesses of capacitive layers were used to study the effects on its performance. In Chapter 2 the MFC was used with an integrated capacitive bioanode of 0.5mm thickness. In this chapter the thickness of the capacitive electrode was varied in three steps: 0.2 mm, 0.5 mm and 1.5 mm. Prior to the use as capacitive bioanode each capacitive electrode was analyzed for their surface properties using BET-Analysis and SEM-pictures were taken. After that each of these capacitive electrodes was tested in the MFC setup using polarization curves to see the constant current density and charge-discharge experiments to see the maximum charge recovery.

The capacitive electrode with a thickness of 0.2 mm outperformed the other electrodes in all experiments: it reached a maximum current density of 2.53 A/m<sup>2</sup> during polarization curves, and was able to store a cumulative total charge of 96013 C/m<sup>2</sup> during charge-discharge experiments. The highest relative charge recovery for this electrode was 1.4, which means that 40 % more current can be gained from this capacitive electrode during intermittent operation compared to continuous operation of a noncapacitive electrode. Compared to the first capacitive bioanode, investigated in Chapter 2, the charge recovery increased another 36%. Surprisingly, the performance of the MFC decreased when the thickness of the capacitive electrode increased, while the opposite was expected. In **Chapter 4** the recipe for the production of the capacitive layer was varied. The capacitive bioanode is produced by casting a mixture of activated carbon powder and PVDF (Polyvinylidene fluoride) on a current collector, where PVDF acts as a binder. In this study the influence of the PVDF-content of capacitive electrodes on bioanode performance was investigated. Six capacitive electrodes were made with PVDF contents (in weight %) of 2%, 4%, 10%, 14%, 21% and 46%. These capacitive electrodes were first tested for their chemical properties using BET-analysis, galvanostatic charge-discharge experiments, and SEM. Their performance as capacitive bioanode was again studied during polarization curves and charge-discharge experiments. In the polarization curves, during constant current generation, the capacitive electrode with the lowest PVDF content of 2% performed best, reaching a maximum current density of 2.4 A/m<sup>2</sup>. However, when the current density of each electrode was expressed per gram of activated carbon, the electrode with the highest PVDF content of 46% reached the highest current density (36.6 mA/g<sub>AC</sub>). During discontinuous current generation in the charge-discharge experiments, the capacitive bioanode with 21% PVDF achieved a relative charge recovery of 1.8, meaning that it produced 1.8 times (80%) more electricity than a noncapacitive electrode in continuous mode. Again an increase in the charge

recovery compared to the best performing capacitive bioanode of Chapter 3 was found.

The results from **Chapters 2-4** show that microorganisms are able to grow on capacitive material and are able to store electrons in an electrode which is not connected to the counter electrode (open electric circuit). The microorganisms are able to adapt to “new” circumstances and to perform even better (increasing charge recoveries). In **Chapter 5** a novel reactor concept was introduced to make use of these properties of the microorganisms. This novel reactor concept was based on the use of activated carbon granules to create a capacitive fluidized bioanode. The use of granular electrodes in MFCs is attractive because granules provide a cost-effective way to create a high electrode surface area, which is essential to achieve high current and power densities. Activated carbon granules are colonized by the microorganisms, which convert organic compounds from the wastewater to protons, carbon dioxide and electrons and store the electrons inside of the granule. The electricity is harvested from the AC granules in an external discharge cell. The proof-of-principle of the fluidized capacitive system had a total anode volume of 2 L. After a start-up period of 100 days, the current density increased from 0.56 A/m<sup>2</sup> with 100 g AC granules, to 0.99 A/m<sup>2</sup> with 150 g AC granules, to 1.3 A/m<sup>2</sup> with 200 g AC granules. Prior to this experiment the contact between the moving AC granules and the current collector was confirmed in an experiment without biofilm. The contact was likely the reason for current production in the fluidized capacitive system with biofilm. SEM pictures confirmed that a biofilm was present on the AC granules after operation in the capacitive fluidized bioanode. Although the current densities reported in **Chapter 5** need further improvement, the high surface area of the AC granules in combination with external discharge offers new and promising opportunities for scaling up MFCs. **Chapter 6** presents a reflection on the work which has been presented in this thesis and an outlook to future application. As presented in

Chapter 1 the development of the power densities of MFCs stagnated during the past few years between 2-3 W/m<sup>2</sup>. This was due to the limitations in electrode spacing, electrolyte conductivity and electrode conductivity. And although the power densities which are achieved in this thesis are not directly an improvement of the power densities, the systems used to achieve these power densities offer a lot of new possibilities. With the flat-plate systems the integrated storage concept was introduced into the world of MFCs. The capacitive bioanodes used for the studies on the flat-plate systems improved charge recovery compared to noncapacitive bioanodes with 80%. Based on this, the integrated system was developed further into a capacitive fluidized bioanode, where the charging and the discharging of the fluidizing granules takes place in two separate reactors. Again the power density of this system did not improve compared to the values of the past years, but it offers the solution to some problems. Due to the intensive mixing of the granules (and thereby the microorganisms) with the electrolyte, the COD-concentration is less important. The separation of the charging and discharging process offers the solution to two problems: Electrode spacing and electrolyte conductivity. Since the granules act as a high surface bioanode, the electrode spacing between the current collector and the cathode can be as small as necessary. And since the electrons are stored inside the granule and the protons are stored inside the double layer around the granule, the electrolyte conductivity also becomes less important. Therefore, no transport of ions through the electrolyte is required. During future research the reactor design of the capacitive fluidized bioanode should be optimized.



## Zusammenfassung

Die Energieversorgung und insbesondere die Elektrizitätsversorgung unserer heutigen Gesellschaft hängen sehr stark von den fossilen Brennstoffen ab. Mit der bevorstehenden Erschöpfung der fossilen Brennstoffe und der wachsenden Erkenntnis der Umweltverschmutzung durch die fossilen Brennstoffe ist es notwendig, um über Alternativen nach zu denken. Der heutige Stand unseres Primärenergieverbrauchs wird in **Kapitel 1** beschrieben. Von 1970 bis 2008 hat sich der weltweite Elektrizitätsverbrauch nahezu verdoppelt und es wird erwartet, dass dieser weiter zunimmt, durch wachsenden Reichtum und den daraus entstehenden Veränderungen im Lebensstil. Da die fossilen Brennstoffe endlich sind, nimmt der Druck nach erneuerbaren Alternativen zu suchen zu. Sonne, Wind, Wasser und Biomasse werden heutzutage bereits als alternative Energiequellen genutzt. Jedoch wird der weitere Ausbau von Sonnen-, Wind- und Wasserenergie gebremst, aufgrund der mangelnden Speicherkapazität für die produzierte Elektrizität. Eine weitere erneuerbare Energietechnologie ist die mikrobielle Brennstoffzelle (MFC). In der MFC werden die organischen Bestandteile aus dem Abwasser direkt in elektrische Energie umgesetzt. MFCs sind eine der aufstrebenden Technologien des letzten Jahrzehnts und viele Forscher haben sich mit der Verbesserung der Strom- und der Leistungsdichte beschäftigt. Die Entwicklung der Strom- und Leistungsdichte stagnierte jedoch während der letzten Jahre und neue Impulse für weitere Forschung werden dringend benötigt, um diese Technologie in die Anwendung zu bringen. Herausforderungen die es zu meistern gilt, sind die Beschränkungen die aus dem Elektrodenabstand, der Leitfähigkeit der Elektrolytlösung, der Elektrodenleitfähigkeit und der notwendigen kontinuierlichen Abwasserreinigung entstehen. Die kontinuierliche Abwasserreinigung erfordert entweder die Speicherung des Abwassers oder die Speicherung der Elektrizität. Die Elektrizitätsspeicherung kann erreicht werden,

wenn die Betreibung der MFC mit dem Betreiben eines Kondensators kombiniert wird.

In **Kapitel 2** wurde ein integriertes System für die Speicherung der erneuerbaren Elektrizität der MFC entwickelt. Das integrierte System besteht aus einer kapazitiven Elektrode, welche in die Anode der MFC eingebaut wurde, und somit eine kapazitive Bioanode formt. Diese kapazitive Bioanode wurde mit einer nichtkapazitiven Bioanode während der Polarisationskurven und während der Lade-Entlade-Experimente hinsichtlich der Leistung und der Speicherkapazität verglichen. Während der Polarisationskurven erreichte die kapazitive Elektrode eine maximale Stromdichte von  $1.02 \pm 0.04 \text{ A/m}^2$ , wohingegen die nichtkapazitive Elektrode nur eine Stromdichte von  $0.79 \pm 0.03 \text{ A/m}^2$  erreichte, beides bei einem Anodenpotential von  $-0.300 \text{ V}$  (vs. Ag/AgCl). Während der Lade-Entlade-Experimente, bei denen 5 min geladen und 20min entladen wurde, konnte die kapazitive Elektrode  $22381 \text{ C/m}^2$  speichern, wohingegen die nichtkapazitive Elektrode lediglich  $12195 \text{ C/m}^2$  speichern konnte. Wenn wir die Ladungsrückgewinnung der beiden Elektroden betrachten, dann war die kapazitive Elektrode in der Lage um 52.9% mehr Ladung während der Lade-Entlade-Experimente zu speichern als die nichtkapazitive Elektrode.

Die kapazitive Elektrode erzielte während aller Lade-Entlade-Experimente bessere Ergebnisse als die nichtkapazitive Elektrode. Dieses Kapitel zeigt, dass die Leistung einer MFC verbessert werden kann, wenn eine kapazitive Elektrode benutzt wird und dass die Elektrizität gespeichert werden kann.

Die Speicherkapazität dieser ersten kapazitiven Elektrode wurde weiter untersucht während der Studien für **Kapitel 3** und **4**. Die kapazitive Schicht der kapazitiven Bioanode wurde in ihrer Materialzusammensetzung variiert, um das Optimum zu ermitteln. In **Kapitel 3** wurden verschiedene Schichtdicken der kapazitiven Schicht untersucht, um den Einfluss auf die Leistung zu bestimmen. In **Kapitel 2** wurde eine kapazitive Elektrode mit einer Schichtdicke von 0.5mm verwendet. In **Kapitel**

3 wurden drei verschiedene Schichtdicken verwendet: 0.2 mm, 0.5 mm und 1.5 mm. Vor der Verwendung der Elektroden als Bioanode wurde die Oberfläche einer jeden kapazitiven Elektrode mit BET-Analyse und REM-Bildern untersucht. Danach wurden die kapazitiven Elektroden im MFC-setup mittels Polarisationskurven zur Bestimmung der Stromdichte und Lade-Entlade-Experimenten zur Bestimmung der Speicherkapazität getestet.

Die kapazitive Elektrode mit einer Dicke von 0.2 mm übertraf die anderen Elektroden während aller Experimente: diese Elektrode erreichte eine maximale Stromdichte von  $2.53 \text{ A/m}^2$  in den Polarisationskurven und war in der Lage während der Lade-Entlade-Experimente  $96013 \text{ C/m}^2$  zu speichern. Die höchste relative Ladungsrückgewinnung für diese Elektrode lag bei 1.4, das bedeutet, dass bei der Benutzung dieser Elektrode 40% mehr Strom gewonnen werden kann. Im Vergleich mit der ersten kapazitiven Bioanode aus **Kapitel 2** bedeutet das eine weitere Zunahme der Ladungsrückgewinnung von 36%. Entgegen der Annahme nahm mit zunehmender Dicke die Leistung der kapazitiven Elektroden ab. In **Kapitel 4** wurde das Rezept für die Herstellung der kapazitiven Elektrode verändert. Die kapazitive Elektrode wird hergestellt, indem eine Mischung aus Aktivkohle und PVDF (Polyvinylidenfluorid) auf einem Stromkollektor ausgestrichen wird, das PVDF ist hierbei das Bindemittel. In dieser Studie wurde der Einfluss der Menge PVDF in der kapazitiven Elektrode untersucht. Sechs kapazitive Elektroden wurden mit verschiedenen Mengen PVDF (Gewichts-%) hergestellt, nämlich 2%, 4%, 10%, 14%, 21% und 46%. Diese kapazitiven Elektroden wurden zuerst mittels einer BET-Analyse, Galvanostatischen Lade-Entlade-Experimenten und REM-Bildern auf ihre chemischen Eigenschaften untersucht. Die Leistung der kapazitiven Bioanoden wurde während Polarisationskurven und Lade-Entlade-Experimenten untersucht. Während der konstanten Stromproduktion in den Polarisationskurven erreichte die kapazitive Elektrode mit nur 2% PVDF-Inhalt die höchste Stromdichte von  $2.4 \text{ A/m}^2$ . Wenn jedoch die

Stromdichte einer jeden kapazitiven Elektrode pro Gramm Aktivkohle ausgedrückt wird, dann erreichte die kapazitive Elektrode mit 46% PVDF-Inhalt die höchste Stromdichte ( $36.6\text{mA/g}_{\text{AC}}$ ). Während der diskontinuierlichen Stromproduktion der Lade-Entlade-Experimente, erreichte die kapazitive Elektrode mit 21% PVDF-Inhalt eine relative Ladungsrückgewinnung von 1.8, was bedeutet, dass diese Elektrode 80% mehr Strom produziert als eine nichtkapazitive Elektrode im kontinuierlichen Modus. Dies bedeutet wiederum eine Steigerung der Ladungsrückgewinnung verglichen mit der besten Elektrode aus **Kapitel 3**.

Die Ergebnisse der **Kapitel 2-4** zeigen, dass die Mikroorganismen in der Lage sind auf dem kapazitiven Material zu wachsen, und dass sie Elektronen in einer Elektrode speichern können welche nicht direkt an eine Gegenelektrode angeschlossen ist (offener elektrischer Schaltkreis). Die Mikroorganismen können sich demnach an die "neuen" Umstände anpassen und sogar bessere Leistungen erzielen (zunehmende Ladungsrückgewinnung). In **Kapitel 5** wird ein neues Reaktorenkonzept eingeführt, um diese Fähigkeiten der Mikroorganismen zu nutzen. Dieses neue Reaktorkonzept basiert auf dem Gebrauch von Aktivkohlegranulat, welches eine kapazitive Wirbelbett Bioanode kreiert. Der Gebrauch von Aktivkohlegranulat ist vorteilhaft, da kostengünstig eine große Elektrodenoberfläche erreicht wird, dies ist essentiell für das Erzielen hoher Strom- und Leistungsdichten. Das Aktivkohlegranulat wird von den Mikroorganismen kolonisiert, welche die organischen Bestandteile des Abwassers in Protonen, Kohlenstoffdioxid und Elektronen umsetzen und die Elektronen in dem Granulat speichern. In einer externen Entladezelle wird dem Aktivkohlegranulat die Elektrizität entzogen. Das Grundsatzexperiment des kapazitiven Wirbelbettsystems bestand aus einem Reaktorvolumen von 2 L. Nach einer Startperiode von 100 Tagen, nahm die Stromdichte von  $0.56\text{ A/m}^2$  mit 100 g Aktivkohlegranulat auf  $0.99\text{ A/m}^2$  mit 150 g Aktivkohlegranulat und auf  $1.3\text{ A/m}^2$  mit 200 g Aktivkohlegranulat zu. Vor diesem Experiment wurde der Kontakt

zwischen dem Aktivkohlegranulat und dem Stromkollektor in einem Experiment ohne Biofilm getestet. Es ist davon auszugehen, dass der Kontakt zwischen dem Aktivkohlegranulat und dem Stromkollektor zur Stromproduktion in den Experimenten mit Biofilm beiträgt. Nach durchführen der Experimente wurde mittels REM-Bilder ein Biofilm auf dem Aktivkohlegranulat nachgewiesen. Wenn auch die Stromdichten, die in **Kapitel 5** gemessen werden weiterentwickelt werden müssen, so bietet die große Oberfläche des Aktivkohlegranulats in Kombination mit der externen Entladezelle neue und vielversprechende Chancen für die Vergrößerung von MFCs. **Kapitel 6** ist eine Reflektion über die Arbeit die für dieses Buch verrichtet wurde und bietet eine Voraussicht für zukünftige Anwendungen. Wie in **Kapitel 1** gezeigt wurde, stagniert die Entwicklung der Leistungsdichte während der letzten Jahre zwischen 2 und 3 W/m<sup>2</sup>. Diese Stagnation wurde durch Beschränkungen bezüglich des Elektrodenabstands, der Elektrolytleitfähigkeit und der Elektrodenleitfähigkeit verursacht. Wenn auch die Leistungsdichten, die während der Experimente für dieses Buch erreicht wurden noch keine Verbesserung darstellen, so bieten die Systeme die zum Erreichen der Leistungsdichten angewendet wurden viele neue Möglichkeiten. Mit dem Platten-Elektroden-System wurde das integrierte Konzept der Stromspeicherung in der MFC in die Welt der MFCs eingeführt. Die kapazitiven Bioanoden die für diese Experimente eingesetzt wurden verbesserten die Ladungsrückgewinnung im Vergleich zu nichtkapazitiven Bioanoden um 80%. Basierend hierauf wurde das integrierte System weiterentwickelt zu der kapazitiven Wirbelbett-Bioanode, wo das Laden und Entladen der Granulate in getrennten Reaktoren stattfindet. Wiederum zeigte die Leistungsdichte dieses Systems keine Verbesserung der Werte der letzten Jahre, aber es bietet die Lösung für einige Probleme. Durch die intensive Mischung der Granulate (und somit der Mikroorganismen) mit dem Elektrolyten ist die CSB-Konzentration nicht mehr so wichtig. Die Trennung des Lade- und Entladevorgangs bietet die Lösung für zwei Probleme:

Elektrodenabstand und Elektrolytleitfähigkeit. Da das Aktivkohlegranulat eine Groß-Oberflächen-Bioanode ist, kann der Abstand zwischen dem Stromkollektor und der Kathode so klein wie nötig sein. Die Elektronen werden im Granulat gespeichert und die Protonen reichern sich in der Doppelschicht außen um das Granulat an, dadurch wird die Elektrolytleitfähigkeit unbedeutend, da kein Transport von Ionen durch den Elektrolyten erforderlich ist. Zukünftige Forschung sollte das Reaktordesign der kapazitiven Wirbelbett-Bioanode optimieren.

## Samenvatting

De energieproductie en in het bijzonder de elektriciteitsverzorging van onze hedendaagse maatschappij zijn sterk afhankelijk van fossiele brandstoffen. Met het opraken van de fossiele brandstoffen en de toenemende bewustwording van de milieuvervuiling, veroorzaakt door het gebruik van fossiele brandstoffen, is het noodzakelijk om over alternatieven na te denken. **Hoofdstuk 1** omschrijft de actuele stand van ons primair energieverbruik. Van 1970 tot 2008 heeft het wereldwijde elektriciteitsverbruik zich bijna verdubbeld en naar verwachting zal dit nog verder toenemen, door toenemende rijkdom over de gehele wereld en de daaruit voortkomende aanpassingen in levensstijl. Denkend aan het opraken van de fossiele brandstoffen, wordt de noodzaak om naar hernieuwbare alternatieven te kijken alleen maar groter. Zon, wind, water en biomassa zijn al hernieuwbare bronnen die actueel gebruikt worden. Maar voor zonne-, wind- en waterenergie beperkt die discontinue aanwezigheid de verdere ontwikkeling en wordt de noodzaak voor elektriciteitsopslag benadrukt. Een andere technologie voor hernieuwbare elektriciteitsopwekking is de microbiële brandstofcel (MFC). In een MFC worden de organische bestanddelen van het afvalwater rechtstreeks in elektrische energie omgezet. MFCs zijn een opkomende technologie van de afgelopen 10 jaar en vele onderzoekers hebben onderzoek gedaan naar de verbetering van de stroomdichtheid en het vermogen. De ontwikkeling van de stroomdichtheid en het vermogen stagneerde gedurende de afgelopen jaren en er zijn nieuwe impulsen noodzakelijk om deze technologie in de praktijk toe te passen. Uitdagingen welke overwonnen moeten worden, zijn de limitaties door de afstand de elektrodes, de geleidbaarheid van de elektrolyt, de geleidbaarheid van de elektrodes en de continue verwerking van het afvalwater. De continue verwerking van het afvalwater vraagt om opslag van het afvalwater of om opslag van de geproduceerde elektriciteit. Opslag van de elektriciteit kan bewerkstelligd worden door het combineren van een MFC met een condensator.

In **Hoofdstuk 2** werd een geïntegreerd systeem voor het opslaan van hernieuwbare elektriciteit in een MFC ontwikkeld. Dit geïntegreerde systeem werd gecreëerd door een capacitieve elektrode in het anode compartiment te plaatsen en daardoor een capacitieve bioanode te vormen. Deze capacitieve bioanode werd met een nietcapacitieve bioanode vergeleken op basis van het vermogen gedurende polarisatiecurves en de opslagcapaciteit gedurende laad-ontlaad-experimenten.

Gedurende de polarisatiecurves wist de capacitieve elektrode een maximale stroomdichtheid van  $1.02 \pm 0.004 \text{ A/m}^2$  te bereiken, terwijl de nietcapacitieve elektrode maar een stroomdichtheid van  $0.79 \pm 0.03 \text{ A/m}^2$  wist te bereiken, allebei gemeten bij een anode potentiaal van  $-0.300 \text{ V}$  (vs.  $\text{Ag/AgCl}$ ). Gedurende het laad-ontlaad-experiment met 5 minuten laden en 20 minuten ontladen wist de capacitieve elektrode  $22831 \text{ C/m}^2$  op te slaan, terwijl de nietcapacitieve elektrode maar  $12195 \text{ C/m}^2$  kon opslaan. Met betrekking tot de ladingsterugwinning van iedere elektrode, was de capacitieve elektrode in staat om 52.9% meer lading terug te winnen, dan de nietcapacitieve elektrode.

De capacitieve elektrode presteerde gedurende alle laad-ontlaad-experimenten beter dan de nietcapacitieve elektrode. Dit hoofdstuk toont aan, dat bij gebruik van de MFC met een capacitieve bioanode het vermogen verbetert wordt en de elektriciteit opgeslagen kan worden.

De opslagcapaciteit van deze eerste capacitieve bioanode werd verder onderzocht gedurende de werkzaamheden voor **Hoofdstuk 3** en **Hoofdstuk 4**. Het capacitieve laagje van de capacitieve bioanode werd in zijn materiaalsamenstelling gevarieerd om de optimale samenstelling te bepalen. In **Hoofdstuk 3** werden verschillende diktes van het capacitieve laagje getest om de invloed op het vermogen te bepalen. In **Hoofdstuk 2** werd de MFC met een geïntegreerde capacitieve bioanode met een dikte van 0.5mm gebruikt. In dit hoofdstuk werd de dikte in drie stappen gevarieerd: 0.2mm, 0.5mm en 1.5mm. Voor het gebruik als capacitieve bioanode

werden van iedere elektrode de oppervlakte eigenschappen bepaald middels BET-Analyse en SEM-beelden. Daarna werd iedere capacitieve elektrode in het MFC-setup getest gedurende polarisatiecurves, voor bepaling maximale continue stroomproductie, en laad-ontlaad-experimenten, voor bepaling maximale ladingsterugwinning.

De capacitieve elektrode met een dikte van 0.2mm presteerde beter dan alle andere elektrodes in alle experimenten: het bereikte een maximale stroomdichtheid van 2.53 A/m<sup>2</sup> gedurende de polarisatiecurves en het was in staat om een totaal van 96013 C/m<sup>2</sup> gedurende laad-ontlaad-experimenten op te slaan. De hoogste ladingsterugwinning voor deze elektrode lag bij 1.4, dit betekent dat 40% meer stroom gewonnen kan worden van deze elektrode gedurende de onderbrokene operatie vergeleken met de continue operatie van een nietcapacitieve elektrode. Vergeleken met de eerste capacitieve bioanode uit **Hoofdstuk 2** is dit wederom een toename in ladingsterugwinning van 36%. Verrassend nam het vermogen van de MFC af met toenemende dikte van de capacitieve elektrode, want het tegenovergestelde werd verwacht. In **Hoofdstuk 4** werd het recept voor de productie van de capacitieve elektrode veranderd. De capacitieve bioanode wordt geproduceerd door het uitstrijken van een mengsel van actieve koolpoeder met PVDF (polyvinylideenfluoride) op een stroomcollector, het PVDF is hierbij het bindmiddel. In deze studie werd de invloed van de hoeveelheid PVDF van de capacitieve elektrode op het vermogen van de capacitieve bioanode getest. Zes capacitieve elektrodes met verschillende PVDF-gehaltenes (gewichts- %) werden geproduceerd, namelijk 2%, 4%, 10%, 14%, 21% en 46%. Deze capacitieve elektrodes werden eerst naar hun chemische eigenschappen onderzocht middels BET-Analyse, galvanostatische laad-ontlaad-experimenten en SEM-beelden. Het vermogen van de capacitieve bioanodes werd weer gedurende polarisatiecurves en laad-ontlaad-experimenten onderzocht. Tijdens de polarisatiecurves met constante stroomproductie, bereikte de capacitieve elektrode met het laagste PVDF-gehalte

van 2% het beste vermogen met een maximale stroomdichtheid van  $2.4\text{A}/\text{m}^2$ . Echter wanneer de stroomdichtheid van iedere elektrode per gram actieve kool uitgedrukt wordt, dan bereikt de capacitieve elektrode met het hoogste PVDF-gehalte van 46% de hoogste stroomdichtheid ( $36.6\text{mA}/\text{g}_{\text{AC}}$ ). Gedurende de intermitterende stroomproductie tijdens de laad-ontlaad-experimenten, wist de capacitieve bioanode met een PVDF-gehalte van 21% een relatieve ladingsterugwinning te bereiken van 1.8, dit betekent dat deze elektrode 80% meer stroom geproduceerd heeft dan een nietcapacitieve elektrode met continue stroomproductie. Wederom werd een toename in de ladingsterugwinning vergeleken met de beste capacitieve elektrode van **Hoofdstuk 3** bereikt.

De resultaten van de **Hoofdstukken 2-4** laten zien dat micro-organismen in staat zijn om op het capacitieve materiaal te groeien en dat ze elektronen in een elektrode op kunnen slaan die niet met de tegenelektrode verbonden is (open elektrisch circuit). De micro-organismen zijn dus in staat om zich aan de “nieuwe” omstandigheden aan te passen en zelfs beter te presteren (toename in ladingsterugwinning). In **Hoofdstuk 5** werd een nieuw reactor concept geïntroduceerd, welke gebruik maakt van deze vaardigheden van de micro-organismen. Dat nieuwe reactor concept is gebaseerd op het gebruik van actieve kool granulen om een capacitieve wervelbed bioanode te vormen. Het gebruik van een granulaire elektrode in een MFC is interessant, want de granulen bieden een gunstige manier voor het creëren van een groot elektrode oppervlak, wat essentieel is voor het bereiken van hoge stroomdichtheden en een hoog vermogen. Actieve kool granulen worden gekoloniseerd door de micro-organismen, welke de organische bestanddelen van het afvalwater in protonen, koolstofdioxide en elektronen omzetten en de elektronen vervolgens in de granulen opslaan. De elektriciteit wordt van de actieve kool granulen gewonnen in een extern ontlaadcel. De proof-of-principle van het capacitieve wervelbed systeem had een totale anode volume van 2L. Na een start-up periode van 100 dagen nam de stroomdichtheid

van  $0.56\text{A}/\text{m}^2$  met 100g actieve kool granulen naar  $0.99\text{ A}/\text{m}^2$  met 150g actieve kool granulen naar  $1.3\text{ A}/\text{m}^2$  met 200g actieve kool granulen toe. Voor dit experiment werd nog het contact tussen de actieve kool granulen en de stroomcollector getest in een experiment zonder biofilm. Het contact tussen de actieve kool granulen en de stroomcollector is de reden voor stroomproductie in het capacitieve wervelbed systeem. SEM-beelden bevestigden de aanwezigheid van een biofilm op de actieve kool granulen na gebruik in de capacitieve wervelbed bioanode. Hoewel de stroomdichtheden die in **Hoofdstuk 5** bereikt worden nog verder verbeterd moeten worden, biedt het grote oppervlak van de actieve kool granulen in combinatie met het externe ontladen nieuwe en veelbelovende kansen voor het scale-up van MFCs. **Hoofdstuk 6** presenteert een reflectie op het werk wat gedaan werd voor dit boek en geeft een vooruitzicht op toekomstige toepassingen. Zoals gepresenteerd werd in **Hoofdstuk 1** stagneert de ontwikkeling van het vermogen van de MFCs sinds een paar jaar tussen de  $2\text{-}3\text{ W}/\text{m}^2$ . Dit is te wijten aan de limitaties door de afstand van de elektrodes, de geleidbaarheid van de elektrolyt en de geleidbaarheid van de elektrodes. En hoewel het vermogen wat tijdens de experimenten voor dit boek bereikt werd niet rechtstreeks een verbetering van het vermogen is, bieden de gebruikte systemen veel nieuwe kansen. Middels het vlakke-plaat systeem werd het geïntegreerde opslag concept geïntroduceerd in de wereld van de MFCs. De capacitieve elektrodes die voor de vlakke-plaat studies gebruikt werden verbeterden de relatieve ladingsterugwinning om 80% vergeleken met een nietcapacitieve elektrode. Gebaseerd op deze resultaten, werd het geïntegreerde opslagsysteem verder ontwikkeld tot een capacitieve wervelbed bioanode, waar het laden en ontladen van de wervelende granulen in gescheiden reactoren plaats vindt. Wederom was het behaalde vermogen van dit systeem geen verbetering van de behaalde waardes van de afgelopen jaren, maar het biedt wel oplossingen voor sommige problemen. Door het intensieve contact tussen de wervelende granulen

(en daardoor de micro-organismen) met de elektrolyt, is de CZV-concentratie minder belangrijk. De scheiding van het laad- en het ontladproces biedt een oplossing voor twee problemen: Afstand van de elektrodes en geleidbaarheid van de elektrolyt. Omdat de granulen als groot oppervlak dienen voor de bioanode, kan de afstand tussen de stroomcollector en de kathode klein zijn. En omdat de elektronen in de granulen opgeslagen worden en de protonen in het dubbellaagje om de granulen heen verrijken, wordt de geleidbaarheid van de elektrolyt ook minder belangrijk. Want er is geen transport van ionen door de elektrolyt meer noodzakelijk. Gedurende het toekomstige onderzoek is het zaak om het design van de capacitieve wervelbed bioanode verder te optimaliseren.

## Acknowledgements

Here we are, after 5 years of work this thesis, My Thesis, is finished and ready to be defended. But without the help of others this would not have been possible, therefore I would like to say 'thanks' to many people.

First of all I would like to thank Gert-Jan and Bert for answering my inquiries after a PhD position on the topic of Microbial Fuel Cells and for inviting me over (all the way from Stuttgart, Germany) for an interview. You were my first contact persons in Wetsus and I still remember our interview.

Furthermore, I would like to express my gratitude to all my supervisors: Cees, thanks for being my promotor and for all the inspring meetings in which you always sketched the bigger picture and showed that you believe in electricity produced from MFCs. Bert, it was one of your many ideas, which turned into my subject for the doctoral research. I enjoyed our meetings were we started off looking at interesting graphs (not looking like expected) and then tried to figure out the possible theory behind it. Michel, as my daily supervisor you managed to give a positive spin to every day. I admire your energy and neverending enthousiasm☺. Thanks a lot for everything.

Tom and Annemiek, you were the last persons to be added to my supervisory team and took over towards the end of my PhD. Thanks a lot for keeping the overview and for all the help at the end.

Also I would like to thank the lab/technical/secretarial/administrative team at Wetsus for their visible/invisible support. Special thanks go out to Harm and Jan for building my first (Harm) and my second (Jan) setup. Also special thanks go out to Jelmer for the support with many BET-Analyses and countless SEM-pictures. Also thanks for the effort in taking AFM-pictures from my black magic stuff.

I would like to thank Tom, Annemiek, Adriaan, Elsemiek, Urania, Philipp, Sam and the other members of the Resource Recovery theme for the fruitful discussions and the support during the work for this thesis.

A lot of practical work was done with the support of several students, therefore I would like to thank Delia, Aura, Joana, Thomas, Girum, Daria and Razan. Guys, you did a great job!

My office mates from Hw 1.03: Joost, Astrid, Tom, Adriaan, Claudia S., Bob, Bruno and Dries thanks for the fun time and all the nice afternoon conversations with or even without coffee.

Then we get to the "German Group" (it started shrinking a lot towards the end of 2013):

Claudia D. (and Norman): Danke, dass du mich als Paranymphe unterstuetzt und vielen Dank fuer alle lustigen Stunden, die wir so am Stall mit den Ponies oder mit den Hunden verbracht haben. Ich hoffe, dass noch viele folgen werden...

Philipp und Sandra (niet duits, maar er toch altijd bij): Danke fuer alle Antworten auf die vielen Fragen und vielen Dank fuer viele leckere Abendessen. Ich besuche euch gerne mal wieder fuer ein paar gefuellte Paprika ☺.

Lena: Danke fuer drei Jahre lustige Hausgemeinschaft, die Anfangszeit in Leeuwarden wurde so doch wesentlich angenehmer. Ich wuensche dir viel Glueck mit deiner neuen "Hausgemeinschaft".

Christina: Vielen Dank fuer unzaehlige Fotos, die mich immer an diese Zeit erinnern werden. Ausserdem vielen Dank fuer etliche schoene Grillabende mit der laufenden "Bratwurst" Emmy.

Ingo und Martina (auch nicht deutsch, aber auch immer dabei): Vielen Dank fuer lustige Abende im Irish Pub und bei zahlreichen Abendessen und Spieleabenden.

Ook nog hartelijk dank aan Rosanne en Henrieke, Tynke, Loes, Inge, Ilse en Nynke jullie hebben ervoor gezorgd, dat ik op stal de nodige afleiding van het promotieonderzoek kon vinden. Bedankt voor talloze leuke buitenritten en jullie

ondersteuning bij menig wedstrijd, waar ik naartoe ben geweest. Rosanne ook nog extra dank aan jou, om als mijn Paranympf erbij te willen zijn.

Ook de familie Leenders en iedereen die erbij hoort mijn dank voor al 16 jaar vriendschap en mijn "tweede familie".

Und zu guter letzt: Mama, Papa vielen Dank fuer alles!!! Ohne eure wirklich grenzenlose Unterstuetzung waere es nicht soweit gekommen. Es ist jetzt zwar ein Jahr spaeter als irgendwann mal angekuendigt, aber es ist vollbracht. Danke, dass ich immer auf euch zaehlen kann.

Alexandra Deeke

Asten-Heusden

September 2014



## **About the author**

Alexandra Deeke was born on the 25th of January in 1982 in Hannover, Germany. After finishing High School, she started her study of Chemical Engineering at the Technical University Clausthal, Clausthal-Zellerfeld, Germany in 2002. Alexandra did her minor thesis on the subject of Microbial Fuel Cells at the Cutec, Clausthal-Zellerfeld, Germany. Her interest in Renewable Energy Technologies awoke and she did her diploma thesis on “Glass seals for the use in solid oxide fuel cells” at the German Aerospace Center, Stuttgart, Germany. After graduation in 2009, she looked for an opportunity to do her PhD. In June 2009, she started her work as a PhD student on the subject of “Capacitive Bioanodes for Electricity Storage in Microbial Fuel Cells” at Wetsus, Leeuwarden, The Netherlands. After finishing her PhD at the end of 2013, she looked for a new challenge in the field of environmental technology. In January 2014 she started working as an Innovation Engineer at Waterboard De Dommel, Boxtel, The Netherlands.